THE EFFECT OF LATERAL FLOW ON EXOSPHERIC DENSITIES*

John Robert McAfee

Department of Physics

University of Pittsburgh

Pittsburgh, Pennsylvania

*Submitted to the Graduate Faculty in the Division of Natural Sciences in partial fulfillment of the requirements for the degree of Doctor of Philosophy.

THE INFLUENCE OF LATERAL FLOW
ON
EXOSPHERIC DENSITIES

John Robert McAfee, Ph.D.
University of Pittsburgh, 1965

15384

Lateral flow in a collisionless exosphere at the top of the earth's atmosphere is calculated for a spherical geometry. The model consists of an exobase surface below which a Maxwellian distribution is assumed and above which particles describe elliptical orbits. The net flux into the exobase surface is the difference between the flow in from all other points on the surface and the flow out from below. The difference arises from both variations in density and temperature on the exobase surface. The net fluxes calculated for atomic oxygen and molecular nitrogen and oxygen are too small to cause a departure from diffusive equilibrium. The flux for helium toward the night side could be supported by diffusion but is sufficiently large to question the assumption of diffusion equilibrium. The hydrogen flux is larger than can be supported by diffusion from below and would necessitate a more complicated approach to calculations of its density distribution. In any case, the hydrogen night-time bulge would persist. The major effect on exospheric densities of helium and hydrogen would come indirectly because of their departure from diffusive equilibrium in the region below and hence their change in density at the exobase surface and corresponding change in exospheric density.

Author

PREFACE

The author is indebted to his advisor, Professor Thomas M. Donahue, for his aid, encouragement, and patience; and to the National Science Foundation, which supported the computer time under NSF contract G-11309. The research was sponsored by NASA under contract NASr-179.

TABLE OF CONTENTS

1.0. INTRODUCTION

The usual method for determining the theoretical composition of the heterosphere is that of solving the problem of diffusing gases for a spherically symmetric atmosphere with time independent parameters (see for instance Kockarts and Nicolet[1,2], Godart and Nicolet[3], or Van Zandt and Knecht[4]). Static (diffusive equilibrium) solutions are found as a function of the altitude temperature profile which is usually assumed to be dependent only upon the exospheric temperature. Hence, the vertical composition in any local region is presumed to be a function only of the exospheric temperature overhead. This is of course an idealization since the atmosphere is not spherically symmetric, nor is it time independent. In fact the temperature of the exosphere varies between night and day as well as with the sunspot cycle. Accordingly, the compositions derived statically as above would then vary in the same manner. Hence, by this reasoning, lateral gradients in density as well as in temperature must exist. A natural question would then be: do these lateral gradients affect the heterospheric composition, and if so, in what way and to what degree?

One non-static effect has already been investigated, namely that of the planetary escape of hydrogen, first proposed by Jeans[5]. The fact that there can be an appreciable hydrogen escape flux necessitates a steady state solution to the diffusion equation which is radically different than the static diffusive equilibrium case (see Kockarts and Nicolet[1,2]

or Figure 11). This is still a case of considering local conditions only since this diffusion is presumed vertical and dependent only upon the overhead exospheric temperature. This model, however, did lead to the first consideration of the possible effect of lateral flow because of the resultant "night-time bulge".

The removal of hydrogen due to escape creates a large diurnal variation in its density if the steady-state diffusion equations are applied. Since the escaping flux is much greater on the hot day side, this removal reduces the daytime hydrogen densities much more severely than on the night side. Hence, there should be more hydrogen on the night side of the earth than on the day side. This diurnal hydrogen variation has been offered as an explanation of the observation of a large night time Lyman - α intensity by Donahue[6]. Calculations by Thomas[7] and Donahue and Thomas[8] have shown that the transport of resonance radiation from the day to night side might produce the observed intensities if there is a sufficiently large diurnal variation in the hydrogen densities.

This approach by Donahue has drawn considerable objection from Hanson and Patterson[9] on the grounds that a large diurnal variation would be quickly wiped out by a lateral mass flow out of this night-time bulge. Their estimate of the lateral flow indicated just this. Improvements in their model by Donahue and McAfee[10], however, suggest that this is not the case, and that furthermore, an appreciable night time bulge is demanded by lateral flow. This is a necessary consequence of the diurnal temperature

variation, since the temperature induced flow would be from the day to the night side.

Experimental evidence for the existence of a lateral flow has been discovered by Reber and Nicolet[11]. In the interpretation of mass spectrometric data from the Explorer XVII satellite, they conclude that at altitudes greater than 400 kilometers any explanation must include horizontal gradients and mass transport near sunrise. The possibility that helium is not in diffusive equilibrium is also suggested by their data, and this might be attributable to a lateral flow of helium.

It would then seem that the possibility that lateral flow is a legitimate and observable effect is one that should be considered. In such a determination several questions must be answered including the obvious ones of the magnitude and form of the lateral flow as well as others such as the times involved, the reaction of the atmosphere to the flow, and how the flow might affect observations. The effort here has then been to calculate this lateral mass flow for as realistic conditions as possible as well as to determine its possible effect upon heterospheric densities.

2.0. MODEL OF THE HETEROSPHERE

Before any meaningful calculations of lateral flow can be performed it is necessary to begin with an initial model of the heterosphere. Since the parameters describing this region are by no means accurately determined at this time, any model must contain a number of assumptions. Ideally, calculations should be made based upon all of the various models which might be applicable. This is unfortunately impractical due to the length of time involved. Therefore, a single type of model has been used which is hoped to at least represent the bulk of the atmospheric properties.

The heterosphere or non-mixing region, assumed here to begin at an altitude of 120 kilometers, can be divided into two main parts, an endosphere (or diffusosphere) and an exosphere. The endosphere is considered to be the region above 120 kilometers where diffusion is the controlling process. At higher altitudes collisions become less frequent due to the reduction in density. At sufficiently high altitudes they become so infrequent that they may be neglected. This region where collisions are neglected is called the exosphere. There will naturally be a transition region between the endosphere and exosphere, but for purposes of calculation, it is assumed that the change is sharp and occurs at the base of the exosphere, or exobase.

2.1. Temperature

Neither the question of vertical profile nor lateral distribution of temperature in the heterosphere has been resolved to the satisfaction of most investigators. However, assumptions for the values of temperature are a necessity since temperature is the primary parameter which will determine the density distributions in the model used here. Hence, it is important to make an attempt to consider the best form possible.

Direct temperature measurements have been made in the lower heterosphere by Blamont et al[12-18] by analysis of the Doppler line profile of resonance radiation from sodium and other elements which have been injected into the atmosphere at various altitudes and allowed to come into thermal equilibrium with the local gas. Some results of this type of experiment are shown in figure 1. They indicate a temperature gradient which is more moderate than that used in some previous models (for instance Kockarts and Nicolet[1,2]) and an isothermal region in the upper heterosphere. The temperature of the isothermal region will be referred to as the exospheric temperature. Unfortunately, this experimental data near 200 km is basically for periods of low solar activity only and some type of extension must be made to higher exospheric temperatures. Two types of behavior were considered: first, a continuation of the temperature gradient and a relatively sharp turnover to an isothermal region at some higher level (Model A); and second, a more

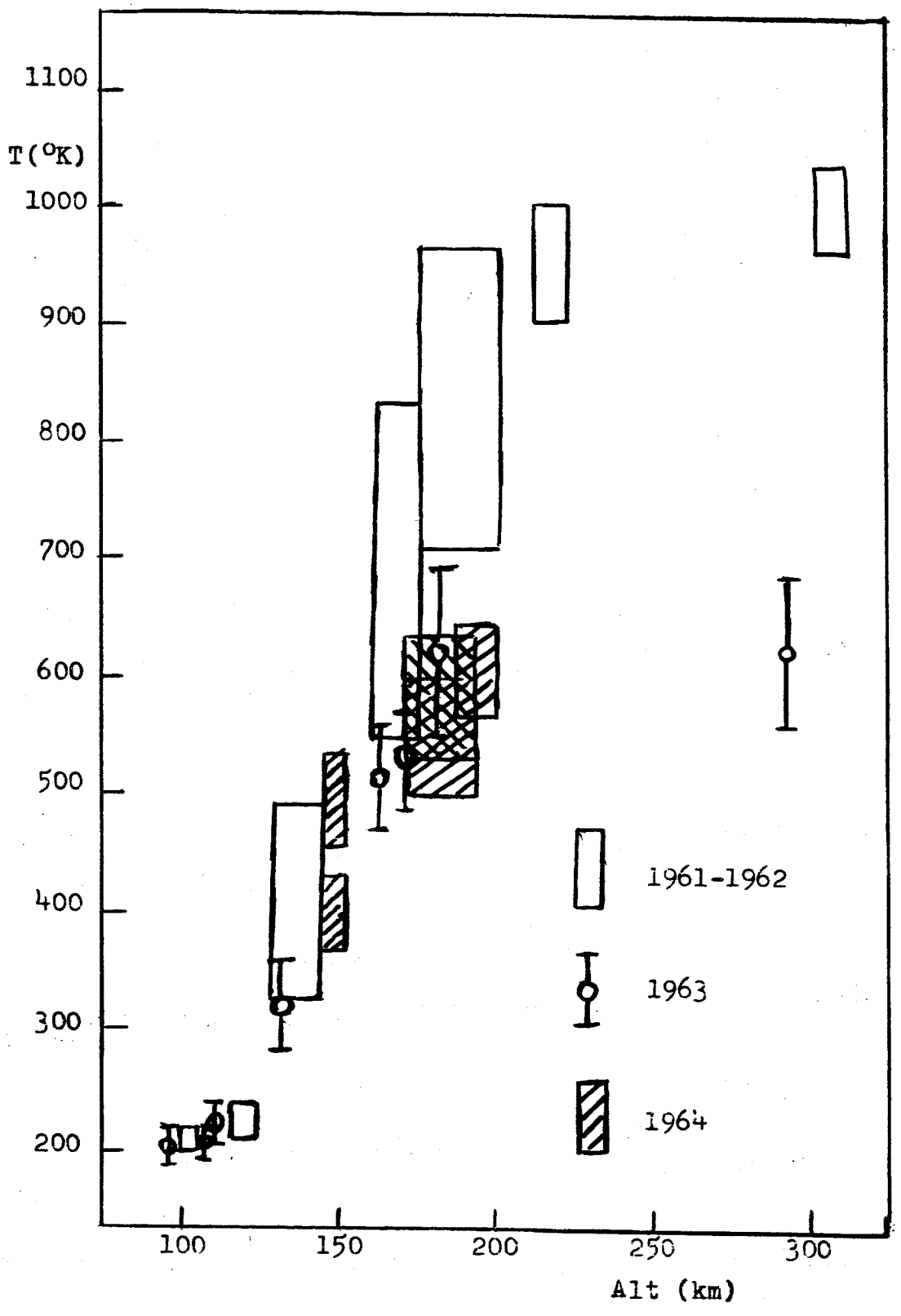

Figure 1. Experimental temperature measurements of Blamont et al 12-18.

and more gradual turnover to the isothermal region as the exosphere temperature becomes larger (Model B). The two models are shown in figure 2.

Further evidence for the validity of these models has been supplied by Hedin, Avery, and Tschetter[19] and Hedin and Nier[20] who have made an independent measurement of the temperature profile with altitude by an analysis of the behavior of mass spectrometric measurements as a function of the angle of rocket attack. These results are in good agreement with the chemical release measurements.

One questionable feature of the models chosen is the fact that the exospheric temperature variation is assumed to affect only the upper part of the temperature profile. The errors involved in the chemical release measurements (see figure 1) are sufficiently large to allow a good deal of fluctuation in the behavior of the temperature profile at lower altitudes. It has been pointed out by Zipf[21] that small changes in the behavior of the temperature near 120 km within the experimental errors can have a large effect upon the eventual densities of the various important constituents at higher altitudes. Such a possibility should be kept in mind; however, for purposes of calculation here, any low altitude temperature fluctuations have been ignored.

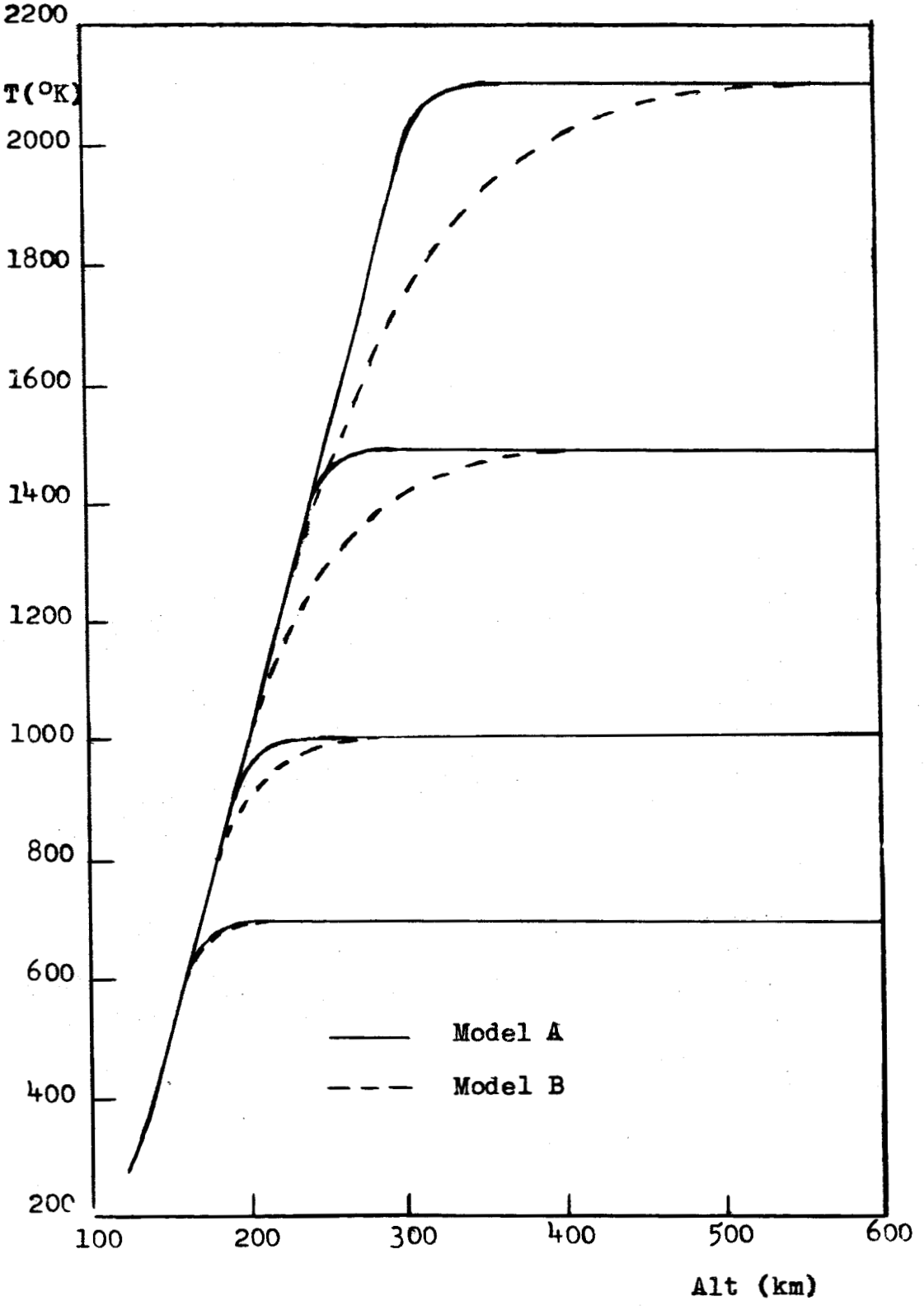

Figure 2. Temperature models of the heterosphere.

2.2. Endosphere

The endosphere is defined as that region of the heterosphere in which diffusion is the dominant process in controlling the distribution of density. Below the lower boundary of the endosphere the atmosphere is mixed by turbulent diffusion so that the ratio of densities between the various constituents remains fixed (disregarding local effects such as caused by chemical or photochemical effects). The altitude at which diffusion replaces mixing, the turbopause, is an important parameter, since the theoretical density profile of individual constituents may be quite different in a mixing as opposed to a diffusing region. It is possible that the turbopause may vary with season, solar cycle, latitude, local time or other parameters.

Experiments such as neutral mass spectrometric rocket probes (see for instance Meadows and Townsend[22], Pokhunkov[23], Meadow-Reed and Smith[24], or Schaefer and Nichols[25]) have placed the turbopause at about 110 km. Kockarts and Nicolet[1] have investigated theoretically the effects of different turbopause levels upon the density distributions above and have found for example that the helium density at 120 km varies by a factor of 10 for turbopause values of 100 or 120 km, since the helium scale height is much greater than the atmospheric scale height in this region. The heavier elements are not affected as severely since their scale heights do not differ greatly from the atmospheric scale height. On the other hand, by the same reasoning hydrogen should show an even larger

discrepancy since its scale height is even larger than that of helium. As has been pointed out by Kockarts and Nicolet[1], however, this is not the case. In fact, as will be shown later, the hydrogen density profile follows the atmospheric density profile fairly closely in this region because hydrogen is probably not in diffusive equilibrium. Furthermore, it has been pointed out by Van Zandt and Knecht[4] that the diurnal variation of the turbopause level can vary only by a few kilometers due to the slowness of diffusion in this region.

Since the interest here is in diurnal effects, and since first, the turbopause level should not show a large diurnal variation, and second, the variation should only affect helium to a noticeable degree, it has been assumed that the densities of the various constituents at 120 km are independent of any turbopause effects. This is to say that densities in the mixing region are unaffected by the variation of other parameters such as exospheric temperature. Hence, for the calculation of densities above 120 km, a constant normalization density at 120 km will be used for each constituent. These normalization densities are shown in Table 1. Values for atomic oxygen, and molecular nitrogen and oxygen were chosen to agree with Hedin and Nier[20] and Nier et al[26]. The helium value is an approximate fit to the Explorer XVII data of Reber and Nicolet[11]. The hydrogen value, very approximate, is about three times that of Kockarts and Nicolet[1], as suggested by Donahue[27] from photometric observations.

Table 1. Density normalization at 120 km.

Constituent	H	He	O	N_2	O_2
Number density at 120 km	6×10^5	2×10^7	4.5×10^{10}	3.5×10^{11}	4×10^{10}

The popular model for the endosphere is to assume that the various constituents are in diffusive equilibrium. The diffusion equations are solved in appendix A and the diffusive equilibrium solution from equation (46) is

$$\overline{n_i(z)} = n_i(120)\left[\frac{T(120)}{T(z)}\right]\exp\left[\frac{-m_i}{k}\int_{120}^{z}\frac{g(z')}{T(z')}dz'\right] \qquad (1)$$

where i refers to the ith constituent. The number densities as so calculated, using the temperature profile of Model A in figure 2, are given in tables 2-5 for exospheric temperatures of 700°K, 1000°K, 1500°K, and 2100°K respectively. Also included in these tables are the temperature, total density, n, where

$$n \equiv \sum_i n_i,$$

and the mean molecular mass, $\bar{m}$, where

$$\bar{m} \equiv \frac{\sum_i m_i n_i}{n}.$$

The same information is plotted in figures 3-9 for n(H), n(He), n(O), $n(H_2)$, $n(O_2)$, n, and $\bar{m}$ respectively. The changes

Table 2. Atmospheric parameters for 700° exospheric temperature and diffusive equilibrium ((k)≡10^k)

z	T	n(H)	n(He)	n(O)	$n(N_2)$	$n(O_2)$	n	$\bar{m}$
120	282	6.0(5)	2.0(7)	4.5(10)	3.5(11)	4.0(10)	4.4(11)	27.1
140	416	3.8	1.0	1.0	3.6(10)	3.1(9)	4.9(10)	25.7
160	609	2.5	5.9(6)	3.5(9)	7.0(9)	5.1(8)	1.1	24.4
180	694	2.1	4.5	1.8	2.4	1.5	4.3(9)	23.2
200	700	2.0	4.0	1.1	9.6(8)	5.4(7)	2.1	22.0
220	700	2.0	3.5	6.3(8)	3.9	1.9	1.1	20.8
240	700	1.9	3.1	3.8	1.6	7.1(6)	5.5(8)	19.7
260	700	1.8	2.7	2.3	6.8(7)	2.6	3.0	18.7
280	700	1.8	2.4	1.4	2.8	9.6(5)	1.7	17.9
300	700	1.7	2.1	8.5(7)	1.2	3.6	1.0	17.2
320	700	1.7	1.9	5.2	5.0(6)	1.3	5.9(7)	16.6
340	700	1.6	1.7	3.2	2.1	5.0(4)	3.6	16.1
360	700	1.6	1.5	2.0	9.1(5)	1.9	2.2	15.6
380	700	1.5	1.3	1.2	3.9	7.1(3)	1.4	15.1
400	700	1.5	1.2	7.5(6)	1.7	2.7	8.9(6)	14.5
420	700	1.4	1.0	4.6	7.2(4)	1.0	5.8	13.7
440	700	1.4	9.0(5)	2.9	3.2	4.0(2)	3.9	12.9
460	700	1.4	8.0	1.8	1.4	1.6	2.7	11.8
480	700	1.3	7.1	1.1	6.0(3)	6.1(1)	2.0	10.7
500	700	1.3	6.4	7.0(5)	2.7	2.4	1.5	9.6
520	700	1.2	5.7	4.4	1.2	9.5(0)	1.1	8.4
540	700	1.2	5.0	2.8	5.3(2)	3.8	8.9(5)	7.4
560	700	1.2	4.5	1.8	2.4	1.5	7.3	6.4
580	700	1.1	4.0	1.1	1.1	-	6.2	5.6
600	700	1.1	3.6	7.0(4)	4.8(1)	-	5.3	5.0
620	700	1.1	3.2	4.5	2.2	-	4.7	4.5
640	700	1.0	2.9	2.9	9.9(0)	-	4.1	4.1
660	700	1.0	2.6	1.8	4.6	-	3.7	3.8
680	700	9.9(4)	2.3	1.2	2.1	-	3.3	3.6
700	700	9.7	2.1	7.6(3)	-	-	3.0	3.4
720	700	9.4	1.8	4.9	-	-	2.8	3.3
740	700	9.1	1.7	3.2	-	-	2.5	3.1
760	700	8.9	1.5	2.0	-	-	2.3	3.0
780	700	8.7	1.3	1.3	-	-	2.1	3.0
800	700	8.4	1.2	8.7(2)	-	-	2.0	2.9
820	700	8.2	1.1	5.6	-	-	1.8	2.8
840	700	8.0	9.6(4)	3.7	-	-	1.7	2.7
860	700	7.8	8.7	2.4	-	-	1.6	2.7
880	700	7.6	7.8	1.6	-	-	1.5	2.6
900	700	7.4	7.0	1.1	-	-	1.4	2.5
920	700	7.2	6.3	6.9(1)	-	-	1.3	2.5
940	700	7.0	5.7	4.6	-	-	1.2	2.4
960	700	6.8	5.2	3.0	-	-	1.2	2.4
980	700	6.7	4.7	2.0	-	-	1.1	2.3
1000	700	6.5	4.2	1.4	-	-	1.0	2.2

Table 3. Atmospheric parameters for 1000° exospheric temperature and diffusive equilibrium ($(k) \equiv 10^k$)

z	T	n(H)	n(He)	n(O)	$n(N_2)$	$n(O_2)$	n	$\bar{m}$
120	282	6.0(5)	2.0(7)	4.5(10)	3.5(11)	4.0(10)	4.4(11)	27.1
140	416	3.8	1.0	1.0	3.6(10)	3.1(9)	4.9(10)	25.7
160	610	2.5	5.9(6)	3.5(9)	7.0(9)	5.1(8)	1.1	24.4
180	810	1.8	3.9	1.6	2.1	1.4	3.8(9)	23.3
200	973	1.5	3.0	8.7(8)	8.9(8)	5.2(7)	1.8	22.3
220	1000	1.4	2.6	5.9	4.6	2.5	1.1	21.5
240	1000	1.4	2.4	4.2	2.5	1.2	6.8(8)	20.6
260	1000	1.3	2.2	2.9	1.4	6.0(6)	4.4	19.9
280	1000	1.3	2.0	2.1	7.3(7)	3.0	2.8	19.2
300	1000	1.3	1.9	1.5	4.0	1.5	1.9	18.5
320	1000	1.2	1.7	9.5(7)	1.9	6.3(5)	1.2	17.9
340	1000	1.2	1.6	7.3	1.2	3.8	8.7(7)	17.5
360	1000	1.2	1.4	5.2	6.6(6)	1.9	6.0	17.1
380	1000	1.2	1.3	3.7	3.6	9.7(4)	4.2	16.7
400	1000	1.1	1.2	2.7	2.0	4.9	3.0	16.3
420	1000	1.1	1.1	1.9	1.1	2.5	2.1	16.0
440	1000	1.1	1.0	1.4	6.3(5)	1.3	1.5	15.7
460	1000	1.1	9.4(5)	9.8(6)	3.5	6.7(3)	1.1	15.3
480	1000	1.0	8.7	7.0	2.0	3.5	8.1(6)	14.9
500	1000	1.0	8.0	5.1	1.1	1.8	6.0	14.5
520	1000	1.0	7.4	3.7	6.3(4)	9.4(2)	4.5	14.0
540	1000	9.8(4)	6.8	2.7	3.6	4.9	3.4	13.5
560	1000	9.6	6.3	1.9	2.0	2.6	2.6	13.0
580	1000	9.5	5.8	1.4	1.2	1.4	2.0	12.3
600	1000	9.3	5.3	1.0	6.7(3)	7.2(1)	1.6	11 6
620	1000	9.2	4.9	7.4(5)	3.8	3.8	1.3	10.9
640	1000	9.0	4.5	5.4	2.2	2.1	1.0	10.2
660	1000	8.8	4.2	4.0	1.3	1.1	8.6(5)	9.4
680	1000	8.6	3.9	2.9	7.5(2)	5.9(0)	7.2	8.7
700	1000	8.5	3.6	2.1	4.3	3.2	6.2	8.0
720	1000	8.4	3.3	1.6	2.5	1.7	5.3	7.3
740	1000	8.2	3.1	1.2	1.5	-	4.6	6.7
760	1000	8.1	2.9	8.5(4)	8.7(1)	-	4.1	6.2
780	1000	7.9	2.7	6.3	5.2	-	3.7	5.8
800	1000	7.7	2.5	4.7	3.0	-	3.3	5.4
820	1000	7.6	2.3	3.5	1.8	-	3.0	5.0
840	1000	7.5	2.1	2.6	1.1	-	2.7	4.7
860	1000	7.3	2.0	1.9	6.4(0)	-	2.5	4.5
880	1000	7.2	1.8	1.4	3.8	-	2.3	4.3
900	1000	7.0	1.7	1.1	2.3	-	2.2	4.1
920	1000	6.9	1.6	8.0(3)	1.4	-	2.0	4.0
940	1000	6.8	1.5	6.0	-	-	1.9	3.9
960	1000	6.7	1.4	4.5	-	-	1.7	3.8
980	1000	6.6	1.3	3.4	-	-	1.6	3.7
1000	1000	6.5	1.2	2.5	-	-	1.5	3.6

Table 4. Atmospheric parameters for 1500° exospheric temperature and diffusive equilibrium ((k) ≡ 10^k)

z	T	n(H)	n(He)	n(O)	$n(N_2)$	$n(O_2)$	n	$\bar{m}$
120	282	6.0(5)	2.0(7)	4.5(10)	3.5(11)	4.0(10)	4.4(11)	27.1
140	416	3.8	1.0	1.0	3.6(10)	3.1(9)	5.0(10)	25.7
160	610	2.5	5.9(6)	3.5(9)	7.0(9)	5.1(8)	1.1	24.4
180	860	1.8	3.9	1.6	2.1	1.4	3.8(9)	23.3
200	1010	1.4	2.8	8.4(8)	8.6(8)	5.0(7)	1.8	22.3
220	1210	1.2	2.2	5.1	4.1	2.2	9.4(8)	21.6
240	1410	1.1	1.8	3.3	2.2	1.1	5.7	20.9
260	1494	1.0	1.6	2.5	1.4	6.4(6)	3.9	20.4
280	1500	9.6(4)	1.5	2.0	9.0(7)	4.0	2.9	19.9
300	1500	9.2	1.4	1.6	6.0	2.5	2.2	19.4
320	1500	8.9	1.3	1.2	3.6	1.4	1.6	18.9
340	1500	8.6	1.2	9.8(7)	2.7	1.0	1.3	18.6
360	1500	8.4	1.2	7.8	1.8	6.4(5)	1.0	18.2
380	1500	8.3	1.1	6.2	1.2	4.1	7.6(7)	17.8
400	1500	8.1	1.0	5.0	8.2(6)	2.6	6.0	17.5
420	1500	8.0	9.8(5)	4.0	5.6	1.7	4.7	17.2
440	1500	7.9	9.3	3.2	3.8	1.1	3.7	17.0
460	1500	7.8	8.8	2.6	2.6	6.9(4)	2.9	16.7
480	1500	7.7	8.3	2.1	1.7	4.4	2.3	16.5
500	1500	7.6	7.9	1.7	1.2	2.9	1.9	16.3
520	1500	7.5	7.5	1.3	8.2(5)	1.9	1.5	16.1
540	1500	7.4	7.1	1.1	5.6	1.2	1.2	15.9
560	1500	7.3	6.7	8.6(6)	3.8	7.9(3)	9.7(6)	15.6
580	1500	7.2	6.4	7.0	2.7	5.1	7.9	15.4
600	1500	7.1	6.0	5.7	1.8	3.4	6.5	15.2
620	1500	7.0	5.7	4.6	1.3	2.2	5.3	15.0
640	1500	6.9	5.4	3.7	8.8(4)	1.5	4.4	14.7
660	1500	6.8	5.2	3.0	6.1	9.6(2)	3.6	14.5
680	1500	6.7	4.9	2.5	4.2	6.3	3.0	14.2
700	1500	6.6	4.7	2.0	3.0	4.2	2.5	13.9
720	1500	6.6	4.4	1.6	2.1	2.8	2.1	13.5
740	1500	6.5	4.2	1.3	1.4	1.9	1.8	13.2
760	1500	6.4	4.0	1.1	1.0	1.2	1.5	12.8
780	1500	6.3	3.8	8.9(5)	7.1(3)	8.2(1)	1.3	12.4
800	1500	6.2	3.6	7.3	5.0	5.5	1.1	12.0
820	1500	6.2	3.4	5.9	3.5	3.7	9.5(5)	11.6
840	1500	6.1	3.3	4.9	2.5	2.5	8.3	11.1
860	1500	6.0	3.1	4.0	1.8	1.7	7.2	10.7
880	1500	5.9	3.0	3.3	1.3	1.1	6.3	10.2
900	1500	5.9	2.8	2.7	9.0(2)	7.7(0)	5.6	9.8
920	1500	5.8	2.7	2.2	6.4	5.2	5.0	9.3
940	1500	5.7	2.6	1.8	4.6	3.6	4.5	8.9
960	1500	5.6	2.5	1.5	3.3	2.4	4.0	8.5
980	1500	5.6	2.3	1.3	2.3	1.7	3.7	8.1
1000	1500	5.5	2.2	1.0	1.7	1.1	3.3	7.7

Table 5. Atmospheric parameters for 2100° exospheric temperature and diffusive equilibrium ((k)≡10^k)

z	T	n(H)	n(He)	n(O)	$n(N_2)$	$n(O_2)$	n	$\bar{m}$
120	282	6.0(5)	2.0(7)	4.5(10)	3.5(11)	4.0(10)	4.4(11)	27.1
140	416	3.8	1.0	1.0	3.6(10)	3.3(9)	4.9(10)	25.7
160	610	2.5	5.9(6)	3.5(9)	7.0(9)	5.1(8)	1.1	24.4
180	722	1.8	3.9	1.6	2.1	1.4	3.8(9)	23.3
200	1010	1.4	2.8	8.4(8)	8.6(8)	5.0(7)	1.8	22.3
220	1092	1.2	2.2	5.1	4.1	2.2	9.4(8)	21.6
240	1280	1.0	1.8	3.3	2.2	1.1	5.7	20.9
260	1471	8.9(4)	1.5	2.3	1.3	6.0(6)	3.7	20.4
280	1664	8.1	1.2	1.7	7.9(7)	3.6	2.5	20.0
300	1858	7.5	1.1	1.3	5.2	2.2	1.8	19.6
320	1948	7.1	9.7(5)	1.0	3.7	1.5	1.4	19.2
340	1965	6.8	9.2	8.3(7)	2.6	1.0	1.1	18.9
360	1977	6.6	8.9	7.4	2.1	8.0(5)	9.6(7)	18.6
380	1989	6.4	8.6	6.3	1.6	5.8	8.0	18.4
400	2001	6.2	8.2	5.3	1.2	4.2	6.7	18.1
420	2100	6.1	7.9	4.6	9.0(6)	3.0	5.6	17.9
440	2100	6.0	7.6	3.9	6.9	2.2	4.7	17.6
460	2100	5.9	7.3	3.3	5.2	1.6	3.9	17.4
480	2100	5.8	7.0	2.8	4.0	1.2	3.3	17.2
500	2100	5.7	6.8	2.4	3.0	8.7(4)	2.8	17.1
520	2100	5.6	6.5	2.1	2.3	6.4	2.4	16.9
540	2100	5.6	6.3	1.8	1.8	4.7	2.0	16.7
560	2100	5.5	6.0	1.5	1.3	3.4	1.7	16.5
580	2100	5.4	5.8	1.3	1.0	2.5	1.5	16.4
600	2100	5.4	5.6	1.1	7.9(5)	1.9	1.3	16.2
620	2100	5.3	5.4	9.7(6)	6.1	1.4	1.1	16.1
640	2100	5.3	5.2	8.4	4.7	1.0	9.4(6)	16.0
660	2100	5.2	5.0	7.2	4.0	7.6(3)	8.1	15.8
680	2100	5.2	4.8	6.2	2.8	5.7	7.0	15.7
700	2100	5.1	4.6	5.4	2.1	4.2	6.1	15.5
720	2100	5.1	4.5	4.6	1.7	3.2	5.3	15.4
740	2100	5.1	4.3	4.0	1.3	2.4	4.6	15.2
760	2100	5.0	4.2	3.5	1.0	1.8	4.0	15.1
780	2100	5.0	4.0	3.0	7.8(4)	1.3	3.5	14.9
800	2100	4.9	3.9	2.6	6.1	1.0	3.1	14.7
820	2100	4.9	3.7	2.3	4.7	7.5(2)	2.7	14.5
840	2100	4.8	3.6	2.0	3.7	5.7	2.4	14.3
860	2100	4.8	3.5	1.7	2.9	4.3	2.1	14.2
880	2100	4.7	3.4	1.5	2.3	3.2	1.8	13.9
900	2100	4.7	3.3	1.3	1.8	2.4	1.6	13.7
920	2100	4.7	3.1	1.1	1.4	1.9	1.5	13.5
940	2100	4.6	3.0	9.8(5)	1.1	1.4	1.3	13.3
960	2100	4.6	2.9	8.5	8.6(3)	1.1	1.2	13.0
980	2100	4.5	2.8	7.4	6.8	8.2(1)	1.0	12.8
1000	2100	4.5	2.7	6.5	5.3	6.2	9.3(5)	12.5

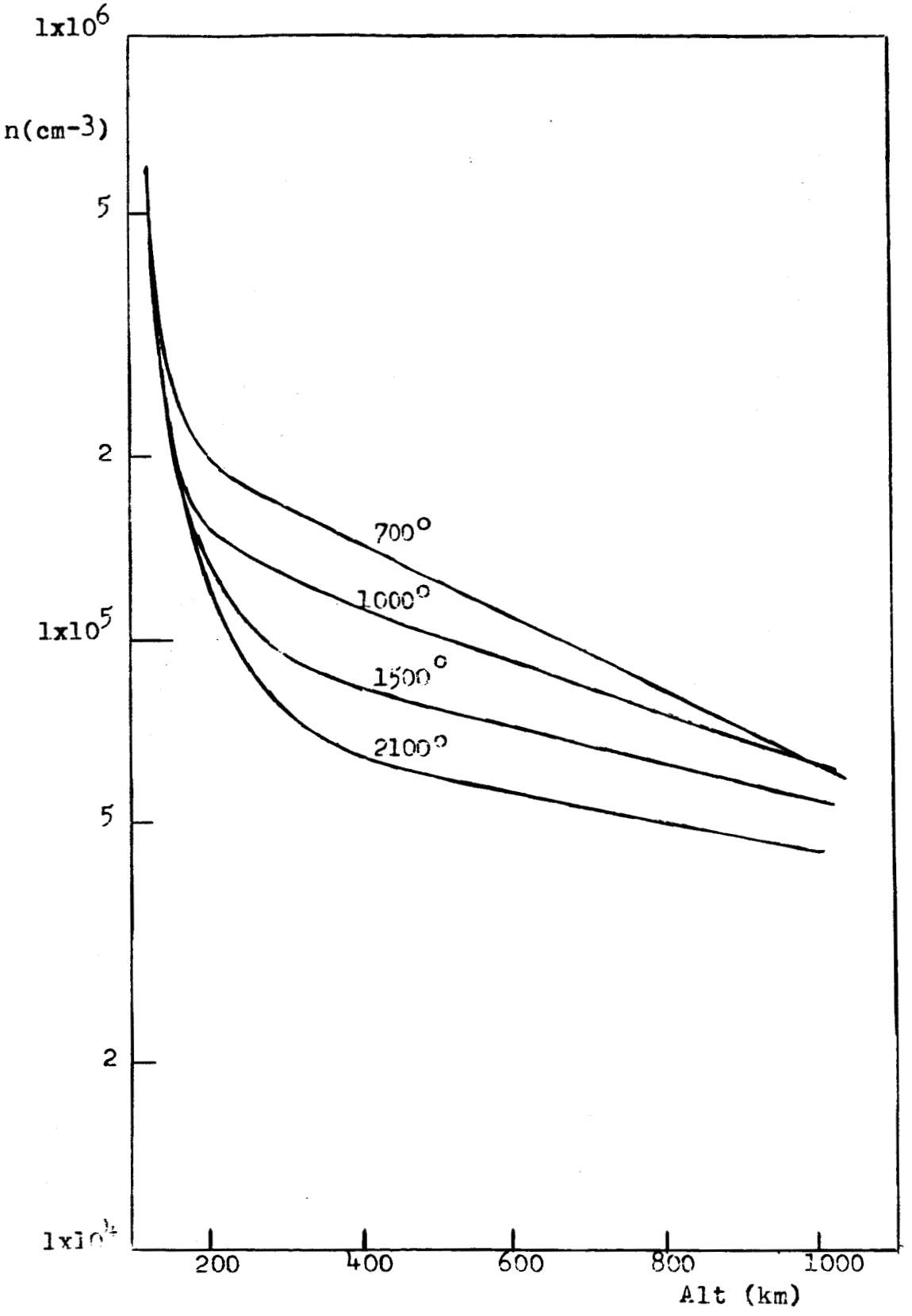

Figure 3. Hydrogen densities for diffusive equilibrium and temperature Model A.

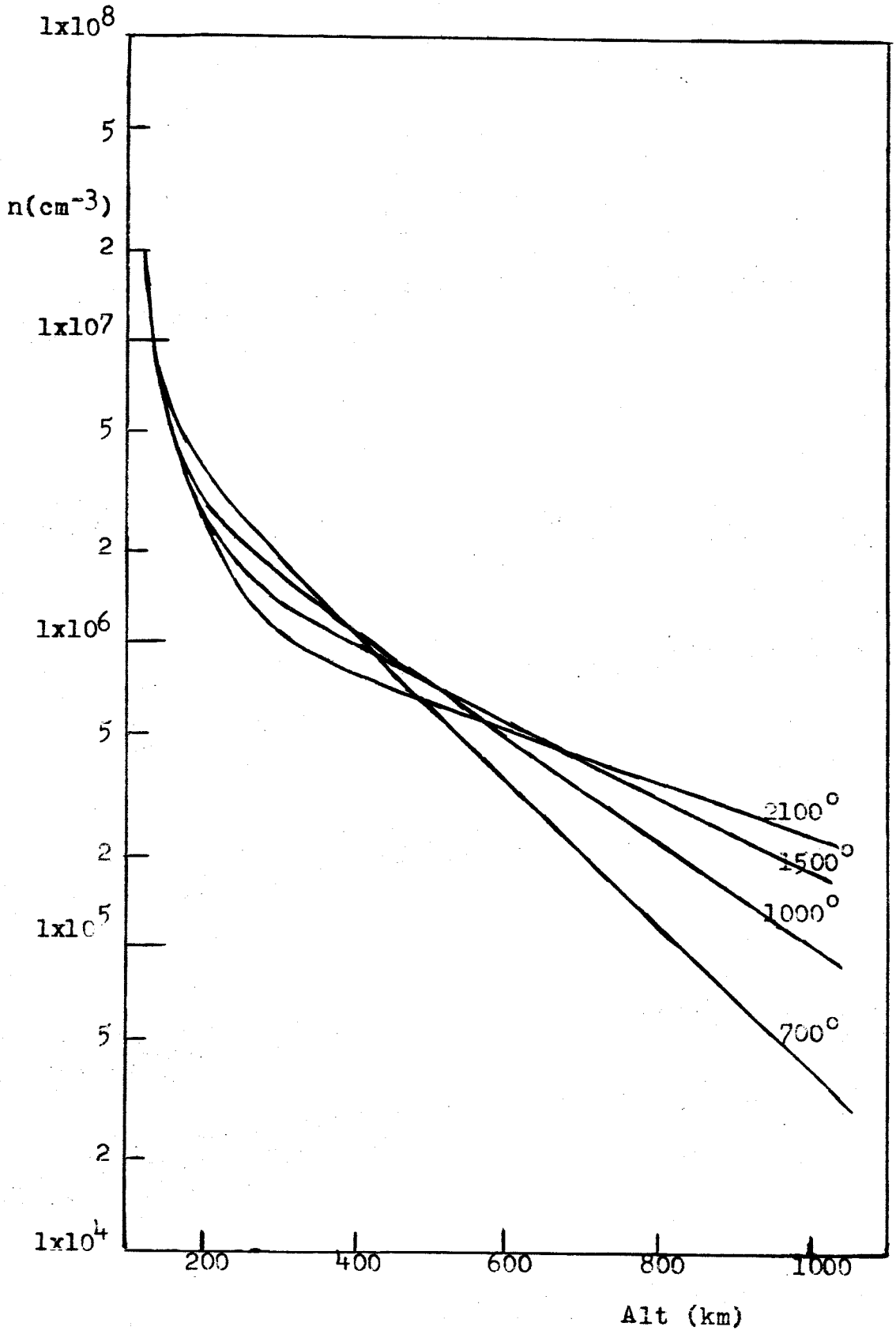

Figure 4. Helium densities for diffusive equilibrium and temperature Model A.

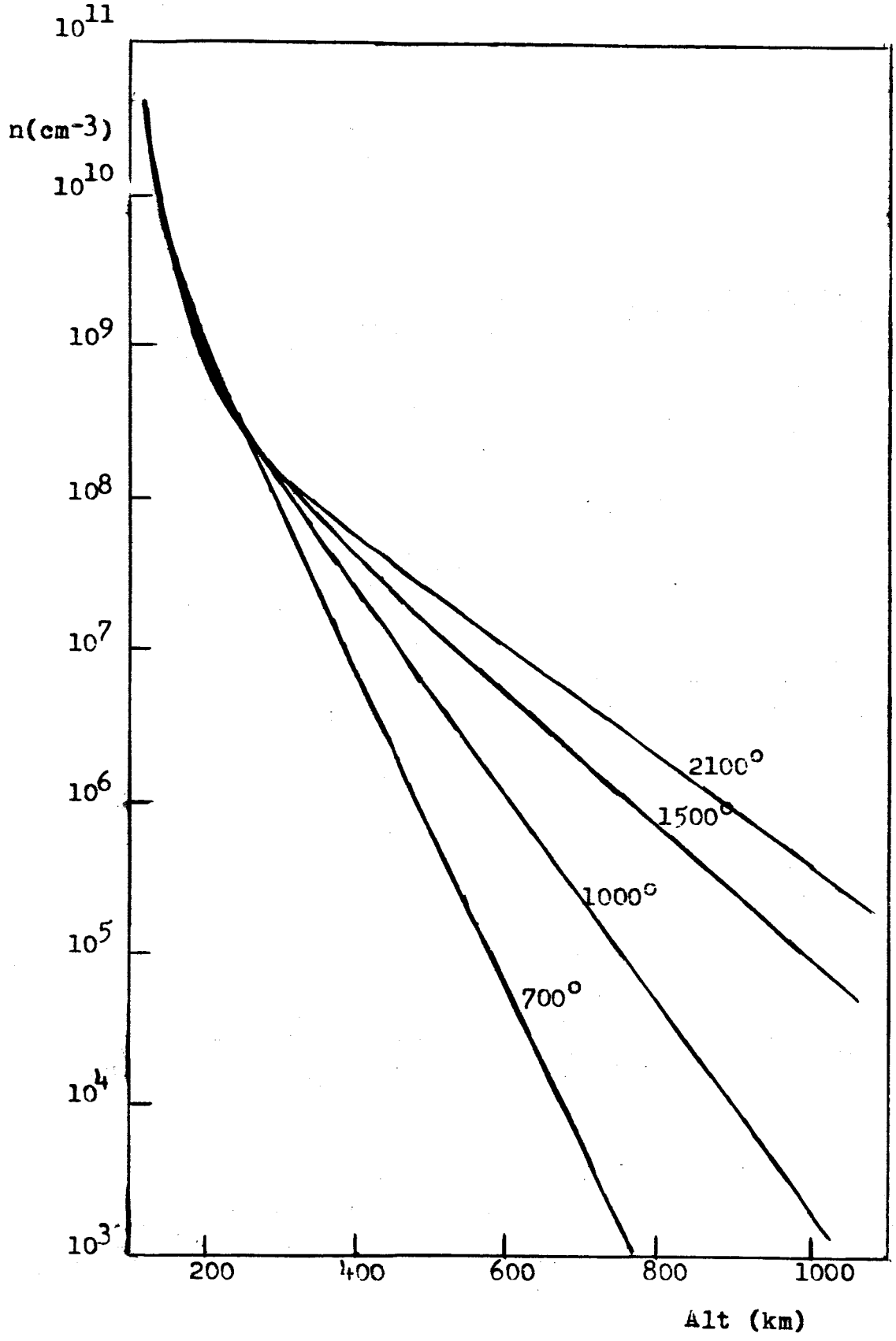

Figure 5. Atomic oxygen densities for diffusive equilibrium and temperature Model A.

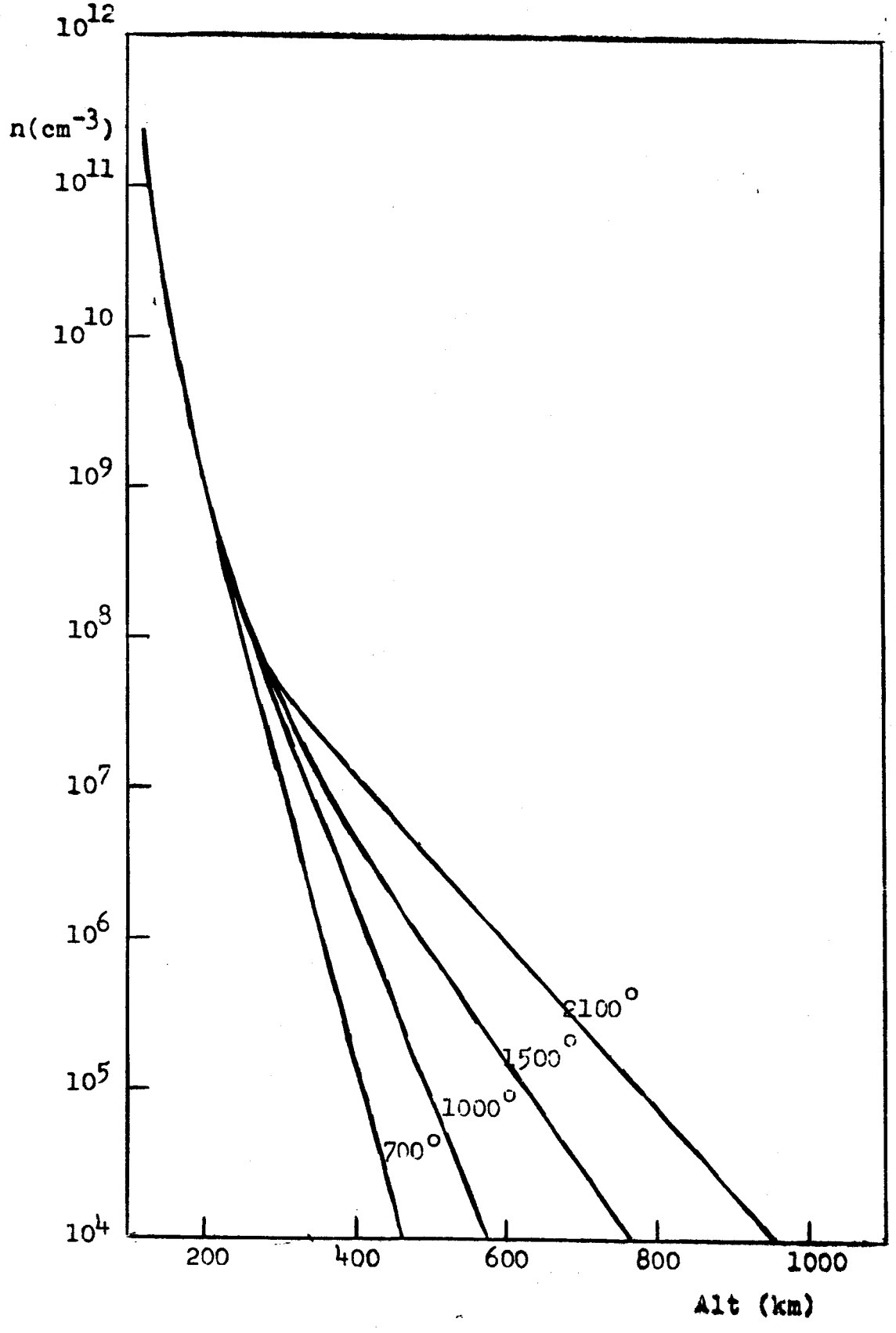

Figure 6. Molecular nitrogen densities for diffusive equilibrium and temperature Model A.

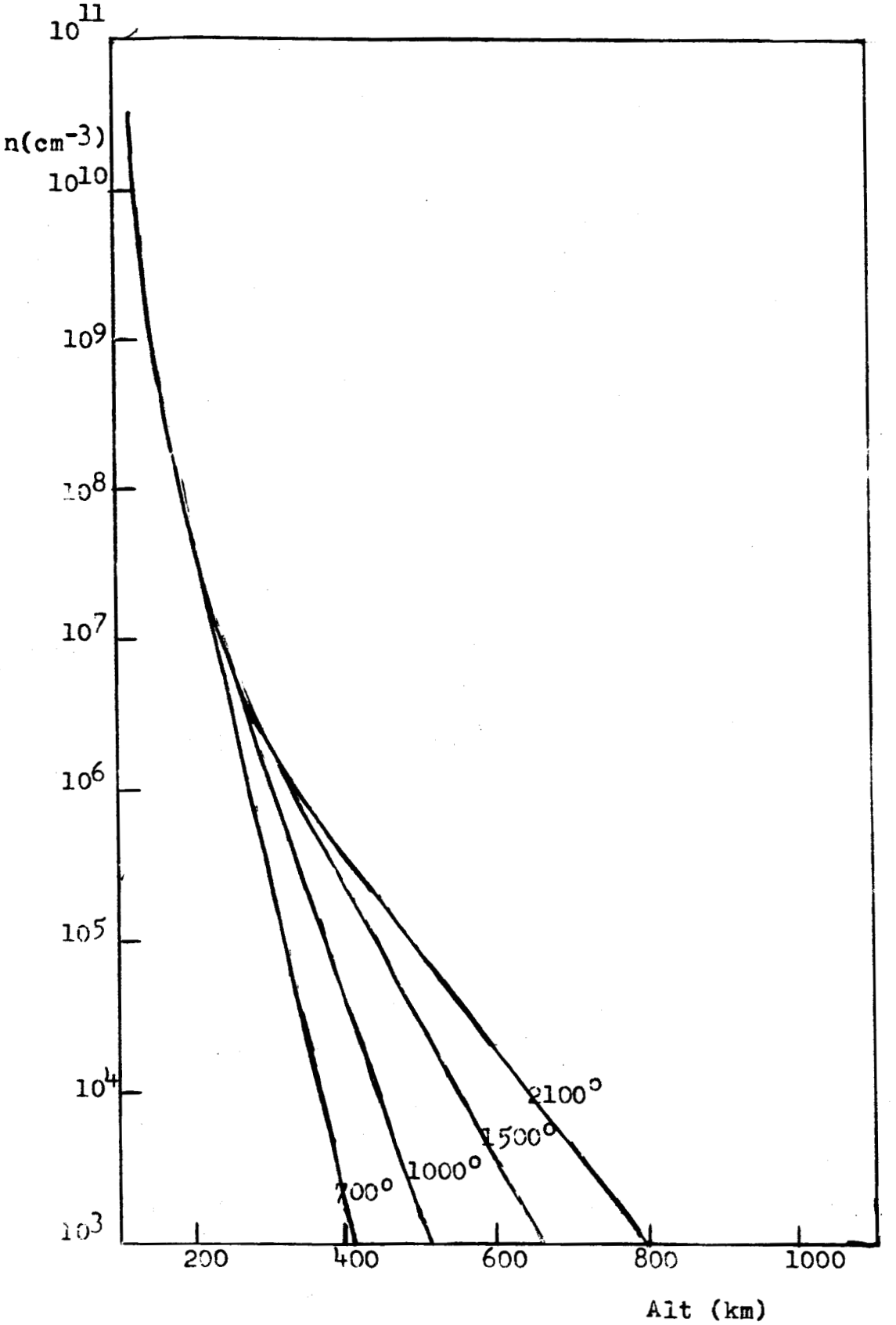

Figure 7. Molecular oxygen densities for diffusive equilibrium and temperature Model A.

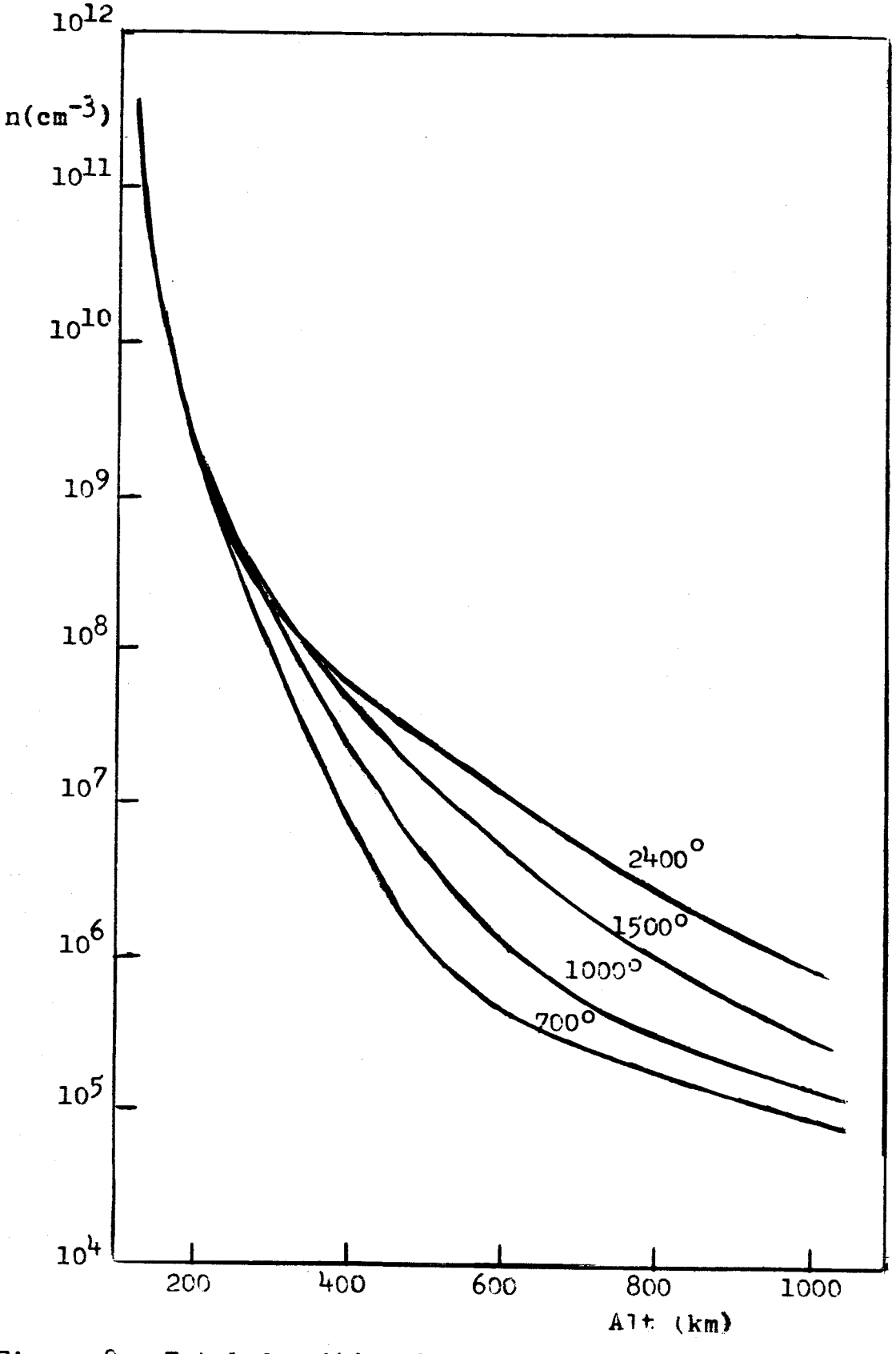

Figure 8. Total densities for diffusive equilibrium and temperature Model A.

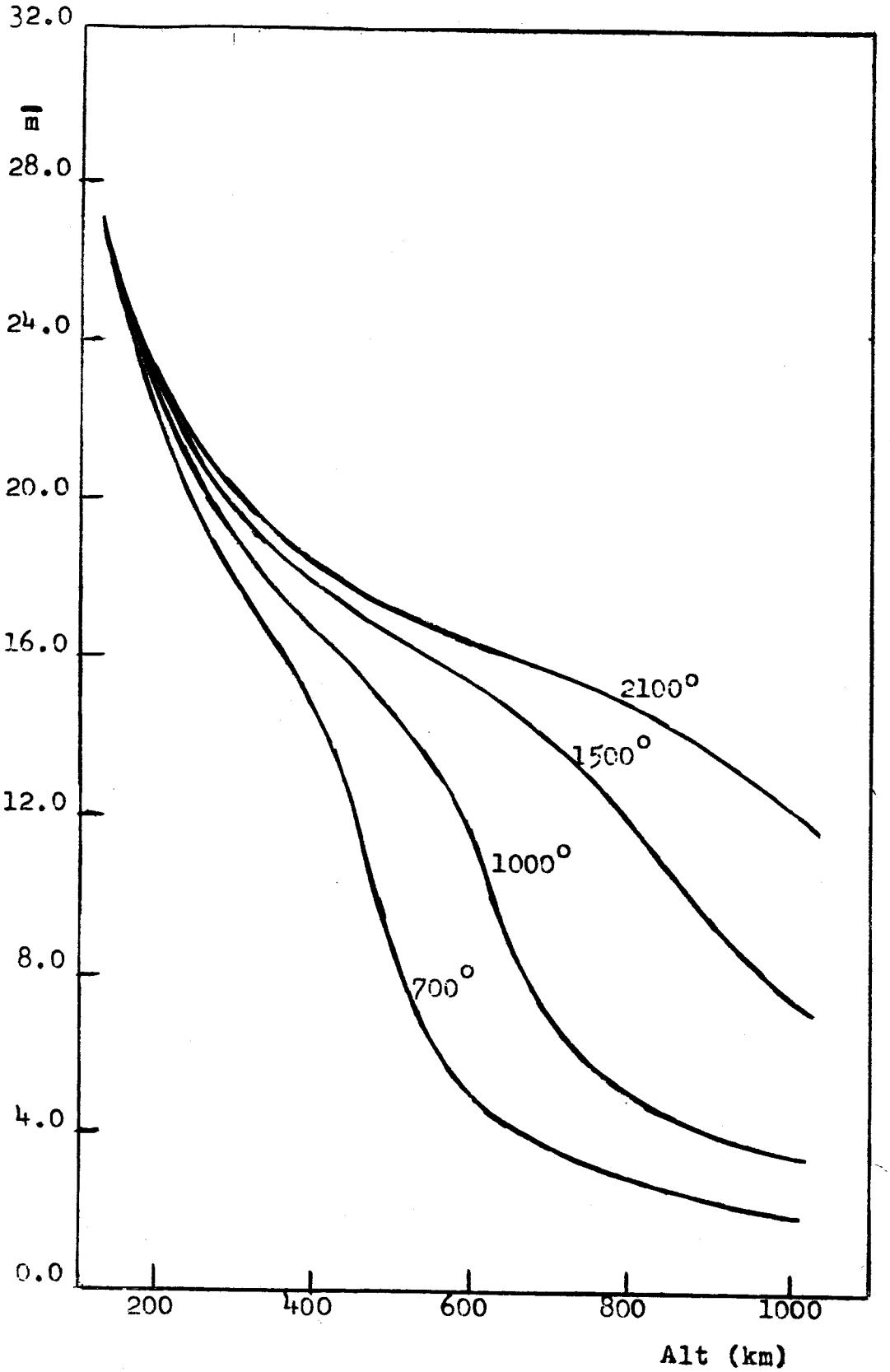

Figure 9. Mean molecular mass for diffusive equilibrium and temperature Model A.

due to using Model B rather than A are not particularly significant as may be seen by the comparison of the two models for the 2100° case (it resulted in the largest difference) in figure 10. Hence for further calculation, Model A has been used.

2.3. Exosphere

The diffusion that determines density distributions in the endosphere is based upon a high frequency of collisions between the various atoms and molecules. At higher altitudes where the density becomes relatively small this is no longer the case. In this region, the exosphere, collisions may be neglected.

For purposes of calculation it is convenient not to separate the endosphere and exosphere by a finite transition region where collisions are few. It is more practical to simply define a single level of transition, the exobase, below which diffusion predominates and there is a Maxwell-Boltzmann, directionally isotropic velocity distribution, and above which no collisions whatsoever take place.

2.31. Exobase

The determination of the exobase altitude is somewhat arbitrary and has been calculated in several different ways. An extremely simple definition is to consider the probability of a collision by a typical particle leaving the level of altitude z and proceeding directly upward to an infinite distance, which is

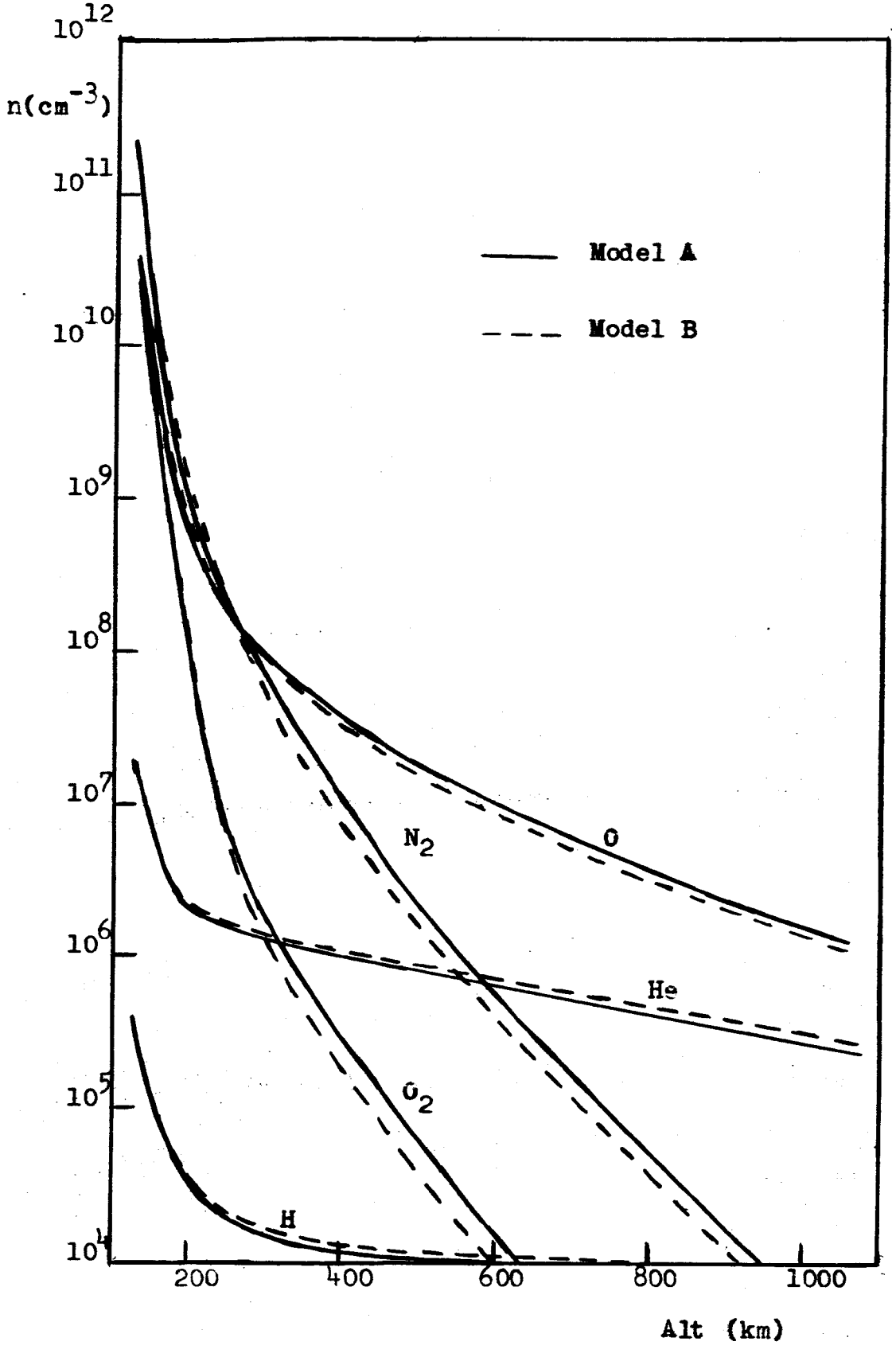

Figure 10. Comparison of diffusive equilibrium densities for temperature Models A and B.

$$P = \sigma \int_{z}^{\infty} n(z')dz' \qquad (2)$$

where σ is the collisional cross-section and n(z') is the total density. The exobase is then defined by the altitude, b, where $P = 1/2$. Since this definition is arbitrary it is important that any effects under consideration will not be highly dependent upon this or any other choice. The exobases as calculated in this manner with $\sigma = 5 \times 10^{-15}$ cm^2 are shown in Table 6.

Table 6. Exobases.

Exospheric temperature (^{o}K)	700	1000	1500	2100
Exobase altitude (km)	360	440	555	680

2.32. Planetary Escape

One obvious effect of the lack of exospheric collisions is the possibility of planetary escape. Some of the particles at the exobase in a Maxwell-Boltzmann distribution will have velocities in excess of the escape velocity. If these suffer no collisions as they proceed outward, they will escape.

The number of particles of constituent i leaving the exobase per unit time per unit area at the angle α from the vertical in the solid angle $d\omega$ with velocity between v and $v + dv$ will be

$$df_i^{esc} = n_i(b) 4\pi \left[\frac{m_i}{2\pi kT}\right]^{3/2} v^2 \exp\left[-\frac{m_i v^2}{2kT}\right] dv \frac{d\omega}{4\pi} v\cos\alpha$$

or

$$dF_i^{esc} = n_i(b)\left(\frac{m_i}{2\pi kT}\right)^{3/2} v^3 \exp\left[-\frac{m_i v^2}{2kT}\right] dv\,d\beta\,d\alpha \sin\alpha \cos\alpha \qquad (3)$$

where

$$d\omega = d\beta\, d\alpha \sin\alpha .$$

The total escape flux will be the integration of equation (3) between the proper limits, namely

$$V_{esc} < v < \infty,$$

$$0 < \beta < 2\pi,$$

$$0 < \alpha < \pi/2,$$

where

$V_{esc} \equiv 2g(b)R_b$ = escape velocity at altitude b,

R_b = geocentric radius appropriate to altitude b.

Integration of equation (3) between these limits yields

$$F_i^{esc} = \frac{n_i(b)}{2}\sqrt{\frac{2g(b)H_i(b)}{\pi}}\left[1 + \frac{R_b}{H_i(b)}\right]\exp\left[-\frac{R_b}{H_i(b)}\right] \qquad (4)$$

where the scale height, $H_i(b)$, is defined as

$$H_i(b) \equiv \frac{kT(b)}{m_i g(b)} . \qquad (5)$$

The effusion velocity, W_i^{esc}, may be defined by

$$W_i^{esc} \equiv \frac{F_i^{esc}}{n_i} = \frac{1}{2}\sqrt{\frac{2g(b)H_i(b)}{\pi}}\left[1+\frac{R_b}{H_i(b)}\right]\exp\left[-\frac{R_b}{H_i(b)}\right]. \qquad (6)$$

The variation of escape flux with the choice of exobase may be seen by considering the escape flux at some level $b+\Delta z = z$, which is

$$F_i^{esc}(z) = \frac{n_i(z)}{2}\sqrt{\frac{2g(z)\,H_i(z)}{\pi}}\left[1+\frac{R_z}{H_i(z)}\right]\exp\left[\frac{-R_z}{H_i(z)}\right]. \qquad (7)$$

Since the region around the exobase is an isothermal one the scale height is dependent only upon the gravitational acceleration:

$$H_i(z) = H_i(b)\left(\frac{R_z}{R_b}\right)^2$$

and the density, assuming diffusive equilibrium, may be written

$$n_i(z) = n_i(b)\exp\left[-\frac{R_b}{H_i(b)}\cdot\frac{\Delta z}{R_z}\right].$$

Substitution of these into equation (7) yields

$$F_i^{esc}(z) = \frac{n_i(b)}{2}\sqrt{\frac{2g(b)H_i(b)}{\pi}}\left[1+\frac{R_b}{H_i(b)}\cdot\frac{R_b}{R_z}\right]\exp\left[-\frac{R_b}{H_i(b)}\right] \qquad (8)$$

The ratio of the escape fluxes at levels $b+\Delta z$ and b is then

$$\frac{F_i^{esc}(b+\Delta z)}{F_i^{esc}(b)} = \frac{1+\frac{R_b}{H_i(b)}\cdot\frac{R_b}{R_{b+\Delta z}}}{1+\frac{R_b}{H_i(b)}} \tag{9}$$

or for $\Delta z << R_b$

$$\frac{F_i^{esc}(b+\Delta z)}{F_i^{esc}(b)} = 1-\frac{\Delta z}{R_b} \tag{10}$$

which is a very small correction.

2.33. Correction to Endosphere Densities

The presence of an escaping flux at the top of the endosphere is inconsistent with the assumption of diffusive equilibrium in the endosphere. The correct solution to the diffusion equation with escape at the top assuming also a source in the mixing region and a steady state is derived in appendix A and given by equation (50). It is

$$n_i(z) = \overline{n_i(z)}\left\{1-\int_{120}^{z}\frac{S_i(120)}{D_i(z')\overline{n_i(z')}}\left[\frac{R_{120}}{R_{z'}}\right]^2 dz'\right\} \tag{11}$$

where

$$S_i(120) \equiv \frac{\overline{n_i(b)}w_i^{esc}\left[\frac{R_b}{R_{120}}\right]^2}{1+\overline{n_i(b)}w_i^{esc}\left[\frac{R_b}{R_{120}}\right]^2\int_{120}^{b}\frac{1}{D_i(z')\overline{n_i(z')}}\left[\frac{R_{120}}{R_{z'}}\right]^2 dz'} \tag{12}$$

is the flux at 120 km. In order to consider the correction to the diffusive equilibrium solution, this flux can be compared with the maximum flux supported by diffusion as defined in appendix A. The diffusion coefficients are estimates based upon experimental values for various gas combinations found in Nawrocki and Papa[28]. The equivalent cross sections vary around 5×10^{-15} cm^2. Table 7 shows the escape fluxes for the important constituents (calculated for diffusive equilibrium densities) as well as these maximum fluxes.

Table 7. Escape and Maximum Diffusive Fluxes.

Exos. Temp.		H	He	O	N_2	O_2
700	Fesc	5.9×10^{6}	4.3×10^{-6}	--	--	--
	Fmax	8.9×10^{7}	5.4×10^{8}	1.3×10^{11}	2.5×10^{10}	3.5×10^{8}
1000	Fesc	7.5×10^{7}	5.7×10^{-1}	1.4×10^{-23}	--	--
	Fmax	8.9×10^{7}	5.3×10^{8}	1.2×10^{11}	2.1×10^{10}	3.0×10^{8}
1500	Fesc	1.1×10^{9}	4.6×10^{3}	1.2×10^{-20}	--	--
	Fmax	8.8×10^{7}	5.3×10^{8}	1.1×10^{11}	1.8×10^{10}	2.5×10^{8}
2100	Fesc	1.2×10^{10}	6.6×10^{5}	2.3×10^{-11}	--	--
	Fmax	8.8×10^{7}	5.3×10^{8}	1.0×10^{11}	1.5×10^{10}	2.0×10^{8}

For hydrogen in particular, the escape fluxes of table 7 are incorrect since its density at the exobase will be modified by the escape flux itself. The correct endospheric solutions for hydrogen are shown in figure 11 along with the diffusive equilibrium solutions for comparison. The corresponding escape fluxes are given in table 8. It should be noted that the modification of the diffusive equilibrium solution takes place entirely in the lower

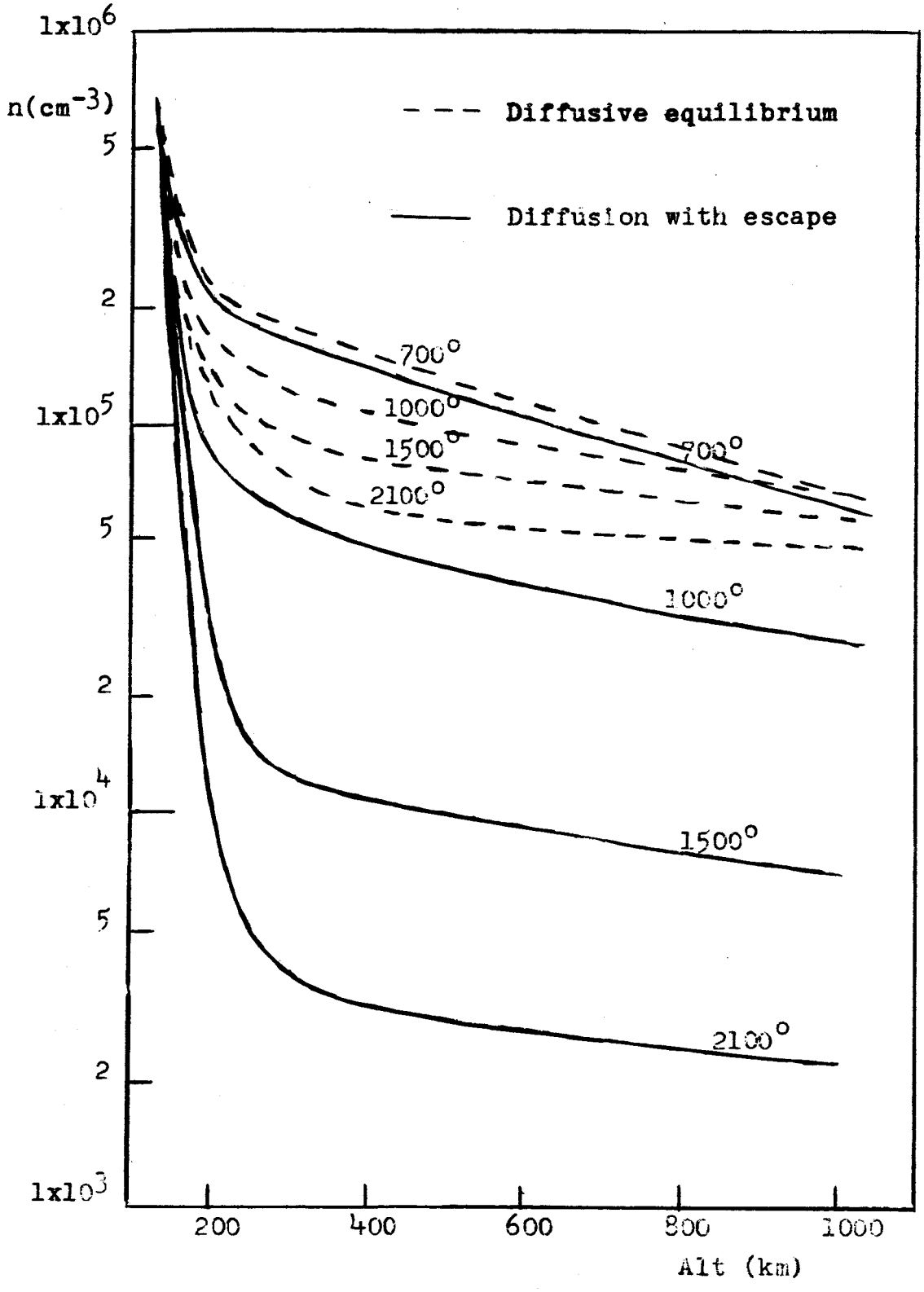

Figure 11. Hydrogen densities for diffusion with escape and temperature Model A.

endosphere and that the hydrogen densities will follow a diffusive equilibrium profile in the upper endosphere.

Table 8. Escape fluxes, corrected.

Exos. Temp.	Fesc(H)	Fmax(H)
700	5.5×10^{6}	8.9×10^{7}
1000	3.7×10^{7}	8.9×10^{7}
1500	5.9×10^{7}	8.8×10^{7}
2100	6.2×10^{7}	8.8×10^{7}

2.34. Exospheric Densities

Densities in the exosphere itself have been calculated in several ways (see Öpik and Singer[29], Herring and Kyle[30], Shen[31], Chamberlain[32], Johnson[33]) by considering the contribution to density at a point above the exobase by particles originating at various points on a spherically symmetric (constant temperature and density) exobase. These densities differ from the diffusive equilibrium densities because they lack certain portions of the isotropic Maxwell-Boltzmann distribution. The first are those particles with velocity greater than escape velocity returning to the earth. The second of these is the so-called bound-orbiting component, which is simply those particles which would have orbits lying entirely in the exosphere such that they never cross the exobase. Since some collisions do occur, it is possible that some of this latter component may indeed be present. However, since these particles spend more than half their time in the presence of the ionizing solar flux, it is felt that they are eventually ionized and removed from consideration.

The lack of a returning escape component creates a discontinuity at the exobase since above it, half the escape region in the Maxwell-Boltzmann distribution is missing, and below it, all regions are full. The real distribution at the exobase due to the absence of returning escape particles has been investigated by Chamberlain[32]. His estimation of the correction is that it does not exceed 20%. For the purpose of the present this error may be neglected.

A comparison of the diffusive equilibrium distributions and the no-collison theory, is given in figures 12 and 13 for hydrogen and helium respectively. The difference is not particularly apparent at small altitudes above the exobase. This is a comforting result since it diminishes the importance of the choice of the exobase in this respect. The correction to the exospheric distribution of the heavier atoms and molecules occurs at altitudes where their presence is negligible and hence may be disregarded.

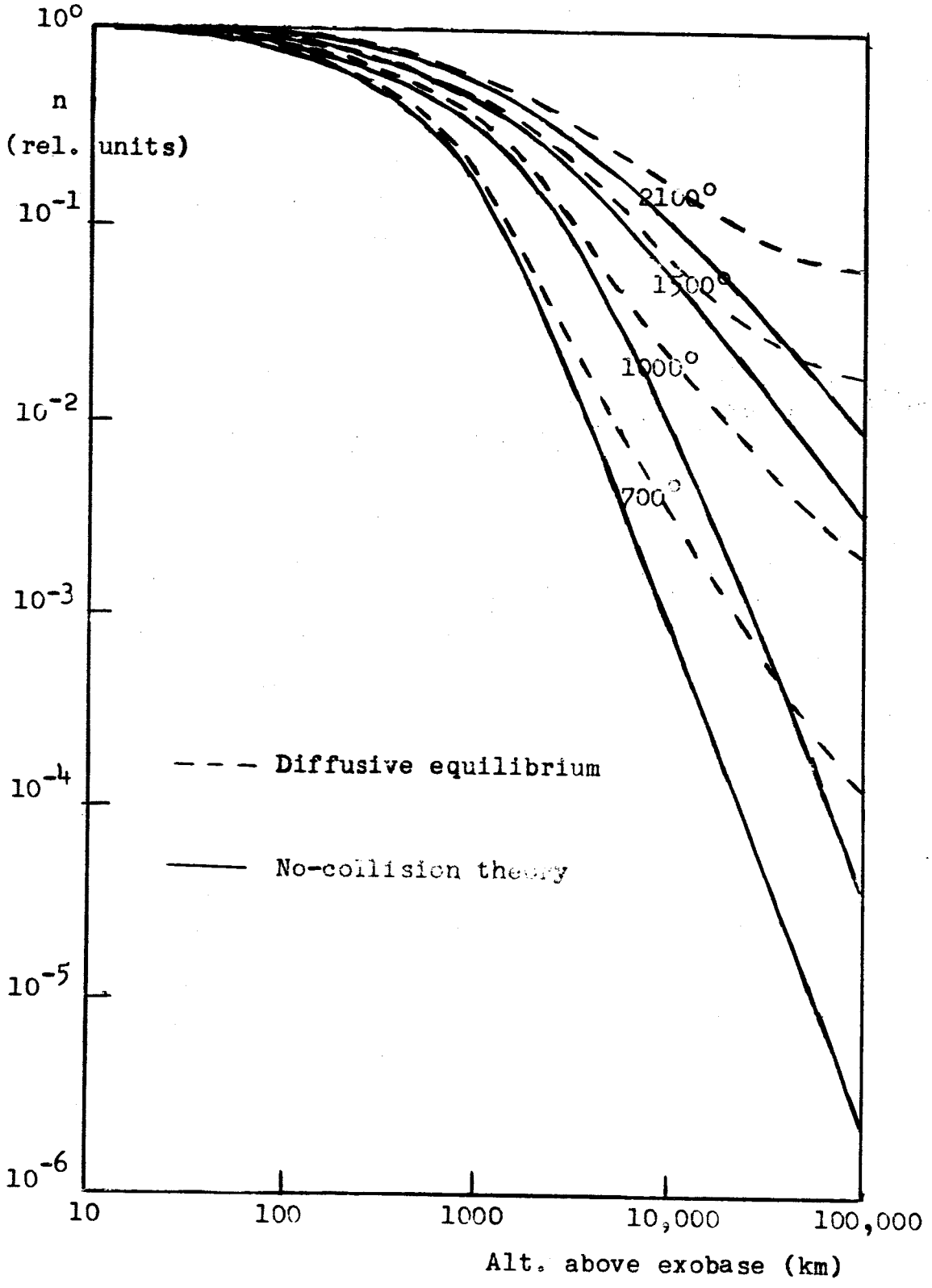

Figure 12. Diffusive equilibrium versus no-collision theory for hydrogen densities.

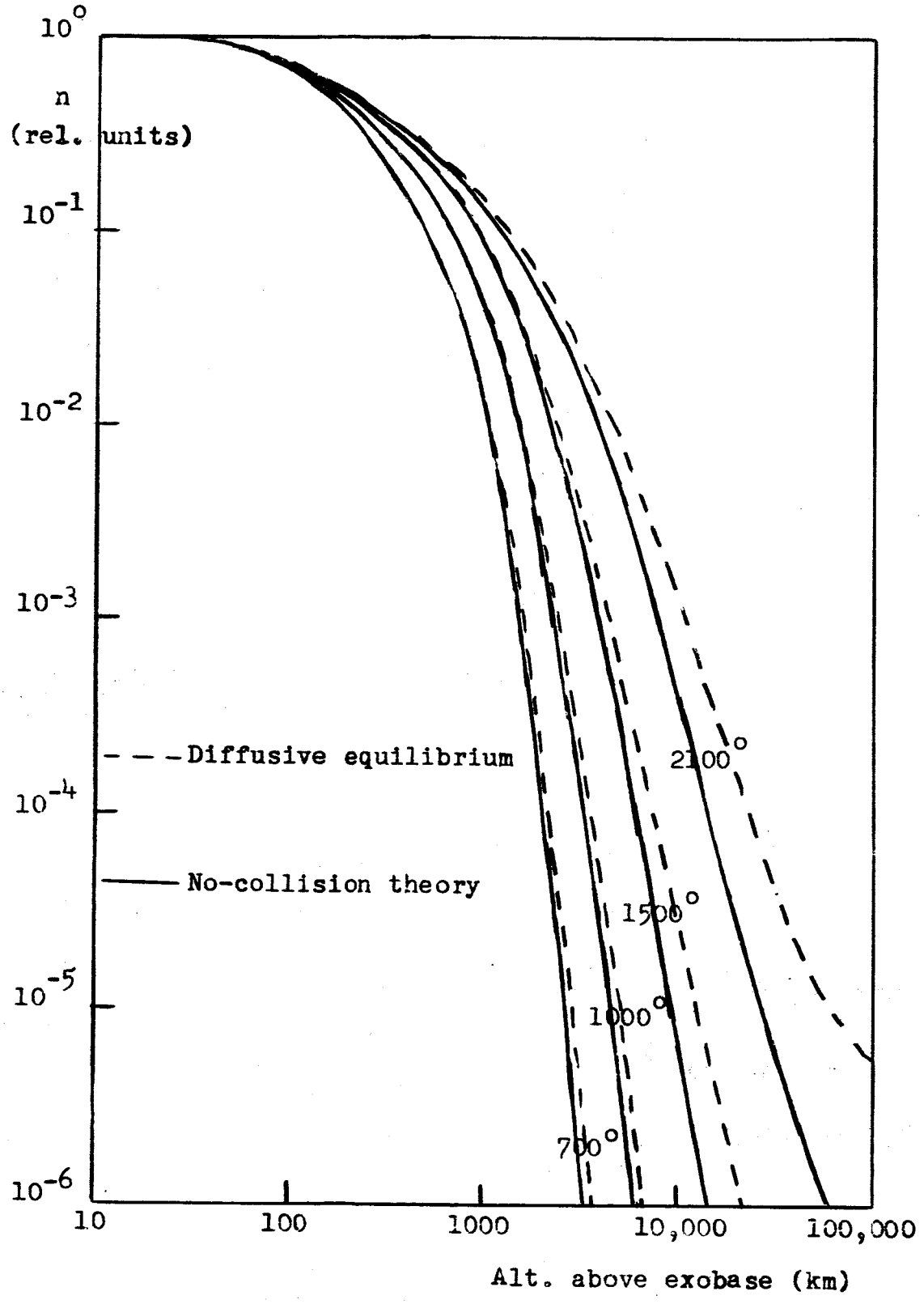

Figure 13. Diffusive equilibrium versus no-collision theory for helium densities.

3.0. LATERAL FLOW

When calculating the escape flux in section 2.32, the flow of particles with velocities greater than the escape velocity was considered. Particles with velocities less than the escape velocity leave the exobase surface at one point, describe ballistic orbits, and re-enter at some other point. If the number density varies on the exobase surface, this process leads to a net flow out of high density regions and into low density regions. Also if the temperature varies on the exobase surface, there will be a net flow out of the high temperature region and into the low temperature region due to the dependence of particle velocities on temperature. The combination of both temperature and density variation over the entire surface will then lead to a net flow into or out of a region because of this lateral motion of individual particles and hence should be called a lateral flow.

3.1. Planar Models

The effect of lateral flow was first investigated for the particular case of hydrogen by Hanson and Patterson[9], who considered the flow through an imaginary semi-infinite strip of unit width with its base at some particular point on the exobase surface, assumed a plane (see Appendix D). The following approximations were made:

1) plane parallel atmosphere
2) parabolic (constant gravitational acceleration) orbits
3) single velocity, Maxwell-Boltzmann rms velocity, $\bar{c}$, for all particles
4) density-temperature variation on the exobase surface determined by

$$n\bar{c}(y) = (n\bar{c})_o + \beta y$$

where y was a lateral coordinate
5) neglect of temperature variations in determining integration limits.

Their conclusion was that the lateral flux dominated the escape flux and would quickly wipe out any night-time bulge due to escape, or more correctly, not allow its establishment.

Further investigation by Donahue and McAfee[10] suggested that this conclusion can not be supported (see Appendix D). The Hanson and Patterson model was modified to the following set of approximations:

1) plane parallel atmosphere
2) parabolic orbits
3) a Maxwell-Boltzmann velocity distribution
4) temperature and density variations

$$n = n_o\left(1 + \delta \sin \frac{y+y_o}{R_b}\right)$$

$$T = T_o\left(1 - \gamma \sin \frac{y+y_o}{R_b}\right)$$

where y_o was the location of the strip on the exobase surface and R_b the exobase radius
5) temperature dependent integration limits.

The resulting fluxes were considerably smaller in magnitude than those of Hanson and Patterson (more comparable to the escape flux) and more favorable to the temperature dependent

part of the flow. This was primarily due to the improvement in using a Maxwell-Boltzmann distribution. A comparative example is shown in figure 14. The flow through the semi-infinite strip has been transformed into a vertical flux into or out of the exobase surface by taking the negative derivative.

3.2. Spherical Models

Although the Donahue-McAfee model was an improvement over the Hanson-Patterson model, several assumptions were still inherent in the derivation. The assumption of the parabolic orbits may underestimate the flows since the physically real elliptical orbits have a longer range. The plane parallel approximation makes the calculations suspect everywhere except near twilight because of the large distortion in the geometry. Hence, it would seem worthwhile to consider the case of the real spherical geometry with the true elliptic orbits.

3.21. First Models

The first spherical model was an extension of the Donahue-McAfee planar model. The change in geometry, however, makes it necessary to discard the semi-infinite strip in favor of a semi-infinite cone described by an angle θ_o. The geometry is shown in figure 15. The model was assumed to be axially symmetric so that any variation in density or temperature would depend only on a colatitude angle. Since particles may pass through a particular cone twice while on the same orbit, it is incorrect just to consider

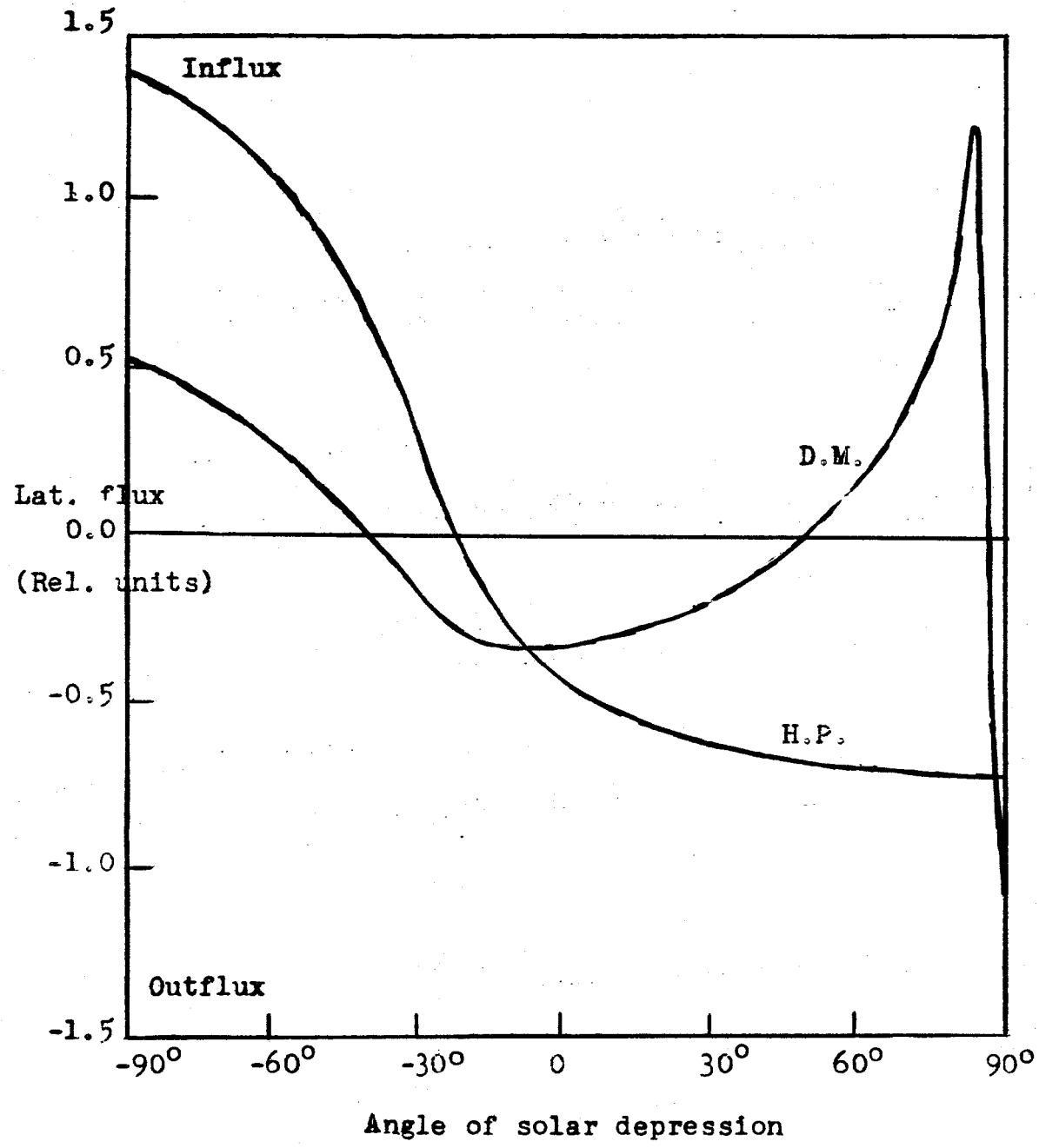

Figure 14. Lateral flux for a sinusoidal 1500-1000°, 2-1, case using the Hanson-Patterson approximations (H.P.) and the Donahue-McAfee approximation(D.M.).

all particles which pass through. Instead, only those which pass through once should be considered.

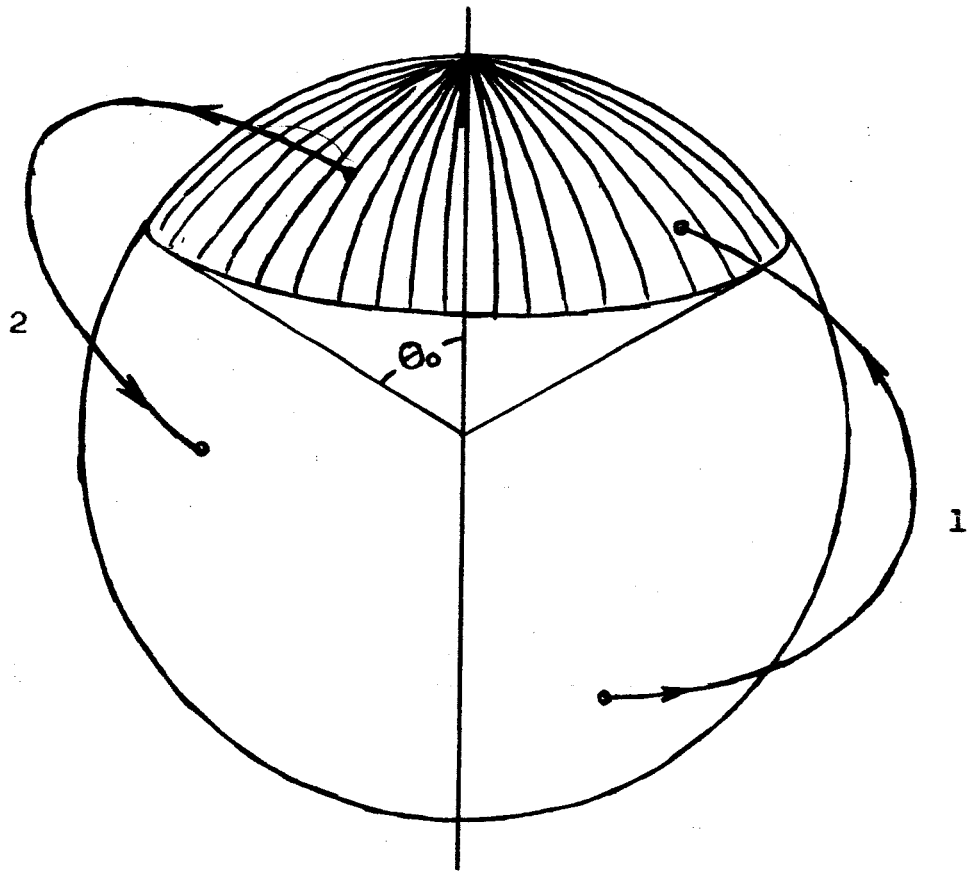

Figure 15. The first spherical model showing particles both leaving and entering each of the areas.

If the net flow, $\mathcal{F}$, into the area governed by $\theta < \theta_o$ (shaded area in figure 15) is the number of particles per unit time leaving the exobase at $\theta > \theta_o$ and entering at $\theta < \theta_o$ (orbit 1 in figure 15) minus those leaving at $\theta < \theta_o$ and entering at $\theta > \theta_o$, (orbit 2 in figure 15), a vertical flux, F, into the endosphere may be calculated by taking the negative derivative of $\mathcal{F}$ with respect to θ_o.

Hence

$$F \equiv - \frac{1}{2\pi R_b^2 \sin\theta_o} \frac{d\mathcal{F}(\theta_o)}{d\theta_o}$$

where R_b is the exobase radius. The problem is then to calculate $\mathcal{F}$.

However, this model has the drawback of excessively long calculations. The calculation of $\mathcal{F}$ must be done for a sufficient number of angles, θ_o, in order to make a graphical calculation of the derivative at all meaningful. For each calculation at a different angle, it is necessary to integrate over the entire surface, and hence there is a good deal of redundancy in the calculations.

An immediate modification which rids the calculation of these redundancies and also eliminates the graphical derivatives consists of dividing the exobase surface into a number of circular strips of width $\Delta\theta$ whose borders are lines of constant reference angles, θ_i, as shown in figure 16. A flux of particles leaving from some point on the surface, θ, will re-enter at another point at an angle, θ', which lies on a particular strip, i, which may be described by

$$\theta_i < \theta' < \theta_{i+1}$$

Then if the integration is carried out over the entire surface once, the total flow into each strip is the sum of the contributions of flow originating from the various parts

of the surface which ended within that strip. Hence, a single integration will simultaneously calculate the flow into each of the strips, $\mathcal{F}$. The vertical flux, F_i, is then simply this divided by the strip area, or

$$F_i = \frac{\mathcal{F}_i}{2\pi R_b^2 \sin\theta_j} \quad . \tag{13}$$

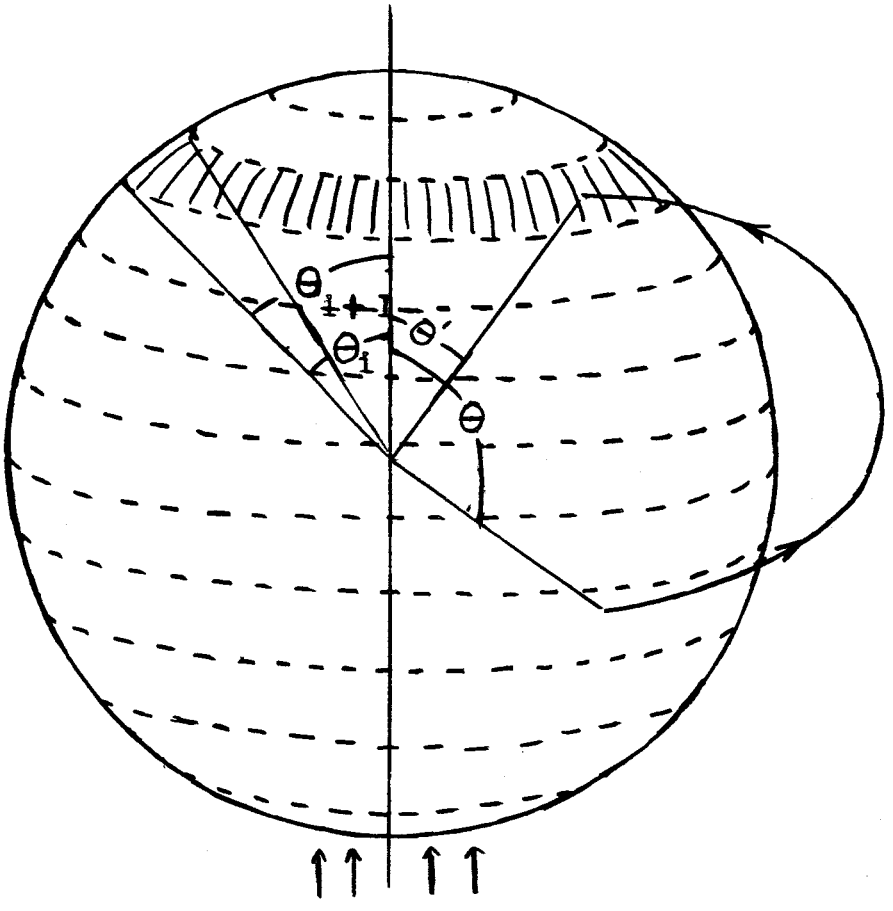

Figure 16. Geometry for spherical model with particle orginating at θ and ending at θ' between θ_i and θ_{i+1}.

The pertinent parameters used in calculating the $\mathcal{F}_i$ are shown in figure 17. The number of particles leaving the surface element

$$dA = R_b^2 \sin\Theta \, d\Theta \, d\phi$$

located at (R_b, Θ, ϕ) with velocity between v and v+dv in the solid angle

$$d\omega = \sin\alpha \, d\alpha \, d\beta$$

per unit time will be

$$d\mathcal{F} = \frac{d\omega}{4\pi} dA \cos\alpha v n(\Theta,\phi) 4\pi \left[\frac{m}{2\pi kT(\Theta,\phi)}\right]^{3/2} v^2 dv \exp\left[\frac{-mv^2}{2kT(\Theta,\phi)}\right] . \quad (14)$$

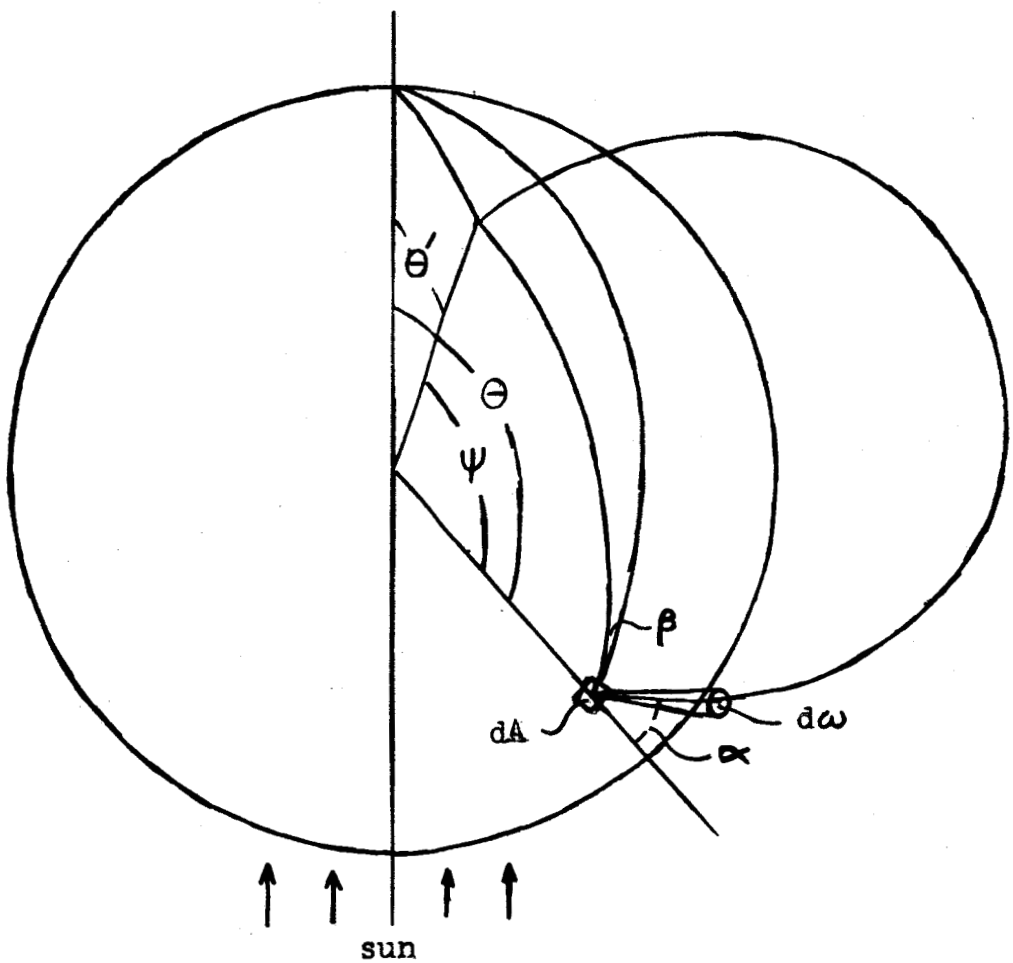

Figure 17. Parameters involved in calculating the lateral flow.

Using azimuthal symmetry,

$$n \neq n(\phi)$$

$$T \neq T(\phi)$$

the limits are also ϕ independent and

$$d\mathcal{F} = 2\pi R_b^2 \left[\frac{m}{2\pi kT(\theta)}\right]^{3/2} dv v^3 d\theta \sin\theta \exp\left[\frac{-mv^2}{2kT(\theta)}\right] d\alpha \sin\alpha \cos\alpha d\beta . \quad (15)$$

If ψ is defined as the angle traversed by these particles between leaving and entering the endosphere, then the angle, θ', where they enter is related to the other parameters by the spherical trigonometric relationship

$$\cos\theta' = \cos\theta\cos\psi + \sin\theta\sin\psi\cos\beta . \quad (16)$$

The expression for ψ is derived in appendix B and is

$$\cos\psi = \frac{[A+\cos\gamma]^2 - \sin^2\gamma}{[A+\cos\gamma]^2 + \sin^2\gamma} \quad (17)$$

where

$$A \equiv \frac{1}{x^2} - 1,$$

$$x \equiv \frac{v}{v_{esc}},$$

$$\gamma \equiv 2\alpha .$$

When the integration of equation (15) is carried out numerically, the element of flux is subtracted from the flow

pertinent to the strip containing θ and added to that containing θ'. The appropriate limits on the integration when summed in this manner are

$$0 < \beta < 2\pi,$$

$$0 < \alpha < \pi/2,$$

$$0 < \theta < \pi,$$

$$0 < v < v_{esc}.$$

This calculation was made on an IBM 7090 computer. An example for hydrogen with a sinusoidal temperature distribution between 1000° at $\theta \simeq 0$ and 1500° at $\theta = \pi$ and a sinusoidal number density distribution of 3-1 with maximum at $\theta = 0$ is shown in figure 18. The points represent the flux, F, of equation (13).

The scatter in the computed points is due to the approximations in the numerical integration. It is more severe near the end points due to the fact that the strips are heavily distorted in these areas. Although for a given set of integration variables in equation (15) this entire flux is assumed to re-enter at a single point, the flow is actually scattered and may enter in part in more than one strip. It would be hoped that errors of this nature would cancel each other. However, this does not occur because the shapes of adjacent strips are not identical.

One solution to this problem is of course to make the integration more accurate by reducing the size of the

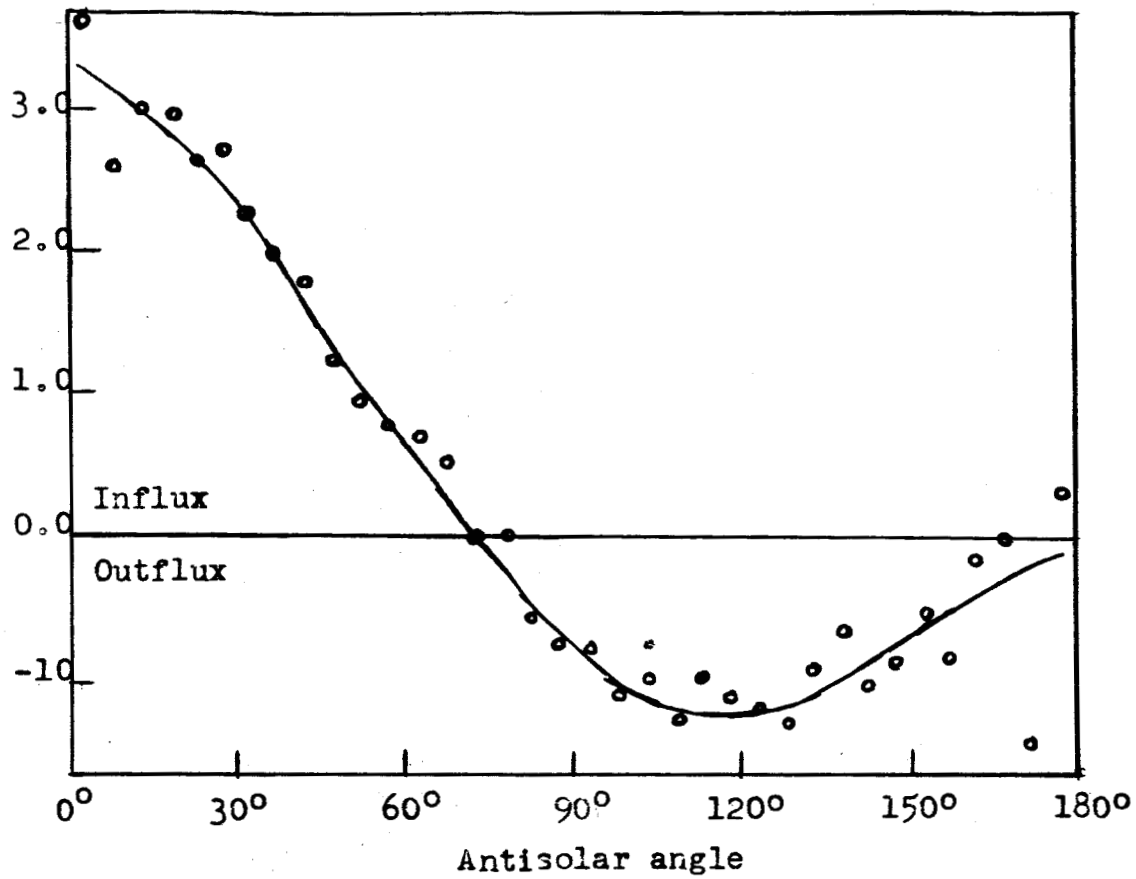

Figure 18. Lateral flux, F, for 1000-1500°, 3-1 hydrogen case. The flux scale is relative.

various integration differentials. However, the computation such as that for the example in figure 18 is already quite lengthy because it is an integration over four variables. Any attempt at an increase in accuracy must be accompanied by a corresponding increase in computing time. This proved to be prohibitive and the method had to be abandoned.

3.22. Final Model

A finally successful approach is to take into account directly the effect of the spreading of a flux element by the time it has re-entered the exobase surface.

Upon leaving the exobase from point 1 the differential flux will be again as in equation (13)

$$d\mathcal{F} = \frac{d\omega}{4\pi} dA \cos\alpha v n 4\pi \left[\frac{m}{2\pi kT}\right]^{3/2} dv v^2 \exp\left[-\frac{mv^2}{2kT}\right]. \qquad (18)$$

If this flow re-enters at point 2, an angle ψ away from its origin, the flux will have spread as shown in figure 19 to an area dA'. The flux into point 2 due to those particles obeying the conditions on $d\mathcal{F}$ will then be

$$dF = \frac{d\mathcal{F}}{dA'}.$$

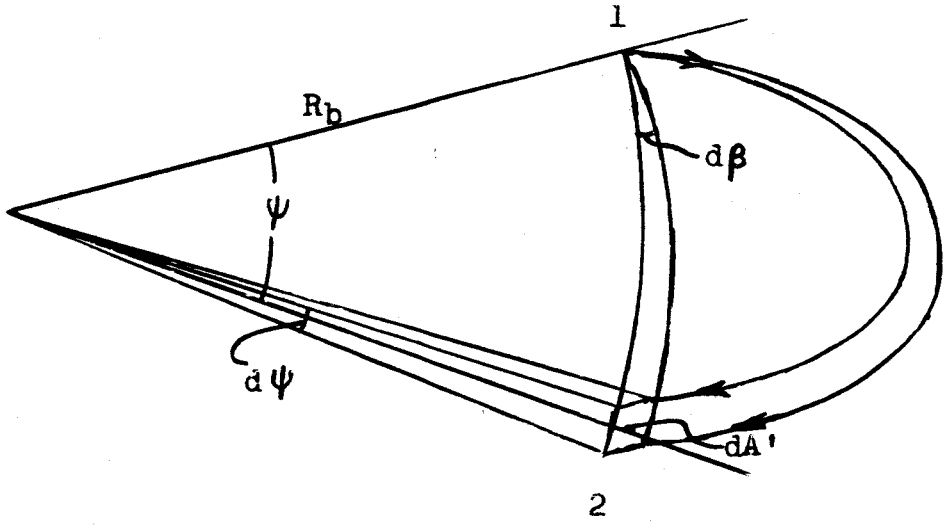

Figure 19. The spread of the differential flux.

If dA' is small it may be written

$$dA' = R_b^2 \sin\psi \, d\psi \, d\beta$$

and equation (18) becomes

$$dF = \frac{d\mathcal{F}}{R_b^2 \sin\psi\, d\psi\, d\beta} \tag{19}$$

The total flux into point 2 is then the sum of these fluxes over other velocities, angles, and positions.

If point 1 is given the coordinates, θ, ϕ, and point 2 the coordinates, θ_o, ϕ_o, in a system the same as in section 2.31, a second spherical coordinate system may be established at point 2 having variables θ' and ϕ' as shown in figure 20. This coordinate system will be related to the original by

$$\cos\theta = \cos\theta_o \cos\theta' + \sin\theta_o \sin\theta' \cos\phi'. \tag{20}$$

By considering an integration in the primed system, the differential flow from the point θ', ϕ' may be written

$$d\mathcal{F} = R_b^2 \left[\frac{m}{2\pi k}\right]^{3/2} dv v^3 d\theta' \sin\theta' d\phi' \frac{n(\theta',\phi')}{[T(\theta',\phi')]^{3/2}} \exp\left[\frac{-mv^2}{2kT(\theta',\phi')}\right] d\alpha \sin\alpha \cos\alpha\, d\beta$$

and equation (19) becomes with $\theta' \equiv \psi$ in this case

$$dF = \left[\frac{m}{2\pi k}\right]^{3/2} dv v^3 \frac{d\theta' d\phi' n(\theta',\phi')}{[T(\theta',\phi')]^{3/2}} \exp\left[\frac{-mv^2}{2kT(\theta',\phi')}\right] \pm \frac{(-d\cos\gamma)}{d\psi} \tag{21}$$

where again

$$\gamma \equiv 2\alpha.$$

The dependence upon β disappears. If $d\psi$ is assumed to be caused by the variation in γ while v, θ', and ϕ' are fixed as they would be if the γ integration were done first,

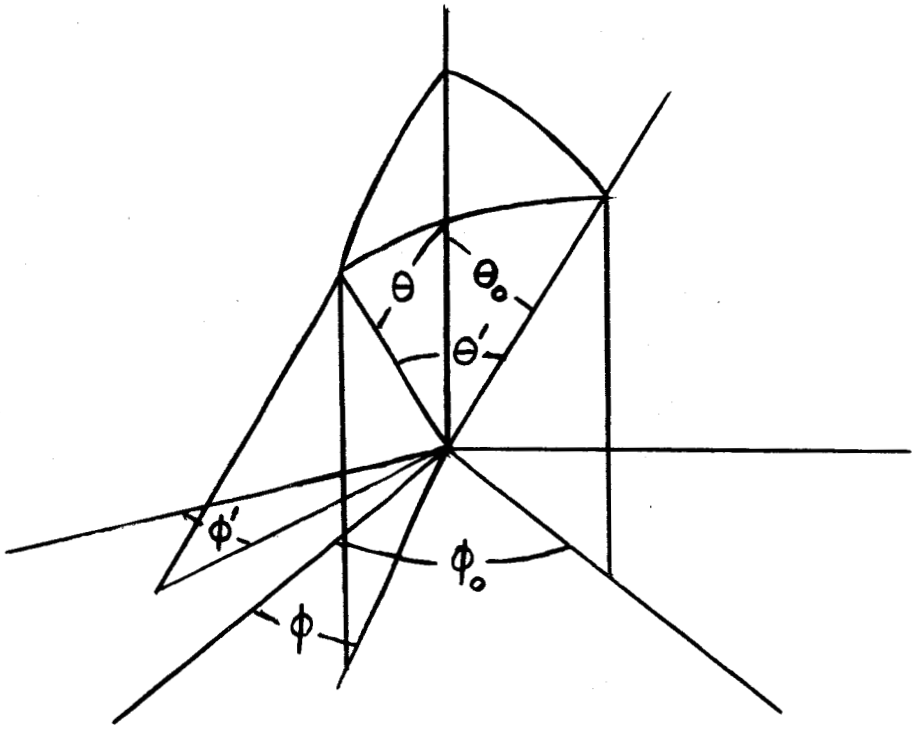

Figure 20. The second spherical coordinate system.

then

$$\frac{(-d\cos\gamma)}{d\psi} \Rightarrow \frac{-\partial\cos\gamma}{\partial\psi} .$$

The relationship between γ and ψ is derived in appendix B and is

$$\cos\gamma = \frac{-A(1-\cos\psi) \pm \sqrt{1+\cos\psi}\,\sqrt{2-(1-\cos\psi)A^2}}{2} . \qquad (22)$$

Differentiation of equation (22) with respect to ψ yields

$$\frac{-\partial\cos\gamma}{\partial\psi} = \frac{\sin\psi\left[1+A^2\cos\psi \mp A\sqrt{1+\cos\psi}\sqrt{2-A^2(1-\cos\psi)}\right]}{2\sqrt{1+\cos\psi}\,\sqrt{2-A^2(1-\cos\psi)}} . \qquad (23)$$

The derivative is double-valued because there are two values of α which give the same range. When the contributions from each of these two is added, the second terms in equation (23) cancel leaving

$$\frac{-\partial \cos\gamma}{\partial\psi} = \frac{\sin\psi\left[1+A^2\cos\psi\right]}{\sqrt{1+\cos\psi}\sqrt{2-A^2(1-\cos\psi)}}. \qquad (24)$$

and with $\psi = \theta'$ the flux, equation (21), becomes

$$dF = \tfrac{1}{4}\left[\frac{m}{2\pi k}\right]^{3/2} \frac{dv v^3 d\theta' \sin\theta'\left[1+A^2\cos\theta'\right]d\phi' n(\theta',\phi')}{\sqrt{1+\cos\theta'}\sqrt{2-A^2(1-\cos\theta')}} \exp\left[\frac{-mv^2}{2kT(\theta',\phi')}\right] \qquad (25)$$

The limits of integration for v and ϕ' are

$$0 < v < v_{esc}$$

$$0 < \phi' < 2\pi$$

respectively. The limits for θ' are more complex. For $v < v_{esc}/\sqrt{2}$ the maximum value for θ' is given by

$$\sqrt{2-A^2(1-\cos\theta)} = 0$$

and hence

$$1 > \cos\theta' > 1 - \frac{2}{A^2}, \qquad v < \frac{v_{esc}}{\sqrt{2}}.$$

For $v > v_{esc}/\sqrt{2}$ the θ' integration may cover the entire sphere and

$$1 > \cos\theta' > -1, \qquad v > v_{esc}/\sqrt{2}.$$

If the substitutions

$$x \equiv \frac{v}{v_{esc}}$$

$$\xi \equiv \cos\theta'$$

are made, then the final form for the flux equation is

$$F_i^{in} = \frac{v_{esc}E^{3/2}}{4}\left\{\int_0^{1/\sqrt{2}} dx x^3 \int_{1-\frac{2}{A^2}}^{1} \frac{d\xi(1+A^2\xi)}{\sqrt{1+\xi}\sqrt{2-A^2(1-\xi)}} \int_0^{2\pi} \frac{d\phi' n(\xi,\phi') \exp\left[\frac{-Ex^2}{T(\xi,\phi')}\right]}{\left[T(\xi,\phi')\right]^{3/2}}\right.$$

$$\left. + \int_{1/\sqrt{2}}^{1} dx x^3 \int_{-1}^{1} \frac{d\xi(1+A^2\xi)}{\sqrt{1+\xi}\sqrt{2-A^2(1-\xi)}} \int_0^{2\pi} \frac{d\phi' n(\xi,\phi') \exp\left[\frac{-Ex^2}{T(\xi,\phi')}\right]}{\left[T(\xi,\phi')\right]^{3/2}}\right\} . \qquad (26)$$

To compute the net flux into or out of the exobase surface, the outgoing flux must be subtracted from the incoming flux of equation (26). The outgoing flux can be calculated directly using equation (14) in the same manner as the escape flux calculation except with the limits on the velocity integration being

$$0 < v < v_{esc}.$$

The solution is then, upon integration,

$$F_i^{out} = \frac{n_i(b)}{2}\sqrt{\frac{2g(b)H_i(b)}{\pi}}\left\{1 - \left[\frac{1+R_b}{H_i(b)}\right]\exp\frac{-R_b}{H_i(b)}\right\} . \qquad (27)$$

This exact solution does turn out to be impractical, however, due to the inexactness of the numerical integration in solving for the incoming flux. Since the net flow is a small difference of two large numbers, even small relative errors between the two terms can lead to grave errors in the difference. This discrepancy can be avoided by integrating the outflow in the same manner as the inflow.

If there were no temperature or density variation the symmetry would demand a zero net flow. Then the outgoing flux in this case is equal to the incoming flux. That this is indeed the case for equation (26) is demonstrated in appendix C. A calculation of the outgoing flux can then be replaced by a calculation of the incoming flux for the symmetric case with a constant density and temperature which is that of the point, θ_o, ϕ_o. The ϕ' integrations in the two terms of equation (26) then become, when computing the net flux:

$$\int d\phi' \Rightarrow \int_0^{2\pi} d\phi' \left\{ \frac{n_i(\xi,\phi') \exp\left[\frac{-Ex^2}{T(\xi,\phi')}\right]}{\left[T(\xi,\phi')\right]^{3/2}} - \frac{n_i(\theta_o,\phi_o) \exp\left[\frac{-Ex^2}{T(\theta_o,\phi_o)}\right]}{\left[T(\theta_o,\phi_o)\right]^{3/2}} \right\} . \quad (28)$$

With this method the errors in calculating each term are similar and the difference would then contain the same approximate error.

The expression for the outgoing flux, equation (27), gives an idea of the problem inherent in the choice of an exobase when concerned with lateral flow. Including the

escape flux term the outgoing flux may be written

$$F_i^{out} = \frac{n_i(b)}{2}\sqrt{\frac{2g(b)H_i(b)}{\pi}} \tag{29}$$

and since $g(b)H_i(b)$ is a constant in this isothermal region the outgoing flux has the same height dependence as the density.

The lateral flow of energy may be calculated in a very similar manner by the inclusion of a kinetic energy term in the flux equations. Hence equation (18) can be multiplied by

$$\tfrac{1}{2}m_i v^2$$

and the integrations carried out as before. The outgoing energy flux in analogy to equation (24) is

$$F_i^{en\text{-}out} = nkT\sqrt{\frac{g(b)H_i(b)}{2\pi}}\left\{1-\exp\left[-E\right]\left[E^2+E+1\right]\right\} . \tag{30}$$

4.0. LATERAL FLOW RESULTS

The numerical integration of equation (26) including equation (28) was performed on an IBM 7090 computer for several values of Θ_o under various temperature and density distributions (azimuthally symmetric in all cases) for the important constituents at the exobase. Table 9 shows the errors of numerical integration by comparing the incoming flux for no density or temperature variation with the outgoing flux of the exact solution of equation (27) for a typical case.

Table 9. Numerical integration errors, 700°K.

	Integrated influx	Exact Outflux	% Error
H	1.32×10^{10}	1.41×10^{10}	6.1
He	7.00×10^{10}	6.53×10^{11}	6.7
O	4.70×10^{11}	4.39×10^{10}	6.7
N_2	1.64×10^{8}	1.53×10^{8}	6.6
O_2	3.19×10^{8}	2.98×10^{8}	6.6

The errors of about 7% are well within the tolerance for this type of calculation, but they certainly necessitate use of the method discussed. Table 10 shows a sample flux for the sinusoidal 1000-1500° case. This comparison, which is fairly typical, shows how the net flux is always a small part of either the influx or outflux.

The dependence of the lateral flow upon density can be seen by a calculation for a constant temperature but a sinusoidally varying density about unity with a maximum at $\Theta = 0$. The obvious result is an antisymmetric flow, outgoing for $\Theta < 90^{\circ}$, ingoing for $\Theta > 90^{\circ}$. Such a result

for maximum to minimum density ratios of 1.5, 3, and 9 is shown for hydrogen at 1000° and 1500° in figures 21 and 22 respectively and for oxygen at 1000° and 1500° in figures 23 and 24 respectively. The oxygen fluxes in general are much smaller as might be expected.

Table 10. Comparison of net flux with outflux at $\Theta = 0$ for 1000-1500°K temperature variation.

	Integrated influx	Integrated outflux	Net flux	% Net flux of outflux
H	$5.6807 \times 10^{9}_{10}$	$5.3454 \times 10^{9}_{10}$	-3.35×10^{8}	6.3%
He	$5.4545 \times 10^{11}_{11}$	$5.4928 \times 10^{11}_{11}$	3.82×10^{8}	0.7%
O	$3.6366 \times 10^{10}_{10}$	$3.6377 \times 10^{10}_{10}$	1.07×10^{6}	0.03%
N_2	1.2661×10^{8}	1.2662×10^{8}	1.20×10^{4}	0.01%
O_2	2.4412×10	2.4414×10^{8}	1.70×10	0.007%

The opposite effect might be expected for a constant density of unity but sinusoidal temperature distributions with the maximum temperature at $\Theta = 180°$. The results for such calculations are shown for hydrogen and oxygen at temperatures varying about 1000° and 1500° in figures 25-28. The flow is not quite antisymmetric due to the nonlinear dependence of the flow on temperature. The oxygen fluxes are again much smaller in magnitude.

The fluxes for both a sinusoidal density and sinusoidal temperature variation are shown in figures 29-34 for hydrogen and oxygen again with an average density of 1.0 and maximum at $\Theta = 0°$ and a maximum temperature at $\Theta = 180°$. The density variations are 2-1, 3-1, and 5-1, while the temperature ranges are 700-1000°, 1000-1500°, and 1500-2100°. For all cases, as the maximum to minimum density

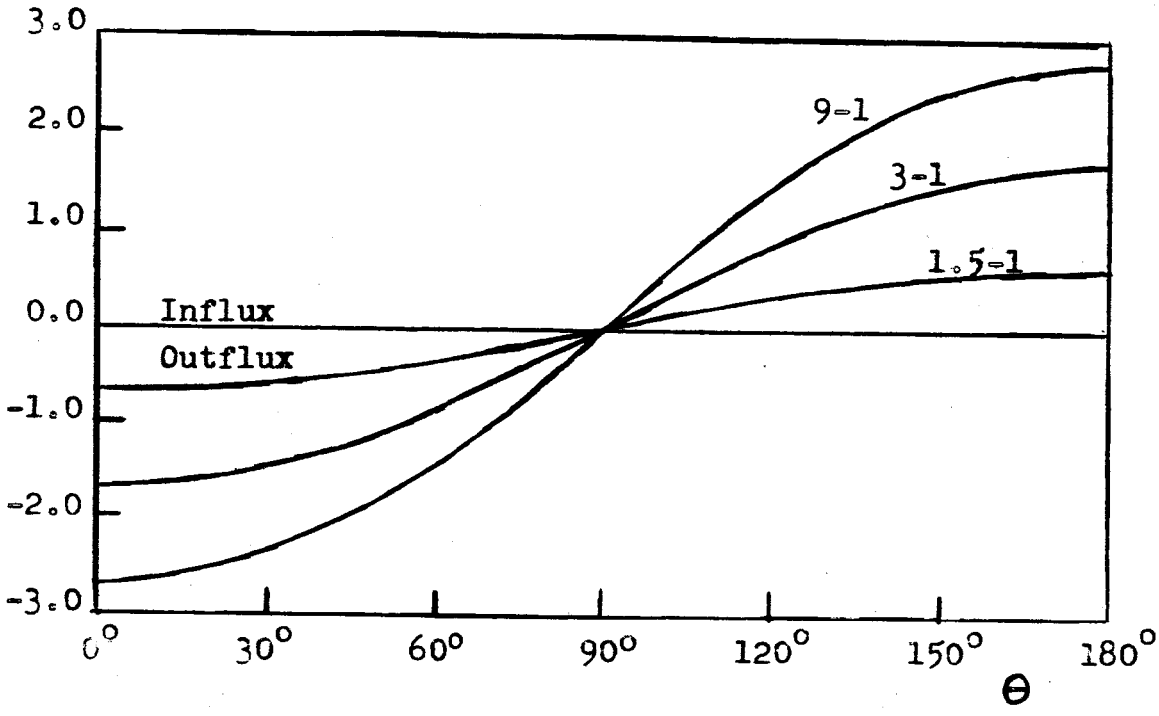

Figure 21. Hydrogen flux in $10^4 cm^{-2} sec^{-1}$ for a constant temperature of 1000° with various sinusoidal density variations about unity, maximum at $\theta = 0$.

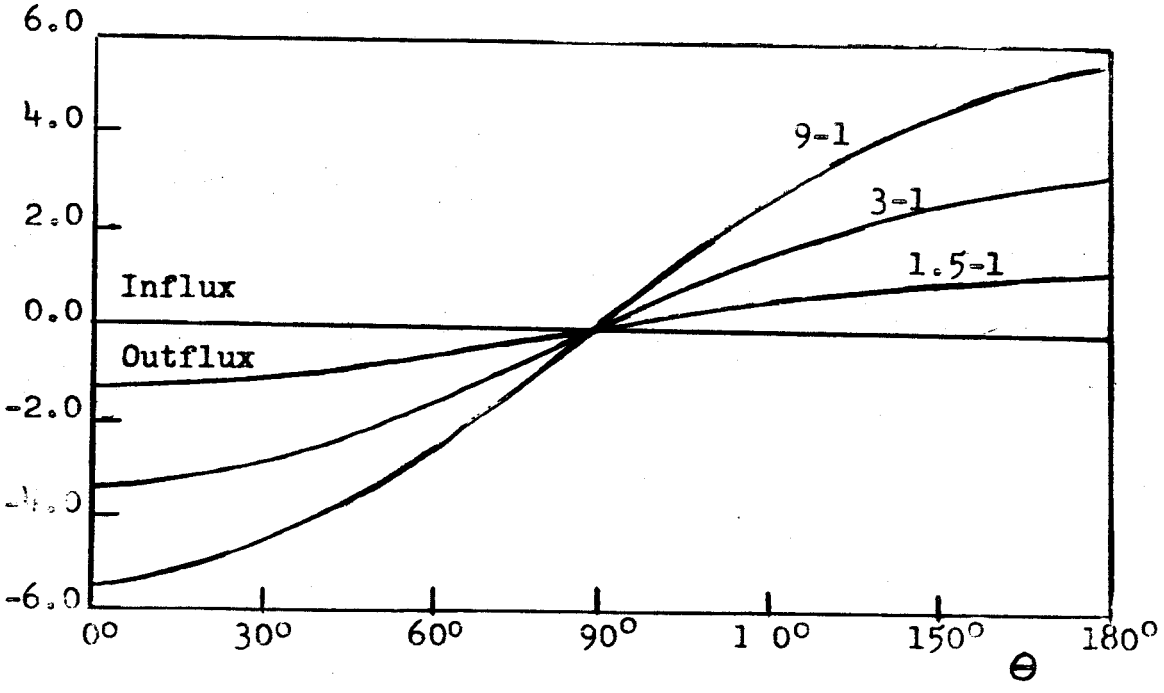

Figure 22. Hydrogen flux in $10^4 cm^{-2} sec^{-1}$ for a constant temperature of 1500° with various sinusoidal density variations about unity, maximum at $\theta = 0$.

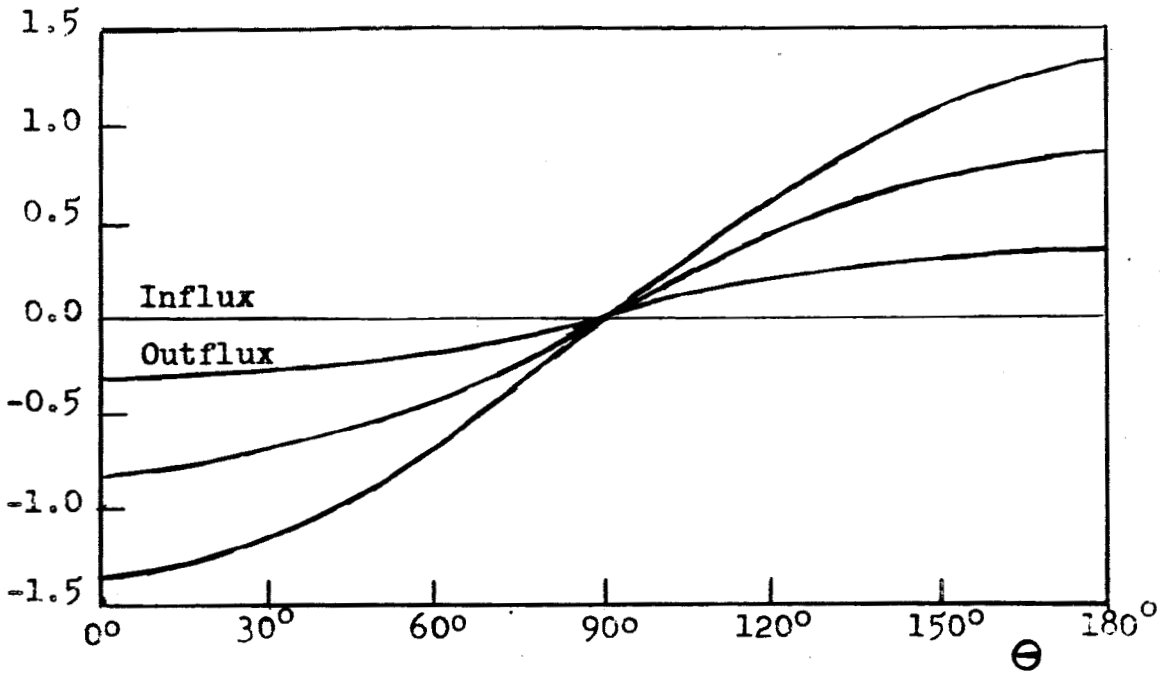

Figure 23. Oxygen flux in $10cm^{-2}sec^{-1}$ for a constant temperature of 1000^{o} with various sinusoidal density variations about unity, maximum at $\Theta = 0$.

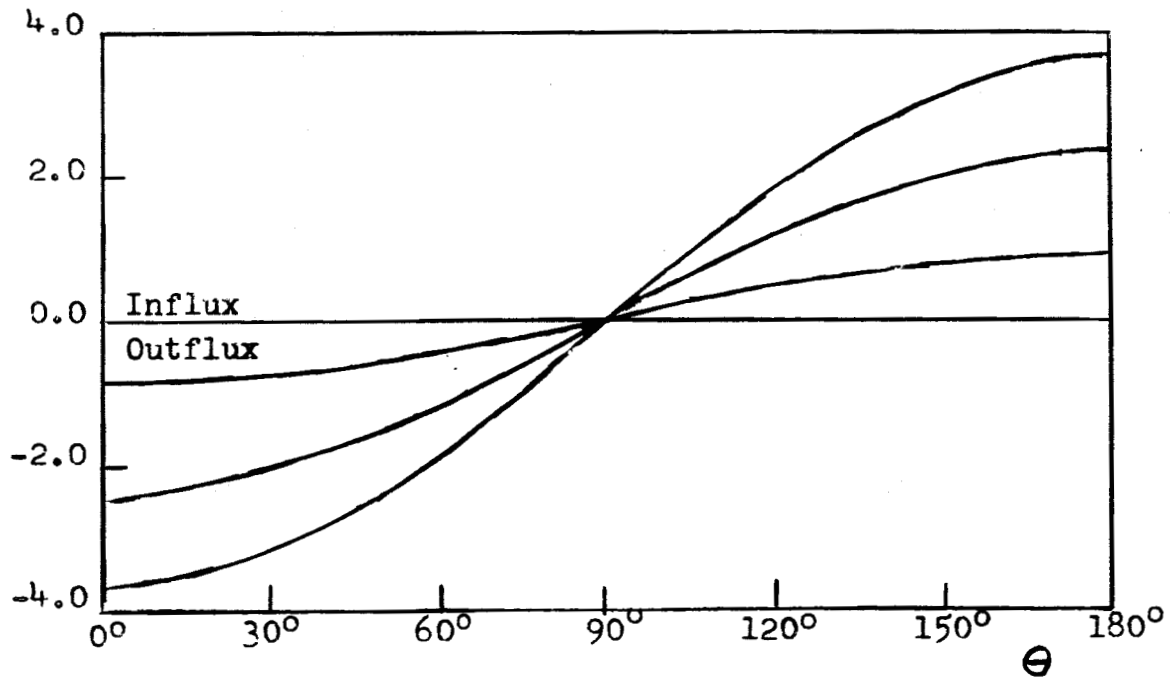

Figure 24. Oxygen flux in $10cm^{-2}sec^{-1}$ for a constant temperature of 1500^{o} with various sinusoidal density variations about unity, maximum at $\Theta = 0$.

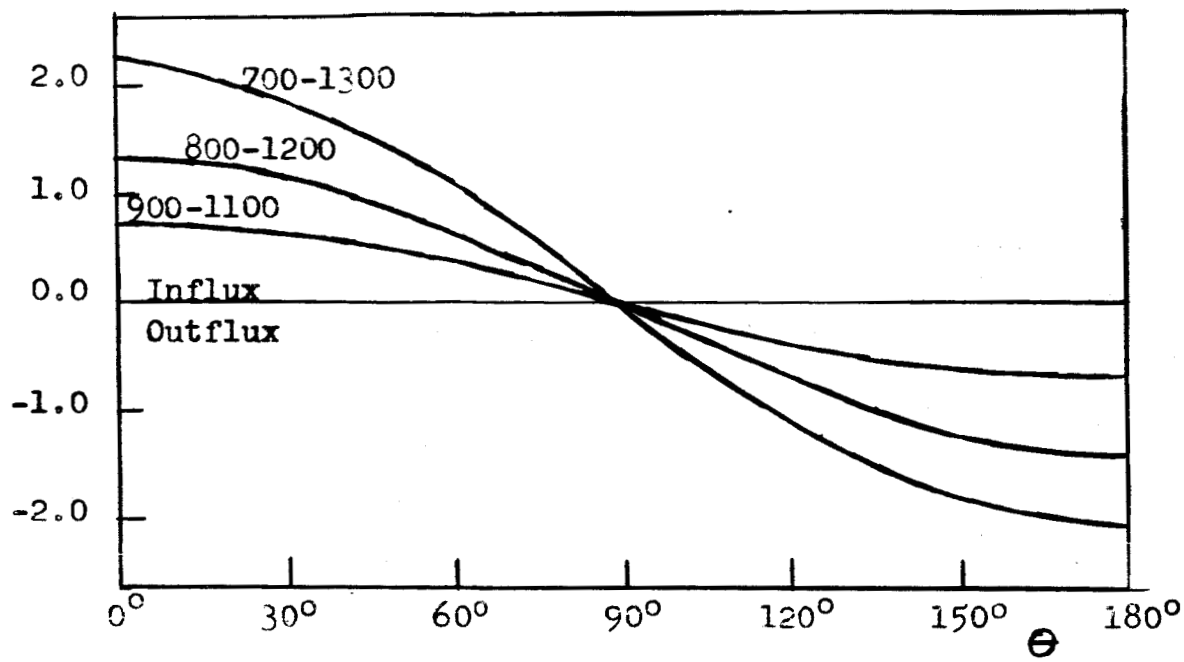

Figure 25. Hydrogen flux in $10^4 cm^{-2} sec^{-1}$ for a constant density of unity and various sinusoidal temperature variations about 1000° with maximum at $\theta = 180^\circ$.

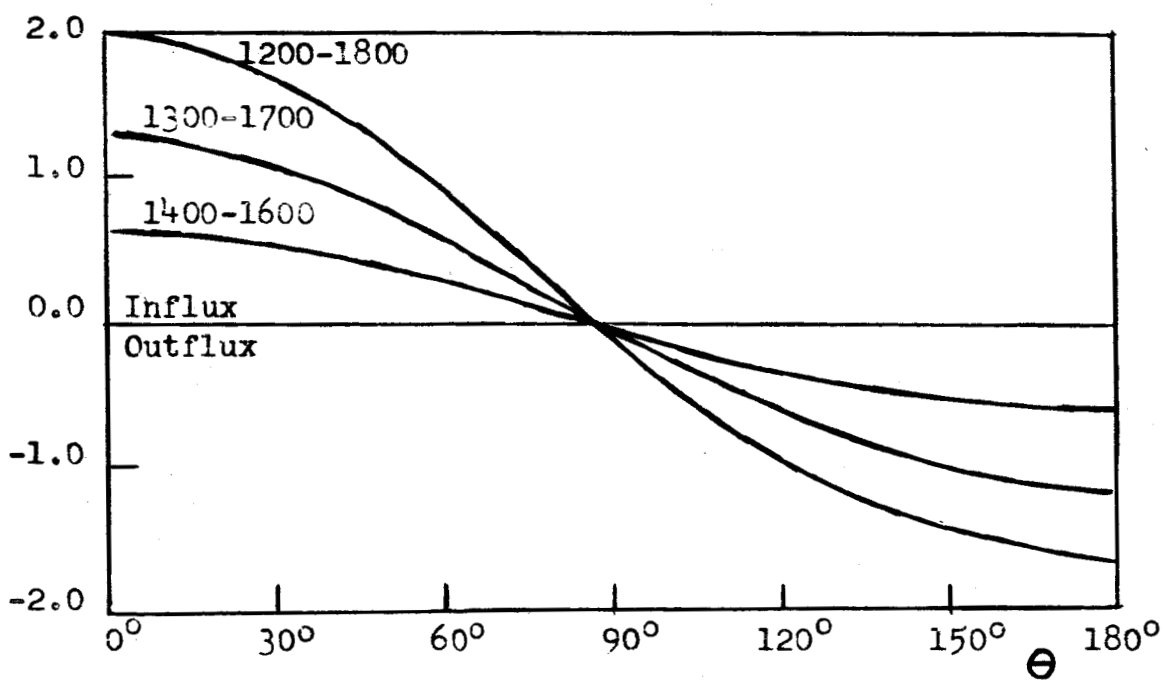

Figure 26. Hydrogen flux in $10^4 cm^{-2} sec^{-1}$ for a constant density of unity and various sinusoidal temperature variations about 1500° with maximum at $\theta = 180^\circ$.

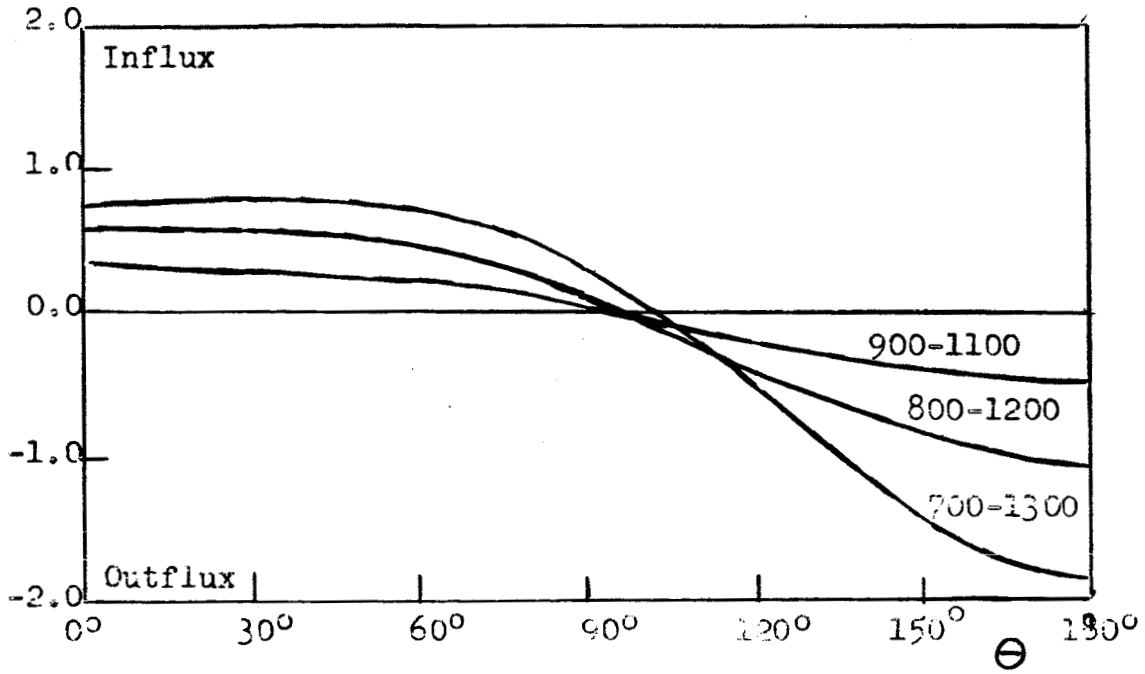

Figure 27. Oxygen flux in $10cm^{-2}sec^{-1}$ for a constant density of unity and various sinusoidal temperature variations about 1000^{o} with maximum at $\Theta = 180^{o}$.

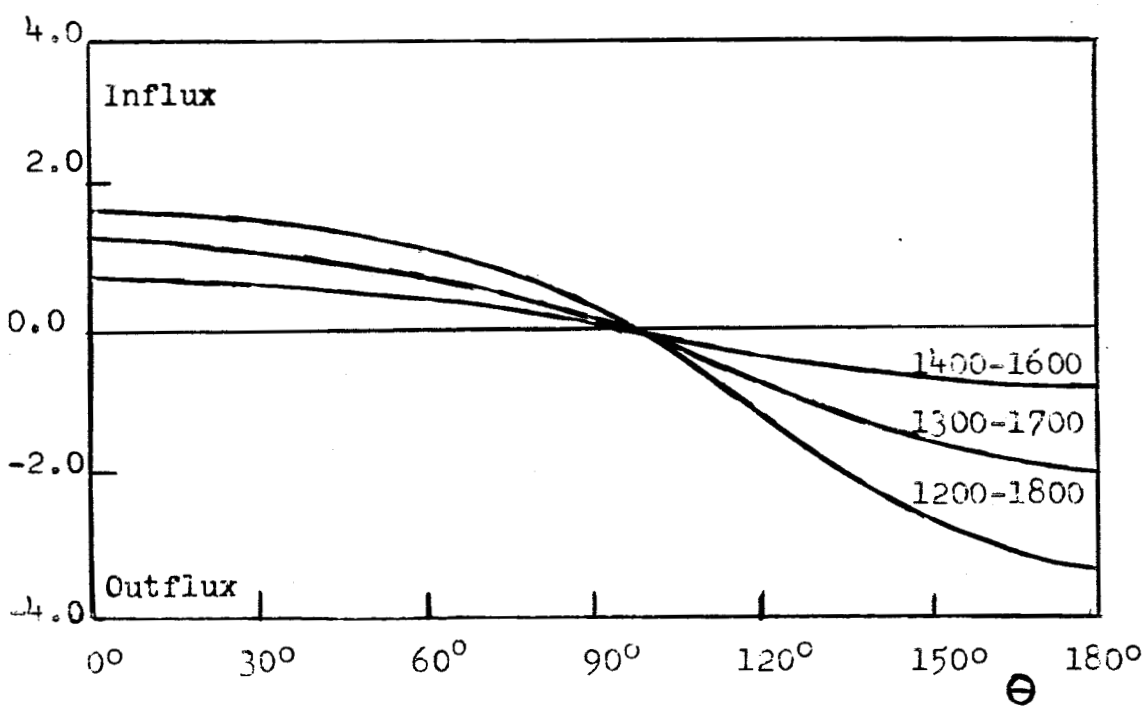

Figure 28. Oxygen flux in $10cm^{-2}sec^{-1}$ for a constant density of unity and various sinusoidal temperature variations about 1500^{o} with maximum at $\Theta = 180^{o}$.

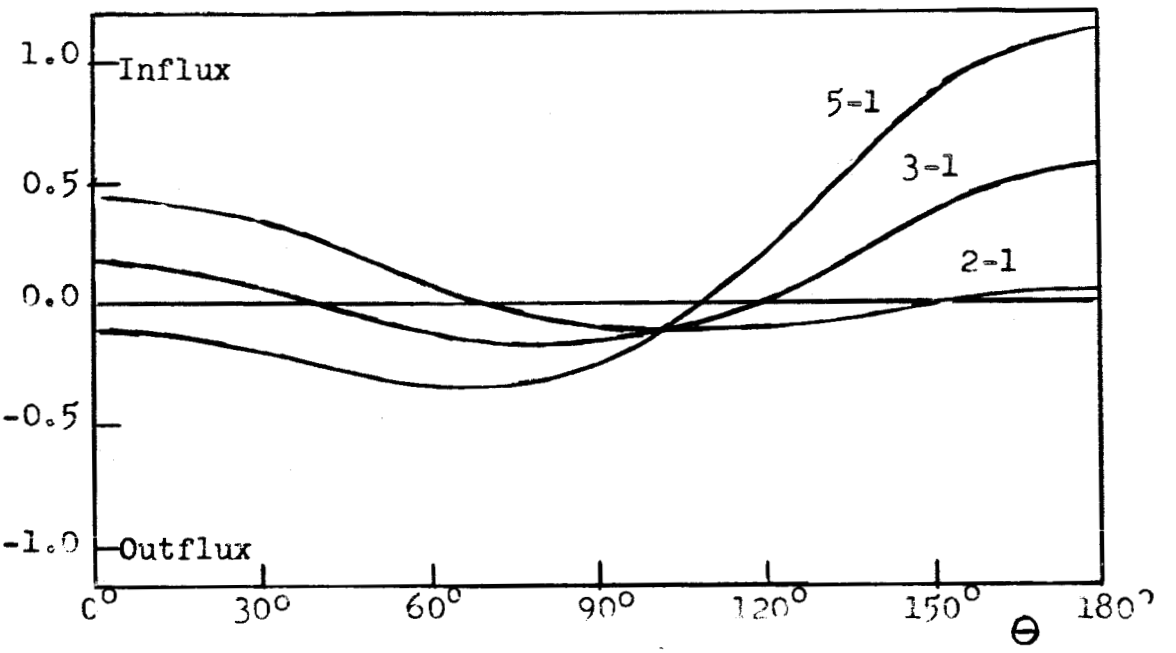

Figure 29. Hydrogen flux in $10^4 cm^{-2} sec^{-1}$ for 700-1000° sinusoidal temperature variation and various sinusoidal density variations about unity. Density maximum at $\Theta = 0$, temperature maximum at $\Theta = 180°$

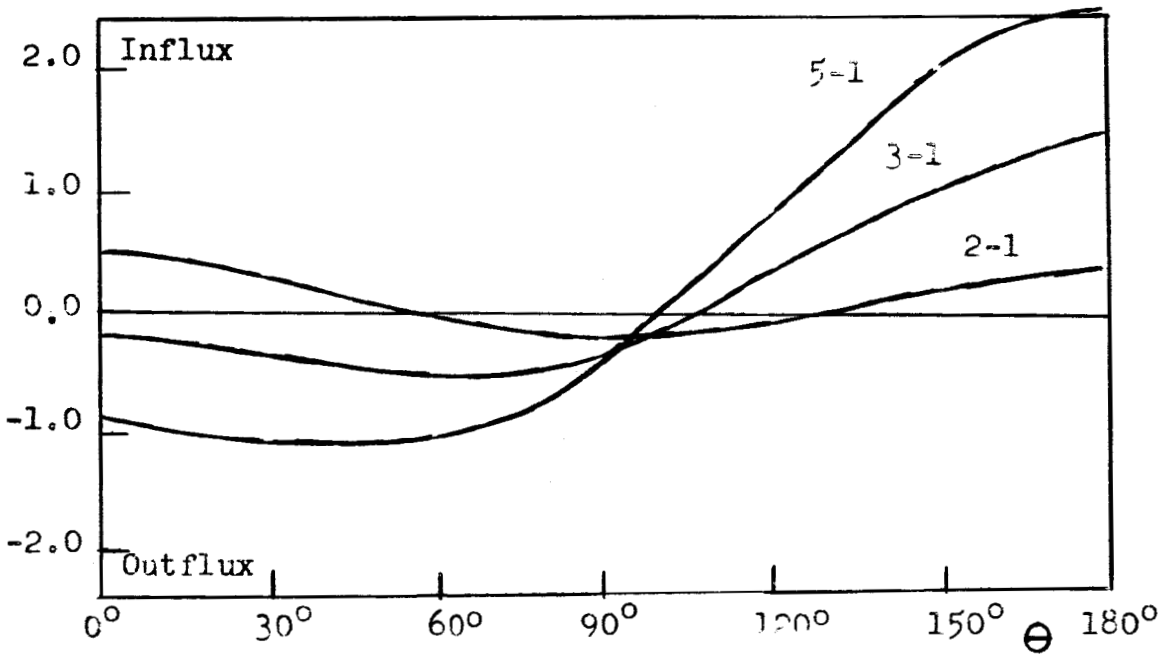

Figure 30. Hydrogen flux in $10^4 cm^{-2} sec^{-1}$ for 1000-1500° sinusoidal temperature variation and various sinusoidal density variations about unity. Density maximum at $\Theta = 0$, temperature maximum at $\Theta = 180°$.

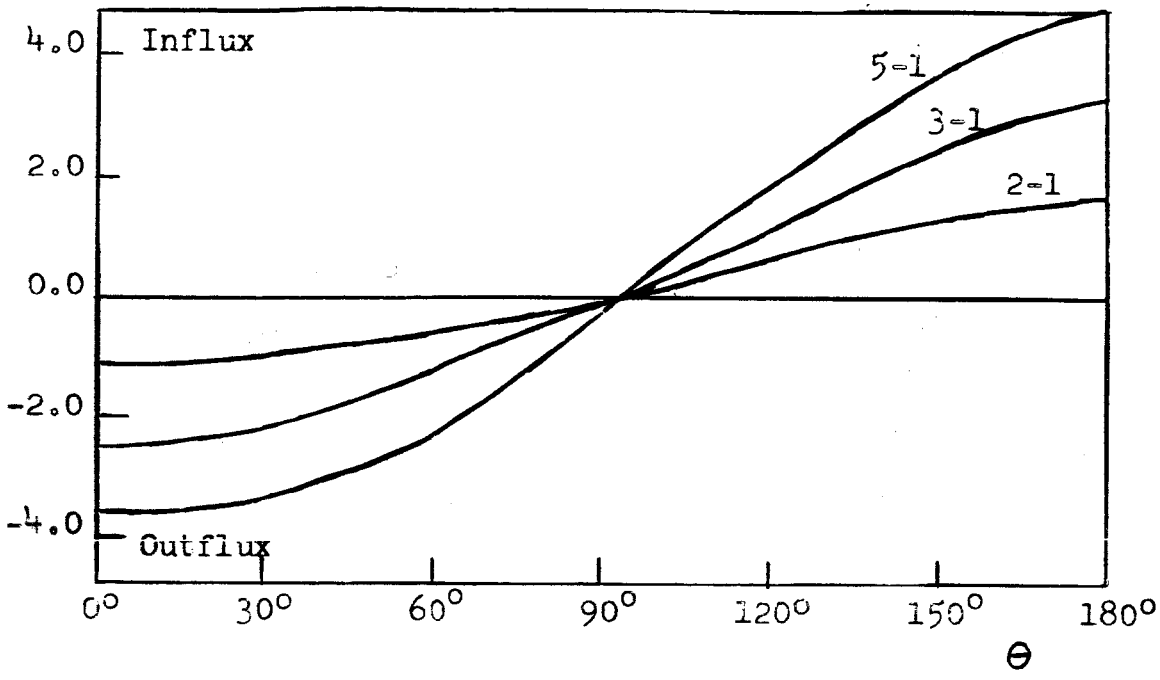

Figure 31. Hydrogen flux in $10^4 cm^{-2} sec^{-1}$ for 1500-2100° sinusoidal temperature variation and various sinusoidal density variations about unity. Density maximum at $\Theta = 0$, temperature maximum at $\Theta = 180°$.

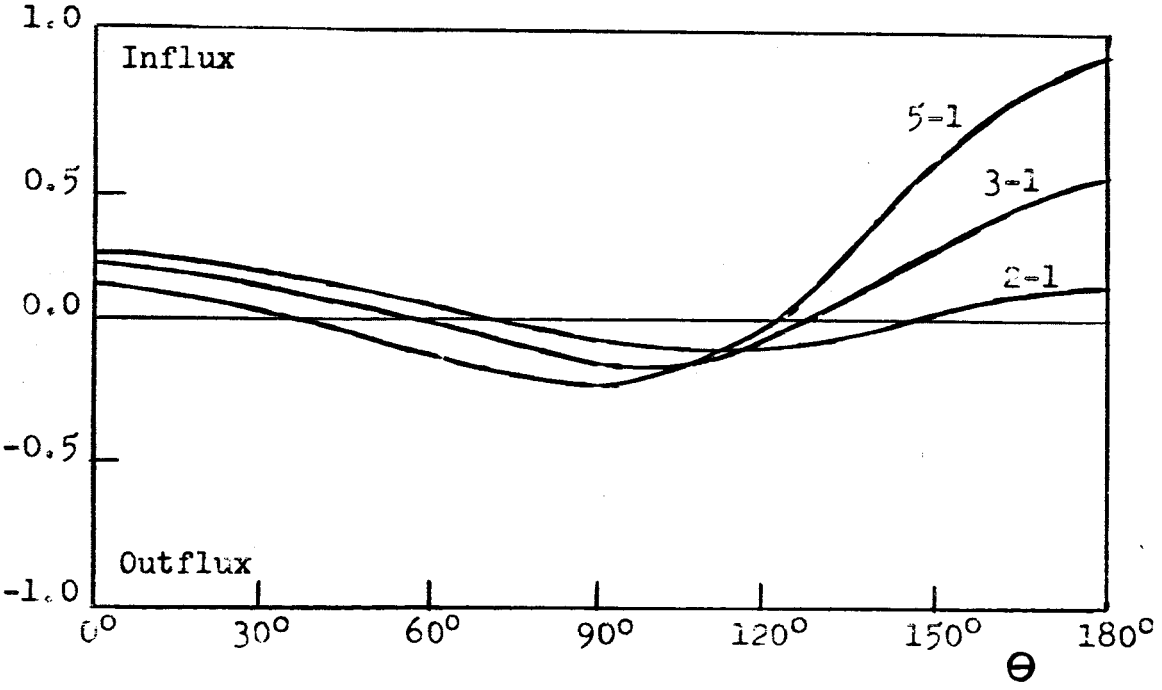

Figure 32. Oxygen flux in $10 cm^{-2} sec^{-1}$ for 700-1000° sinusoidal temperature variation and various sinusoidal density variations about unity. Density maximum at $\Theta = 0$, temperature maximum at $\Theta = 180°$.

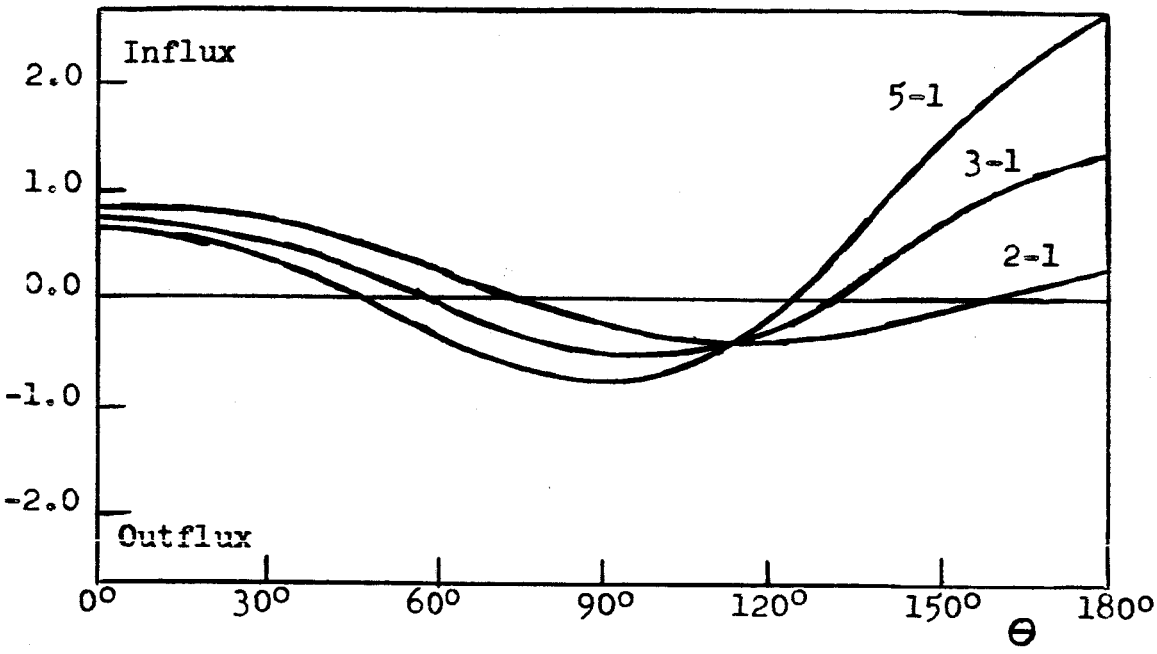

Figure 33. Oxygen flux in $10cm^{-2}sec^{-1}$ for 1000-1500° sinusoidal temperature variation and various sinusoidal density variations about unity. Density maximum at $\Theta = 0$, temperature maximum at $\Theta = 180^{0}$.

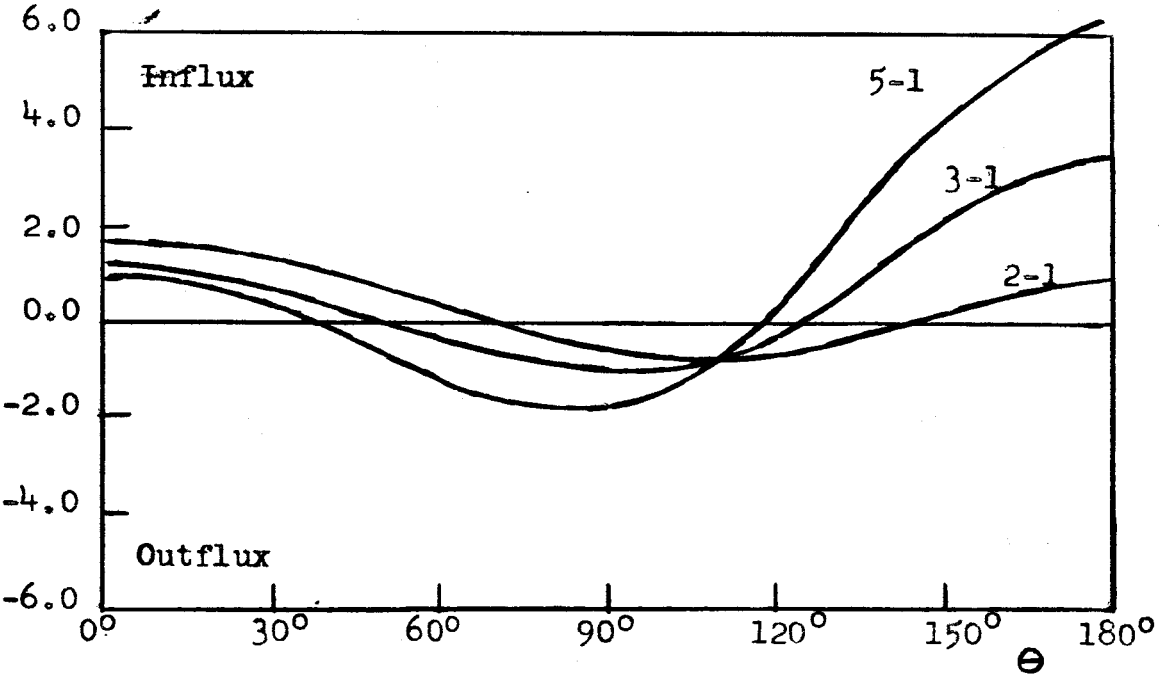

Figure 34. Oxygen flux in $10cm^{-2}sec^{-1}$ for 1500-2100° sinusoidal temperature variation and various sinusoidal density variations about unity. Density maximum at $\Theta = 0$, temperature maximum at $\Theta = 180^{0}$.

ratios are varied, the fluxes range from a day to night flow for a small ratio to a night to day flow for a large ratio. A comparison with the old models is shown in figure 35.

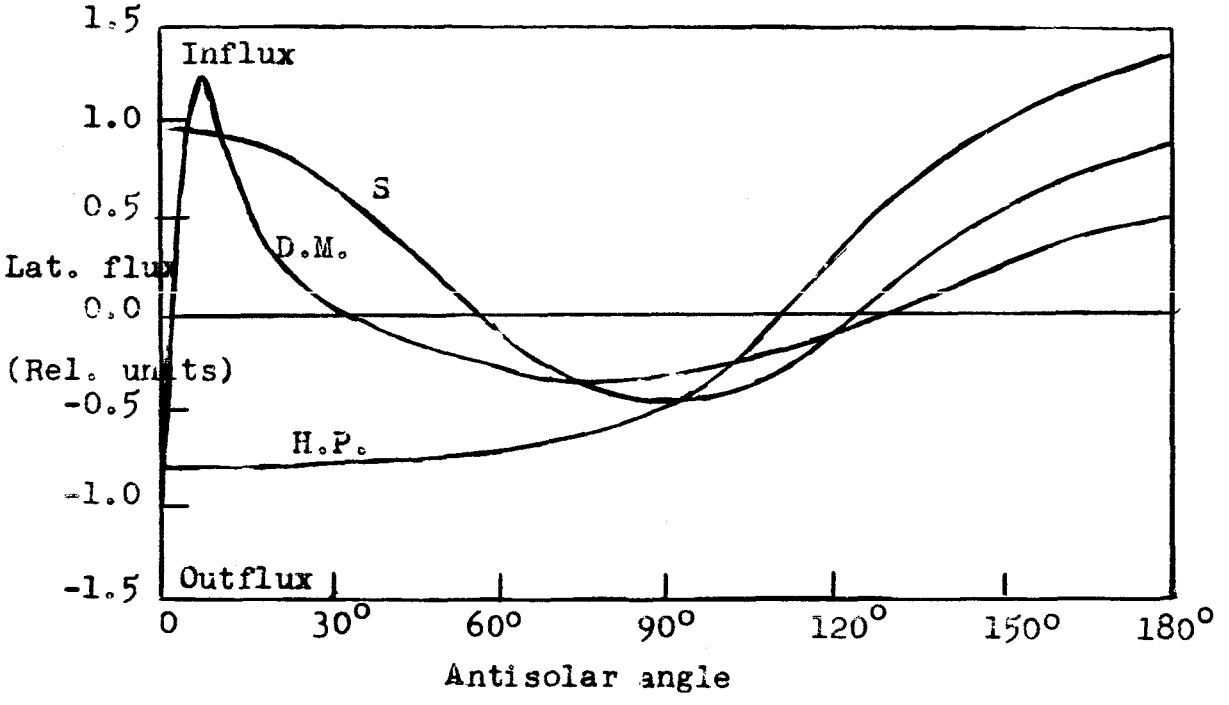

Figure 35. Comparison of lateral flow models including the Hanson-Patterson (H.P.), Donahue-McAfee (D.M.) and spherical (S).

The previous results of a general nature tend to demonstrate the functional dependence of the lateral flow. In order to estimate the magnitude of the effect upon a real atmosphere, it is necessary to use real parameters. The densities of the various constituents at the exobase can be taken from tables 2-5 for helium, atomic oxygen, molecular nitrogen, and molecular oxygen and from figure 11 for hydrogen. In practice, for a given temperature variation the densities were found for the maximum and minimum

temperature and corresponding exobases, and then assumed to vary sinusoidally in the region between. Since the exobase altitude is a function of the temperature it is apparent that the exobase surface is not spherical but has a day-night asymmetry, being at a larger altitude on the day side. This variation was not considered in the calculations involving the various orbital relationships since the criterion of importance is the change in exobase height as compared with its geocentric distance. The variation in exobase height is small compared with this radius so that it does not alter the solutions significantly. The important feature is in the fact that the densities used are not for the same altitudes at different points on the exobase surface. The pertinent data concerning the parameters at the exobase for various temperatures is given in table 11.

Table 11. Exobase parameters.

T(°K)	b(km)	n(H)	n(He)	n(O)	$n(N_2)$	$n(O_2)$
700	360	1.47×10^{5}	1.46×10^{6}	1.96×10^{7}	9.05×10^{5}	1.88×10^{4}
1000	440	5.26×10^{4}	1.02×10^{6}	1.36×10^{7}	6.26×10^{5}	1.29×10^{3}
1500	555	8.78×10^{3}	6.81×10^{5}	9.12×10^{6}	4.22×10^{5}	8.73×10^{3}
2100	680	2.57×10^{3}	4.81×10^{5}	6.21×10^{6}	2.77×10^{5}	5.68×10^{3}

The results of calculations of lateral flow (along with the escape fluxes and maximum fluxes) using the data from table 11 are shown in tables 12-14 for temperature variations of 700°-1000°, 1000°-1500°, and 1500°-2100° respectively. They are also shown in graphical form in figures 36-38 for hydrogen and helium.

Table 12. Pertinent fluxes for 700-1000° temperature variation.

Constituent	Angle	Lateral flux	Escape flux	Max.Diff.flux
H	0	2.29×10^{8}	0.55×10^{7}	8.9×10^{7}
	30	1.11×10^{8}	0.69×10^{7}	8.9×10^{7}
	60	-1.14×10^{8}	1.20×10^{7}	8.9×10^{7}
	90	-1.82×10^{8}	2.12×10^{7}	8.9×10^{7}
	120	0.24×10^{8}	3.11×10^{7}	8.9×10^{7}
	150	3.44×10^{8}	3.63×10^{7}	8.9×10^{7}
	180	4.97×10^{8}	3.73×10^{7}	8.9×10^{7}
He	0	1.56×10^{8}	4.26×10^{-6}	5.4×10^{8}
	30	1.36×10^{8}	1.29×10^{-5}	5.4×10^{8}
	60	0.78×10^{8}	2.00×10^{-4}	5.4×10^{8}
	90	-0.10×10^{8}	4.64×10^{-3}	5.3×10^{8}
	120	-0.86×10^{8}	6.31×10^{-2}	5.3×10^{8}
	150	-1.22×10^{8}	3.26×10^{-1}	5.3×10^{8}
	180	-1.27×10^{8}	5.65×10^{-1}	5.3×10^{8}
O	0	5.12×10^{7}	-	1.3×10^{11}
	30	4.44×10^{7}	-	1.3×10^{11}
	60	2.38×10^{7}	-	1.3×10^{11}
	90	-0.40×10^{7}	-	1.2×10^{11}
	120	-2.69×10^{7}	-	1.2×10^{11}
	150	-3.58×10^{7}	-	1.2×10^{11}
	180	-3.65×10^{7}	-	1.2×10^{11}
N_2	0	5.57×10^{5}	-	2.5×10^{10}
	30	4.80×10^{5}	-	2.5×10^{10}
	60	2.53×10^{5}	-	2.4×10^{10}
	90	-0.52×10^{5}	-	2.3×10^{10}
	120	-3.00×10^{5}	-	2.2×10^{10}
	150	-3.88×10^{5}	-	2.1×10^{10}
	180	-3.90×10^{5}	-	2.1×10^{10}
O_2	0	8.10×10^{3}	-	3.5×10^{8}
	30	7.00×10^{3}	-	3.5×10^{8}
	60	3.84×10^{3}	-	3.4×10^{8}
	90	-0.81×10^{3}	-	3.2×10^{8}
	120	-4.52×10^{3}	-	3.1×10^{8}
	150	-5.68×10^{3}	-	3.0×10^{8}
	180	-5.71×10^{3}	-	3.0×10^{8}

Table 13. Pertinent fluxes for 1000-1500° temperature variation.

Constituent	Angle	Lateral flux	Excape flux	Max.Diff.flux
H	0	-3.34×10^{8}	3.73×10^{7}	8.9×10^{7}
	30	-3.59×10^{8}	4.39×10^{7}	8.9×10^{7}
	60	-3.38×10^{8}	6.28×10^{7}	8.9×10^{7}
	90	-1.23×10^{8}	8.45×10^{7}	8.8×10^{7}
	120	2.77×10^{8}	8.86×10^{7}	8.8×10^{7}
	150	6.67×10^{8}	7.13×10^{7}	8.8×10^{7}
	180	8.28×10^{8}	5.92×10^{7}	8.8×10^{7}
He	0	3.82×10^{8}	5.65×10^{-1}	5.3×10^{8}
	30	3.34×10^{8}	1.38×10^{0}	5.3×10^{8}
	60	1.91×10^{8}	1.20×10^{1}	5.3×10^{8}
	90	-0.30×10^{8}	1.34×10^{2}	5.3×10^{8}
	120	-2.19×10^{8}	9.33×10^{2}	5.3×10^{8}
	150	-2.97×10^{8}	3.07×10^{7}	5.3×10^{8}
	180	-3.07×10^{8}	4.56×10^{3}	5.3×10^{8}
O	0	1.07×10^{8}	-	1.2×10^{11}
	30	0.94×10^{8}	-	1.2×10^{11}
	60	0.53×10^{8}	-	1.2×10^{11}
	90	-0.08×10^{8}	-	1.1×10^{11}
	120	-0.59×10^{8}	-	1.1×10^{11}
	150	-0.78×10^{8}	-	1.1×10^{11}
	180	-0.79×10^{8}	-	1.1×10^{11}
N_2	0	1.16×10^{6}	-	2.1×10^{10}
	30	1.03×10^{6}	-	2.1×10^{10}
	60	0.57×10^{6}	-	2.0×10^{10}
	90	-0.09×10^{6}	-	1.9×10^{10}
	120	-0.64×10^{6}	-	1.9×10^{10}
	150	-0.85×10^{6}	-	1.8×10^{10}
	180	-0.86×10^{6}	-	1.8×10^{10}
O_2	0	1.71×10^{4}	-	3.0×10^{8}
	30	1.50×10^{4}	-	2.9×10^{8}
	60	0.83×10^{4}	-	2.8×10^{8}
	90	-0.13×10^{4}	-	2.7×10^{8}
	120	-0.95×10^{4}	-	2.6×10^{8}
	150	-1.26×10^{4}	-	2.5×10^{8}
	180	-1.28×10^{4}	-	2.5×10^{8}

Table 14. Pertinent fluxes for 1500-2100° temperature variation.

Constituent	Angle	Lateral flux	Escape flux	Max.Diff.flux
H	0	-1.52×10^{8}	5.92×10^{7}	8.8×10^{7}
	30	-1.40×10^{8}	6.34×10^{7}	8.8×10^{7}
	60	-0.95×10^{8}	7.31×10^{7}	8.8×10^{7}
	90	-0.13×10^{8}	8.04×10^{7}	8.8×10^{7}
	120	0.89×10^{8}	7.75×10^{7}	8.8×10^{7}
	150	1.71×10^{8}	6.73×10^{7}	8.8×10^{7}
	180	2.03×10^{8}	6.16×10^{7}	8.8×10^{7}
He	0	7.90×10^{8}	4.56×10^{3}	5.3×10^{8}
	30	6.71×10^{8}	7.28×10^{3}	5.3×10^{8}
	60	3.45×10^{8}	2.31×10^{4}	5.3×10^{8}
	90	-0.63×10^{8}	8.75×10^{4}	5.3×10^{8}
	120	-3.75×10^{8}	2.64×10^{5}	5.3×10^{8}
	150	-5.16×10^{8}	5.27×10^{5}	5.3×10^{8}
	180	-5.46×10^{8}	6.64×10^{5}	5.3×10^{8}
O	0	1.54×10^{8}	-	1.1×10^{11}
	30	1.31×10^{8}	-	1.1×10^{11}
	60	0.69×10^{8}	-	1.1×10^{11}
	90	-0.16×10^{8}	-	1.0×10^{11}
	120	-0.80×10^{8}	-	1.0×10^{11}
	150	-0.99×10^{8}	-	1.0×10^{11}
	180	-0.97×10^{8}	-	1.0×10^{11}
N_2	0	1.60×10^{6}	-	1.8×10^{10}
	30	1.35×10^{6}	-	1.8×10^{10}
	60	0.67×10^{6}	-	1.7×10^{10}
	90	-0.22×10^{6}	-	1.6×10^{10}
	120	-0.79×10^{6}	-	1.6×10^{10}
	150	-0.84×10^{6}	-	1.5×10^{10}
	180	-0.75×10^{6}	-	1.5×10^{10}
O_2	0	2.31×10^{4}	-	2.5×10^{8}
	30	1.94×10^{4}	-	2.4×10^{8}
	60	0.95×10^{4}	-	2.3×10^{8}
	90	-0.35×10^{4}	-	2.2×10^{8}
	120	-1.14×10^{4}	-	2.1×10^{8}
	150	-1.16×10^{4}	-	2.0×10^{8}
	180	-1.00×10^{4}	-	2.0×10^{8}

The result for the heavier constituents, O, N_2, and O_2 is that the computed lateral flow may be neglected since it is much smaller than the maximum diffusive flux. Hence the vertical distribution should remain one of diffusive equilibrium in these three cases. This is of special importance for the case of atomic oxygen. It is the dominant constituent in the exobase region and a change in its density would necessitate a consistent change in the exobase level. Therefore, since there should be no change in its density, the exobase can be assumed unaffected by the lateral flow.

The lateral fluxes for helium, however, are comparable to its maximum diffusive flux, and hence bear consideration. The hydrogen fluxes are of even more concern since they are actually larger than the maximum diffusive fluxes.

The lateral energy fluxes turn out to be small compared with other energy sources. Even the total flux out of a surface as from equation (30) is only on the order of 10^{-3} ergs cm^{-2} sec^{-1}. A sample calculation for hydrogen and oxygen at constant density of 1.0 with a 900-1100° temperature variation is shown in figures 39 and 40. Since the real densities are on the order of 10^5 or 10^6 times the unity used, realistic flows would include this approximate factor also.

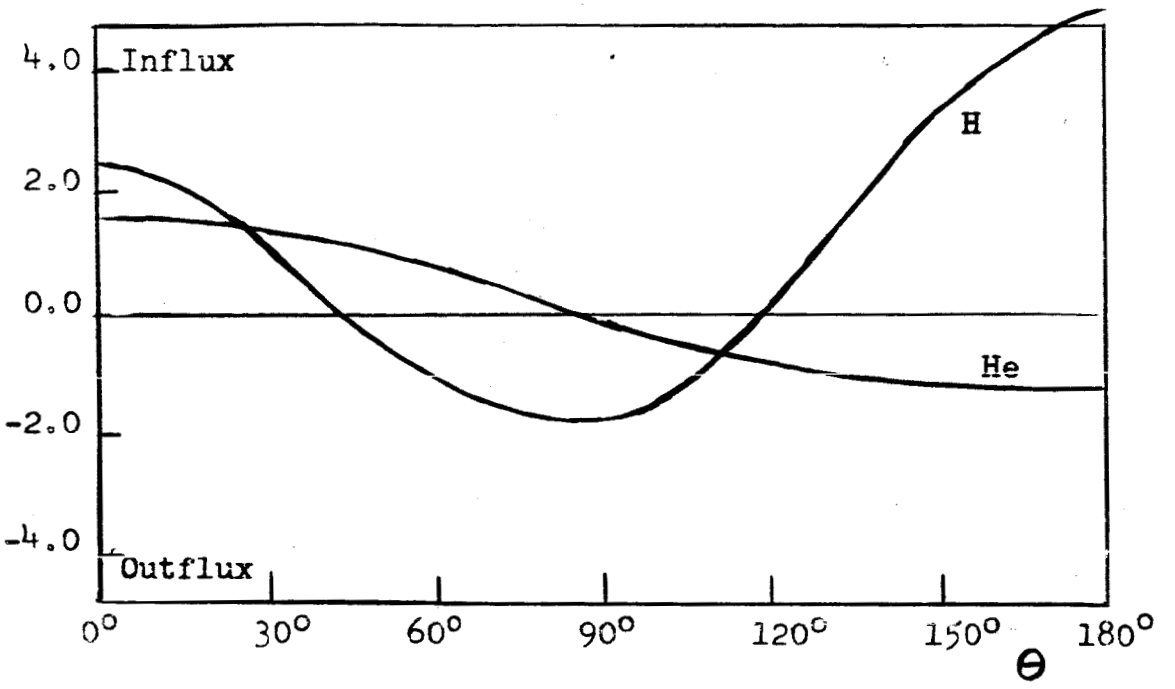

Figure 36. Hydrogen and helium fluxes in $10^8 cm^{-2} sec^{-1}$ for 700-1000° sinusoidal temperature variation with corresponding densities as in table 11.

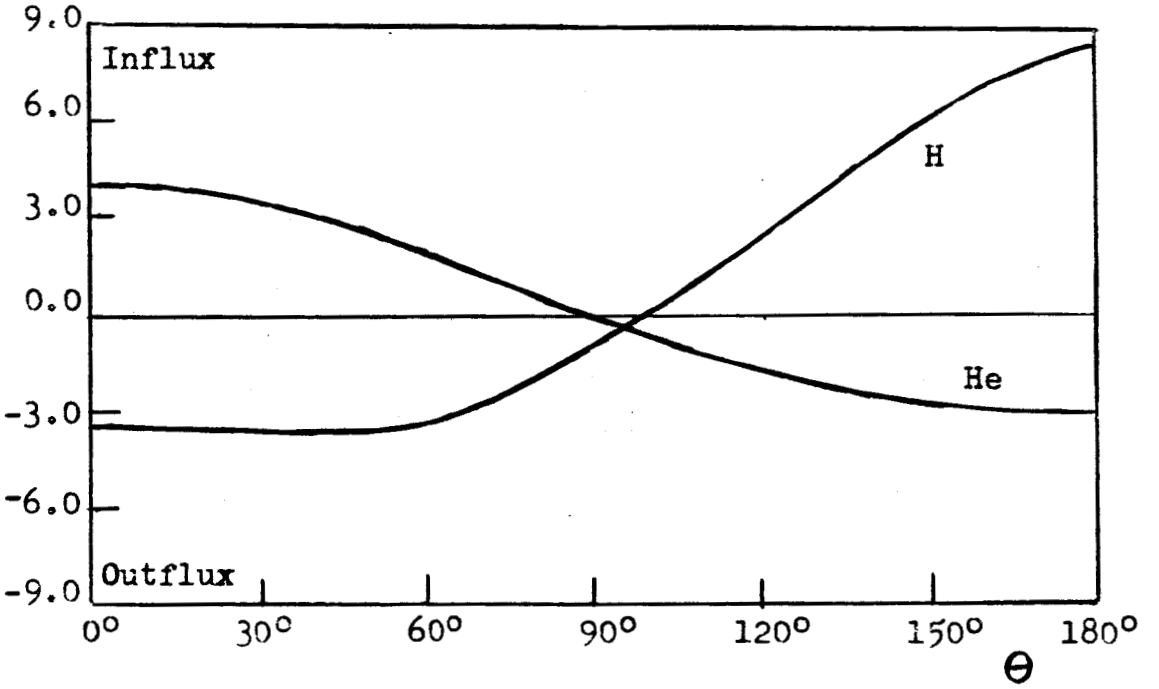

Figure 37. Hydrogen and helium fluxes in $10^8 cm^{-2} sec^{-1}$ for the 1000-1500° sinusoidal temperature variation with corresponding densities as in table 11.

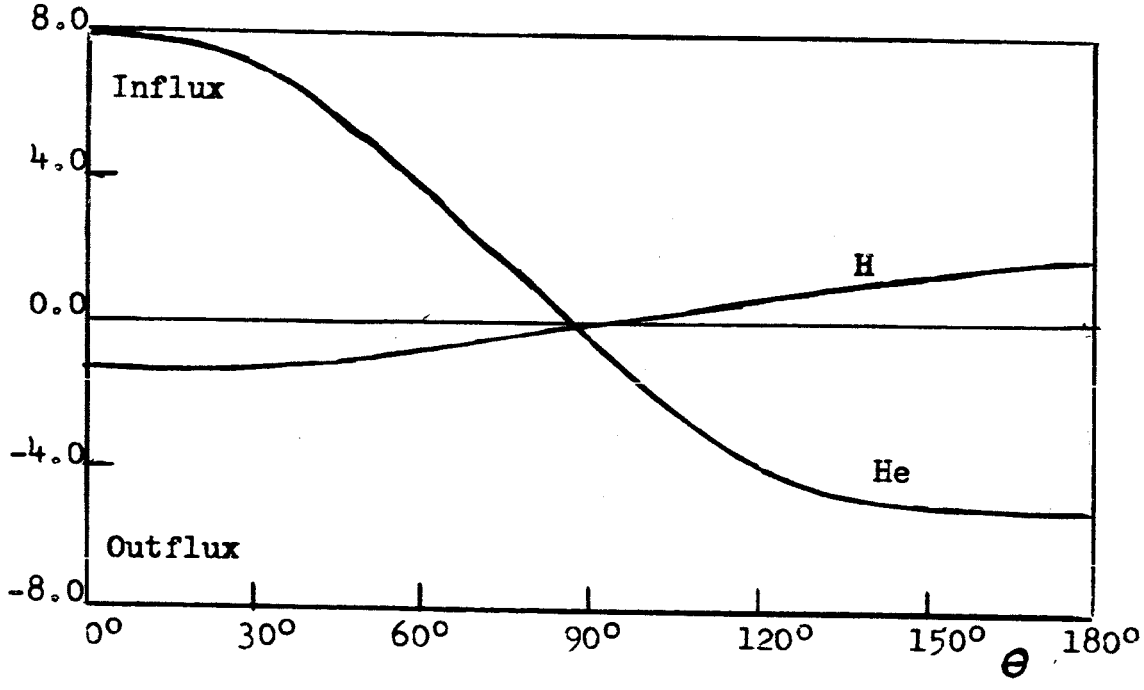

Figure 38. Hydrogen and helium fluxes in 10^{8} cm^{-2} sec^{-1} for the 1500-2100° sinusoidal temperature variation with corresponding densities as in table 11.

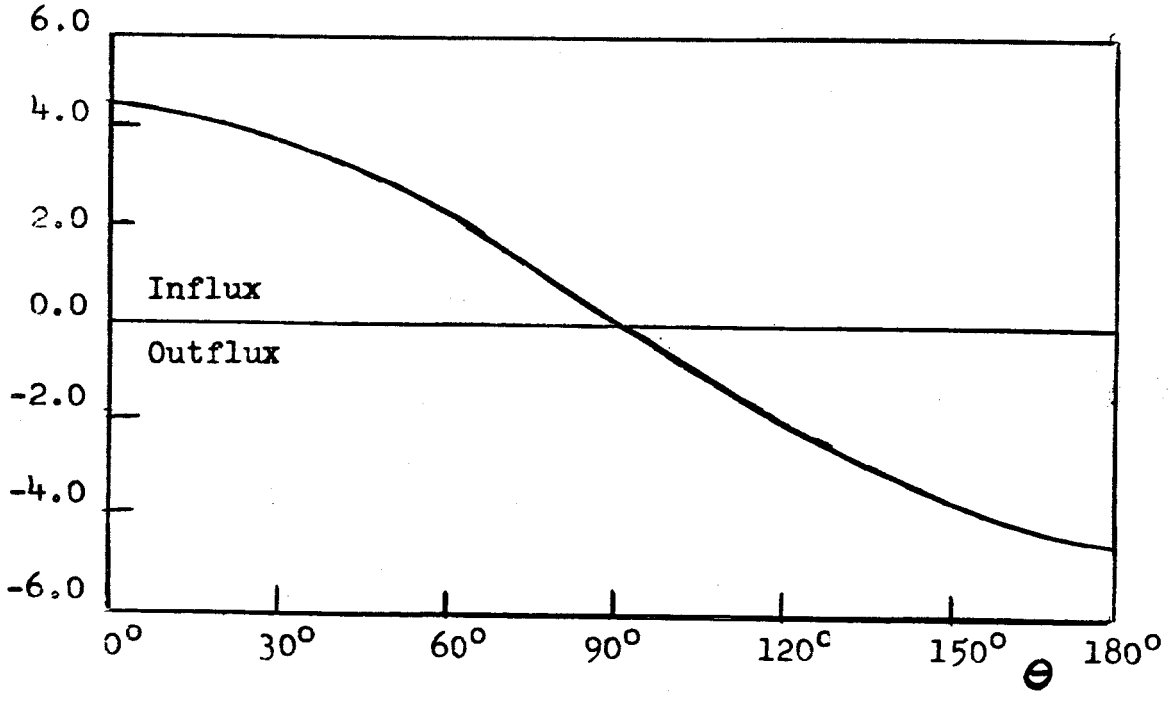

Figure 39. Lateral energy fluxes for hydrogen in 10^{-9} ergs cm^{-2}sec^{-1} for 900-1100° sinusoidal temperature variation and constant density of 1.0.

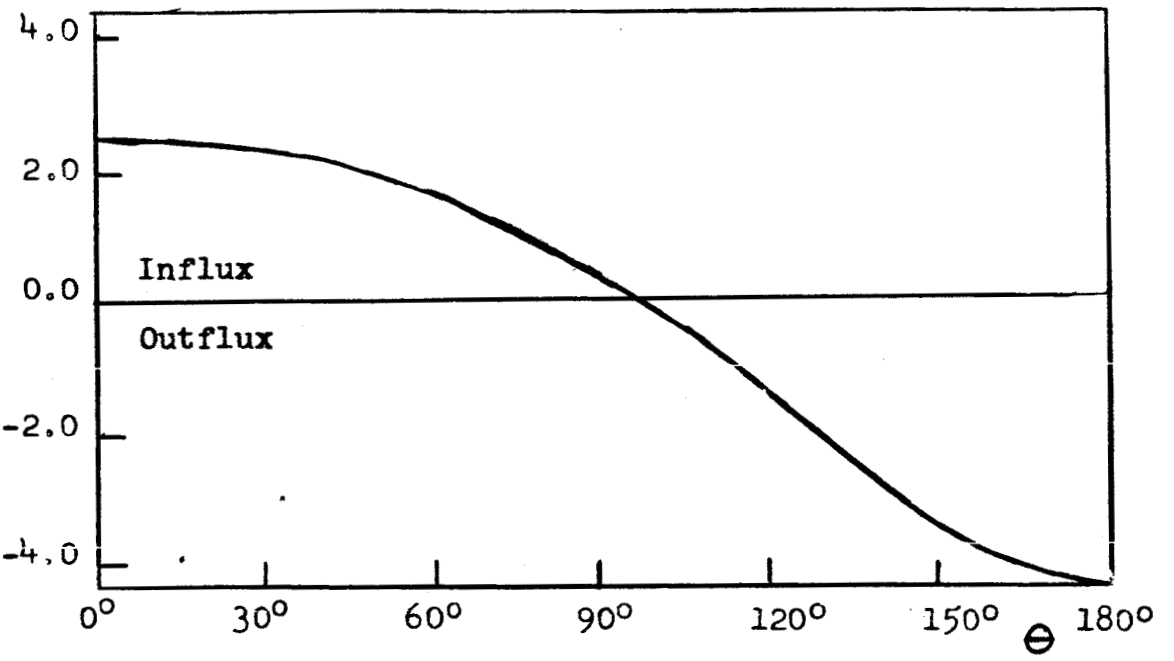

Figure 40. Lateral energy fluxes for oxygen in 10^{-12} ergs $cm^{-2}sec^{-1}$ for 900-1100° sinusoidal temperature variation and constant density of 1.0.

5.0. LATERAL FLOW INFLUENCE

5.1. Endosphere

The lateral fluxes derived in the previous section will influence the vertical density distributions in the endosphere by destroying the assumption of zero flux necessary to a diffusive equilibrium situation. As was shown, the fluxes are so small for O, N_2, and O_2 that they make no appreciable difference and may be ignored. The fluxes for H and He are significant and their effect on the endospheric densities could be large.

5.11. Zero Lateral Flow Distributions

The endospheric effect of the lateral flow can be simply described as follows. In a region where the flux is into the endosphere the density will build up. The reverse is true in a region where the flux is out. These density changes in turn decrease the lateral flux and in this manner the density distributions would tend toward those which would yield no lateral flow. Such distributions can be found by successive approximations to the density distributions consistent with the calculated lateral flow. These are compared in figures 41-43 with the distributions from table 11 which were used in calculating the actual flux.

Even if conditions in the heterosphere were kept fixed for a sufficient length of time, however, the final distribution would not be a no lateral flow distribution. This is due to the fact that a zero flow distribution on

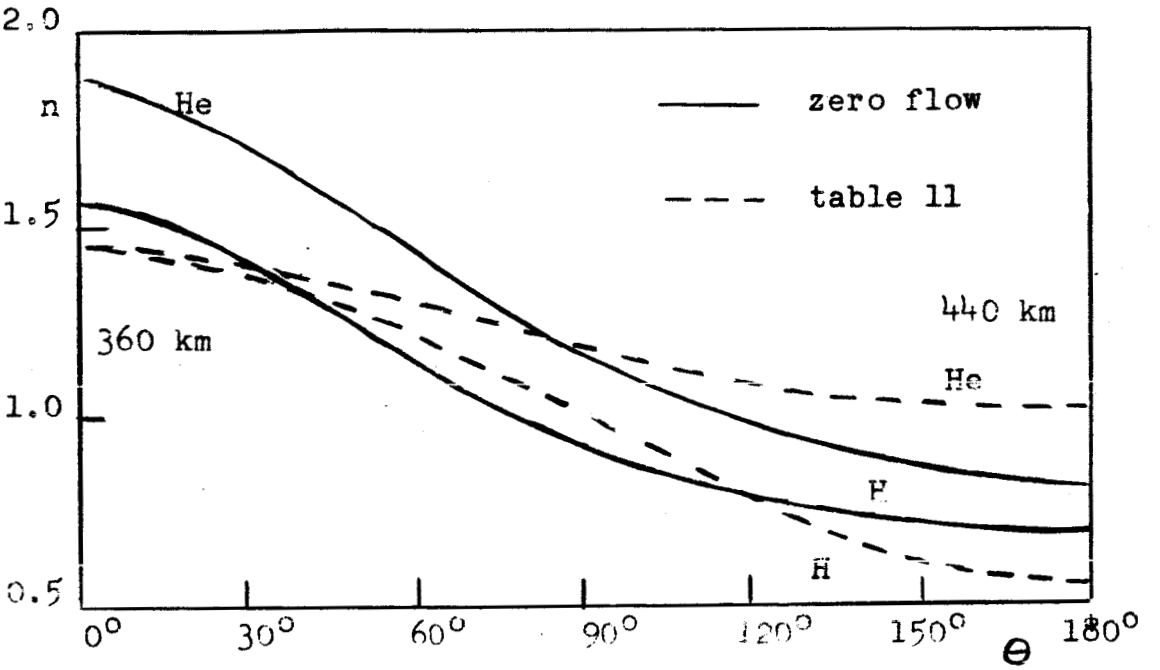

Figure 41. Hydrogen and helium densities in 10^4 and $10^6 cm^{-3}$ respectively for zero flow and as in table 11. for a 700-1000° sinusoidal temperature variation.

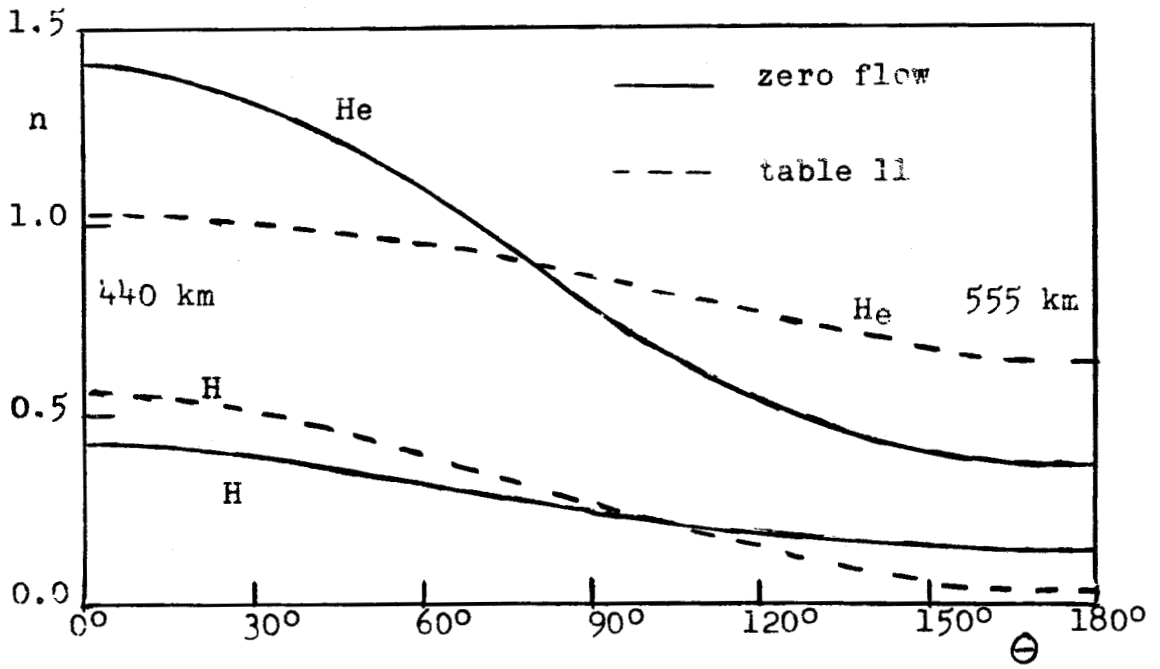

Figure 42. Hydrogen and helium densities in 10^5 and $10^6 cm^{-3}$ respectively for zero flow and as in table 11. for a 1000-1500° sinusoidal temperature variation.

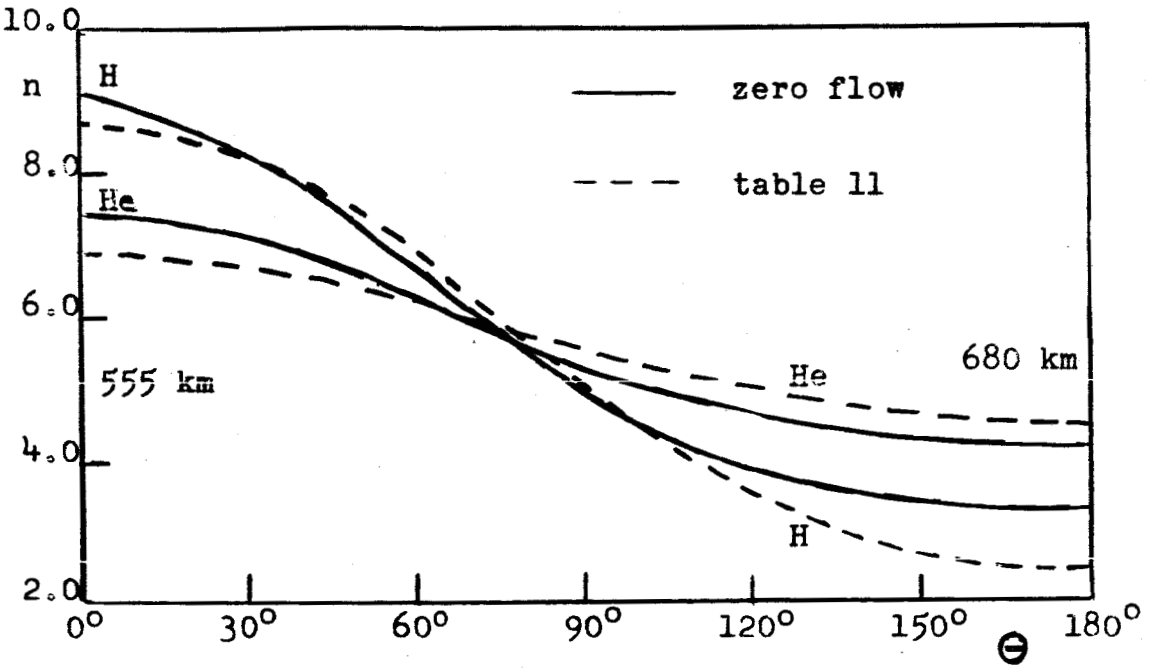

Figure 43. Hydrogen and helium densities in 10^3 and $10^5 cm^{-3}$ respectively for zero flow and as in table 11 for a 1500-2100° sinusoidal temperature variation.

the exobase surface would mean that the endospheric distributions were not ones of diffusive equilibrium and would yield a flow by diffusion. Hence the distributions would tend toward a zero lateral flow situation but would not reach one.

5.12. Steady State

If the homosphere is assumed to be able to act as either a sink or a source as endospheric conditions warrant, then a steady state distribution can be imagined similar to a steady state with escape in which the lateral flows for a given exobase distribution are matched by the vertical diffusive fluxes in the endosphere which give that same distribution at the exobase when used in the diffusion equation. This distribution would have to lie somewhere between the

diffusive equilibrium model and the zero flow model by virtue of the correlation between the lateral flow and the diffusive flow created by the resultant change in density.

This type of steady state distribution depends upon two major assumptions, however. The first is that of a source and/or sink at the turbopause. If these are not sufficient to supply or accept the steady state fluxes, then of course a steady state distribution would be impossible. The second assumption is that a new steady state will be quickly assumed by the gas as the parameters, temperature in particular, change with time.

5.13. Time Considerations

A representative time for lateral flow is desirable when considering the ability of the lateral flow to quickly adjust density distributions. The lateral flow itself is made up of particles which take a finite time between leaving and re-entering the endosphere. Some times, τ, for typical orbits designated by the initial conditions at the exobase, velocity, v, and an angle from the radial direction of 45^{o}, are shown in table 15. Since the escape velocity is 10.9×10^{5} $cm \cdot sec^{-1}$, it is apparent that the majority of particles take less than an hour in flight. It should be pointed out in all fairness that much of the hydrogen flux comes from higher velocity particles (~ 8 or 9×10^{5}) so that one hour might be a little small as a useful time. Anyway, in the period of one or even two hours conditions will not have changed drastically and the lateral flow itself can be thought of as taking a negligible amount of time.

Table 15. Orbital times for lateral flow particles.

V(cm sec^{-1})	τ(hr)
$2x10^5$	0.04
$4x10^5$	0.11
$6x10^5$	0.31
$8x10^5$	0.95
$10x10^5$	11.19

In a steady state the total amount of either helium or hydrogen in a column would differ with lateral position. Hence it would be necessary for a diffusive flow in the endosphere (in this case equivalent to the lateral flow) to remove the excess or build up the deficiency in 12 hours. To get an idea of what this would involve, it can be done for the hydrogen steady state escape distributions of figure 11. If the difference between column densities above 120 km at maximum and minimum temperature is divided by 12 hours, an average flux for removal between day and night is the result. Using the hydrogen densities of figure 11 these fluxes turn out to be $1.67x10^8 cm^{-2}sec^{-1}$, $1.37x10^8 cm^{-2}sec^{-1}$, and $2.72x10^7$ $cm^{-2}sec^{-1}$ for 700-1000°, 1000-1500° and 1500-2100° respectively. In this case they are even larger than possible which immediately suggests that these diurnal variations are too large. However, a steady state with lateral flow would not be as extreme and fluxes derived from differences in this case might be tolerable.

5.14. Alternative to Steady State

If a steady state distribution as formulated is not possible, the alternative is a distribution dependent upon

the lateral flow and how it can be supported or absorbed by diffusion in the endosphere. Since diffusion rates vary inversely with the total density, diffusion is much quicker in the upper endosphere than in the lower endosphere. In a region of removal by lateral flow, densities in the near exobase region could quickly diminish the lateral flow.

5.2. Exosphere

The influence of the lateral flow on the exosphere may be regarded as in two parts. The first is the alteration of the exospheric densities. This is an obvious consequence since the density in the lower exosphere is simply an extension of that in the endosphere. The second is the presence of a net flow in the exosphere itself.

5.21. Exospheric Densities with Lateral Flow

The effect upon exospheric densities of lateral flow in the exosphere region may be seen by consideration of the origin of particles contributing to the density at any point. These particles originate from all points on the exobase surface and hence come from regions of different density and temperature. The density at an exospheric point is then no longer a simple function of the local temperature and density variation.

It should be expected that at small altitudes above the exobase, such an effect would be small since most of the density contributions come from locally originating particles. At higher altitudes the origin of particles is much less

localized and modification should take place. At extremely high altitudes particles contributing to the local density have an almost equal chance of originating from any position, a necessary fact already pointed out by Chamberlain[32]. In this case the density at these high altitudes should be spherically symmetric regardless of the temperature and density distributions below.

Without the assumption of spherical symmetry exospheric density calculations become more complex but can be handled in a manner similar to the calculation of the lateral flux. The pertinent geometry for such a calculation is shown in figure 44. The contribution to the density at point 2 from the flux originating at point 1 is that flux divided by its velocity at point 2, v(2), and divided by the flux area at point 2, dA(2).

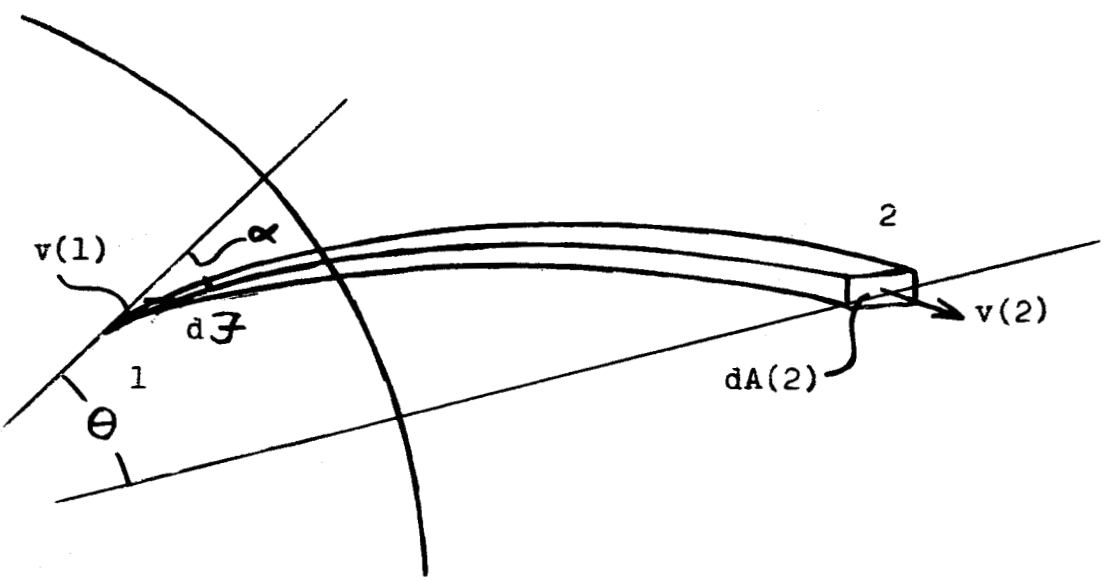

Figure 44. Geometry for exospheric density calculation.

Hence,

$$dn(2) = \frac{d\mathcal{F}(1)}{dA(2)v(2)} \quad . \tag{31}$$

For practical purposes the area and velocity as specified may be replaced by the lateral component of velocity, W_θ, and the area normal to W_θ, dA'. Then

$$dn(2) = \frac{d\mathcal{F}(1)}{dA' W_\theta} \quad . \tag{32}$$

By conservation of angular momentum with velocity v at point 1

$$W_\theta = v_\theta \, y = x v_{esc} y \sin\alpha \tag{33}$$

where

$$y \equiv R_b/r$$

$$x \equiv v/v_{esc} .$$

The area dA' may be expressed in terms of useful variables

$$dA' = r dr d\beta \sin\theta = \frac{R_b^2 d\beta \sin\theta \, d(-y)}{y^3} \tag{34}$$

where β is an azimuthal angle at point 1. The flux is the familiar form of equation (13)

$$d\mathcal{F} = n(\theta,\phi) v_{esc} \left[\frac{E}{\pi}\right]^{3/2} R_b^2 \frac{\sin\theta d\theta d\phi}{[T(\theta,\phi)]^{3/2}} d\alpha \sin\alpha\cos\alpha d\beta dx x^3 \exp\left[\frac{-Ex^2}{T(\theta,\phi)}\right] \tag{35}$$

Substituting equations (33), (34) and (35) into equation (31) yields

$$dn(2) = y^2 n(\theta,\phi)\left[\frac{E}{\pi}\right]^{3/2} \frac{d\phi\, d\theta}{\left[T(\theta,\phi)\right]^{3/2}} d\alpha \cos\alpha x^2 \exp\left[\frac{-Ex^2}{T(\theta,\phi)}\right] \frac{dx}{d(-y)}. \quad (36)$$

By first performing the x integration,

$$\frac{dx}{d(-y)} \Rightarrow -\frac{\partial x}{\partial y}.$$

From appendix B, differentiating equation (67), and inverting:

$$-\frac{\partial x}{\partial y} = \frac{x^3 \sin^2\alpha}{1-\cos\theta}, \quad (37)$$

and substitution of equation (37) into (36) gives

$$dn(2) = y^2 n(\theta,\phi)\left[\frac{E}{\pi}\right]^{3/2} \frac{d\phi\, d\theta}{(1-\cos\theta)} \frac{d\alpha \cos\alpha}{\left[T(\theta,\phi)\right]^{3/2}} \sin^2\alpha x^5 \exp\left[\frac{-Ex^2}{T(\theta,\phi)}\right]. \quad (38)$$

For azimuthal symmetry (directly above the temperature minimum or maximum) the ϕ integration gives the factor, 2π. The functional form of x from Appendix B, equation (67) is

$$x^2 = \frac{(1-\cos\theta)}{2\sin^2\alpha\left[y-\cos\theta+\cot\alpha\sin\theta\right]}. \quad (39)$$

The integration for θ is over the whole surface, i.e.,

$$0 < \theta < \pi.$$

The limits for the α integration are determined by the relationship for α and x^2. From $\alpha = 0$ until x^2 becomes negative there is always a velocity such that the orbit will pass through R_b, θ and $y, 0$. Hence

$$0 < \alpha < \cot^{-1}\left[\frac{y-\cos\theta}{\sin\theta}\right] .$$

The numerical results from an IBM 7090 computer are shown in figures 45-50. In all cases these are for hydrogen and helium at points of maximum and minimum temperatures. Figures 45 and 46 show the dependence upon density for the particular case of a 3-1 density ratio and various constant temperatures. Figures 47 and 48 show the temperature dependence. In figures 49 and 50 a continuation of the real density curves has been shown where between 120 km and the exobase diffusion is presumed and above the exobase densities are calculated from the orbital theory. Since definite changes from diffusion theory do not appear until large altitudes are reached, no correction need be made for the fact that the exobase is non-spherical.

The gross features are readily apparent. The height density profile is ignorant of lateral conditions in the region immediately above the exobase. At higher altitudes the lateral flow tends to smooth the densities toward a spherical symmetry between the extremes. These variations occur at such large altitudes, however, that for all intents and purposes a diffusive equilibrium type distribution can be assumed in the lower exosphere.

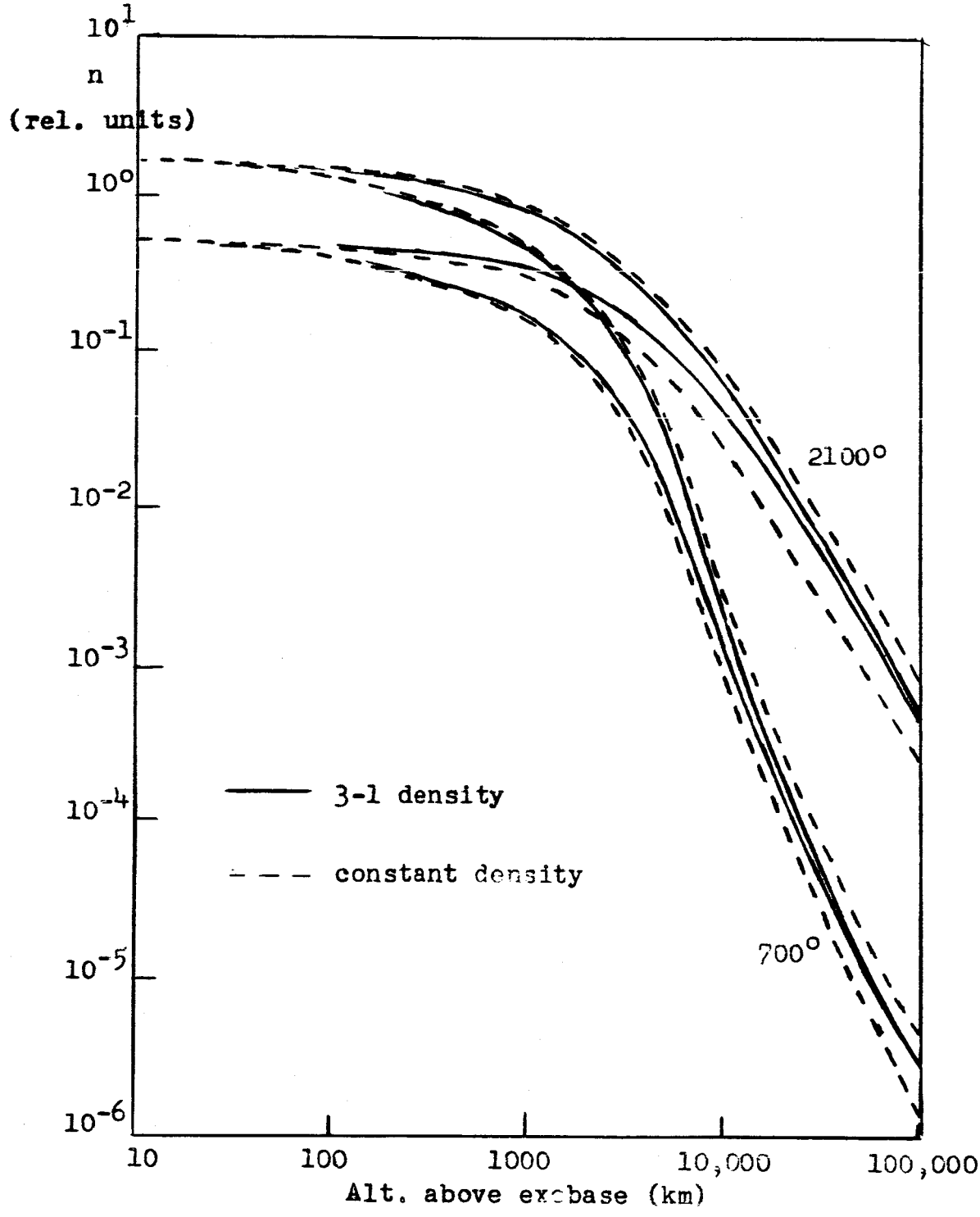

Figure 45. Exospheric hydrogen densities for constant and sinusoidal 3-1 density exobases and 700° and 2100° exospheric temperatures.

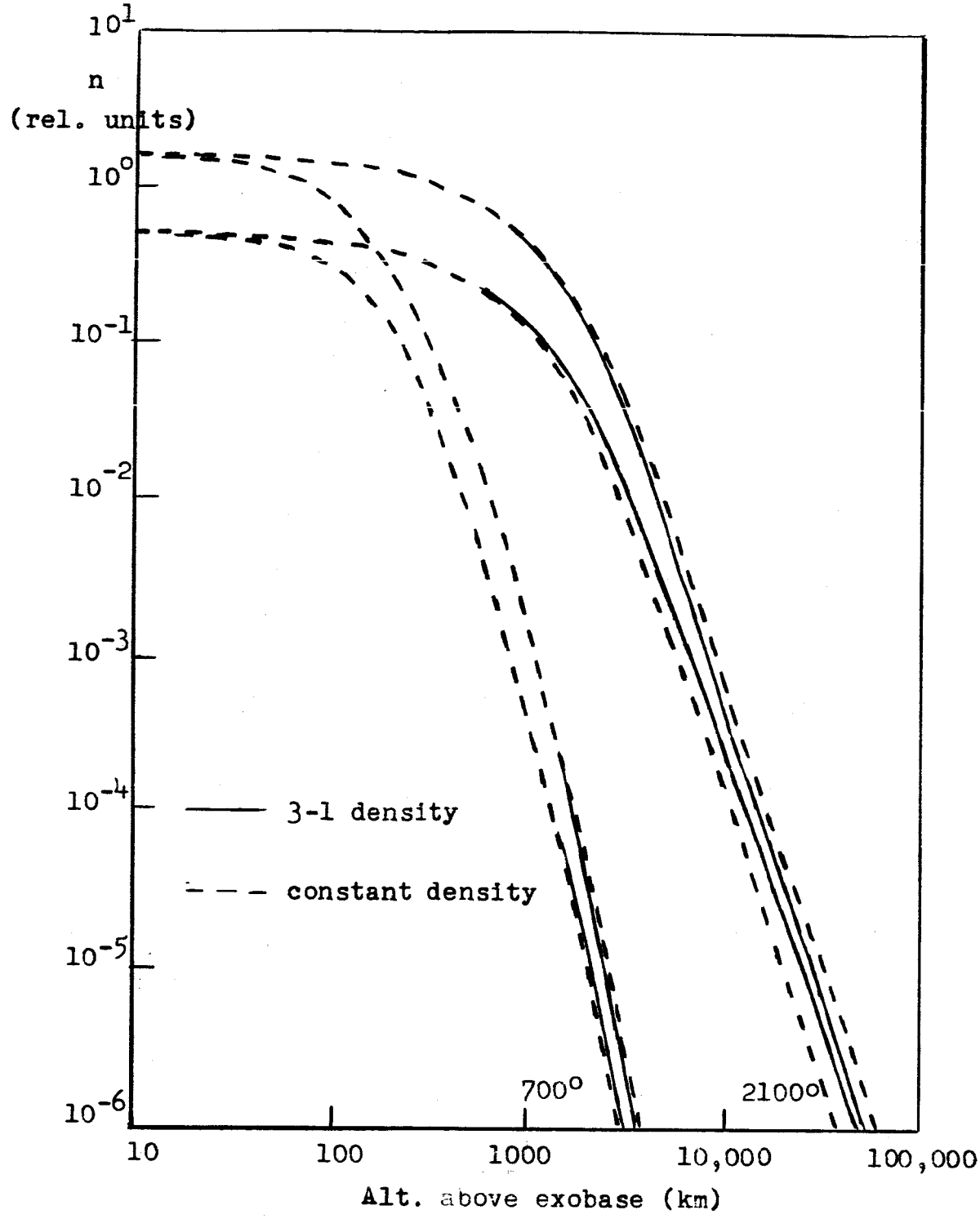

Figure 46. Exospheric helium densities for constant and sinusoidal 3-1 density exobases and 700° and 2100° exospheric temperatures.

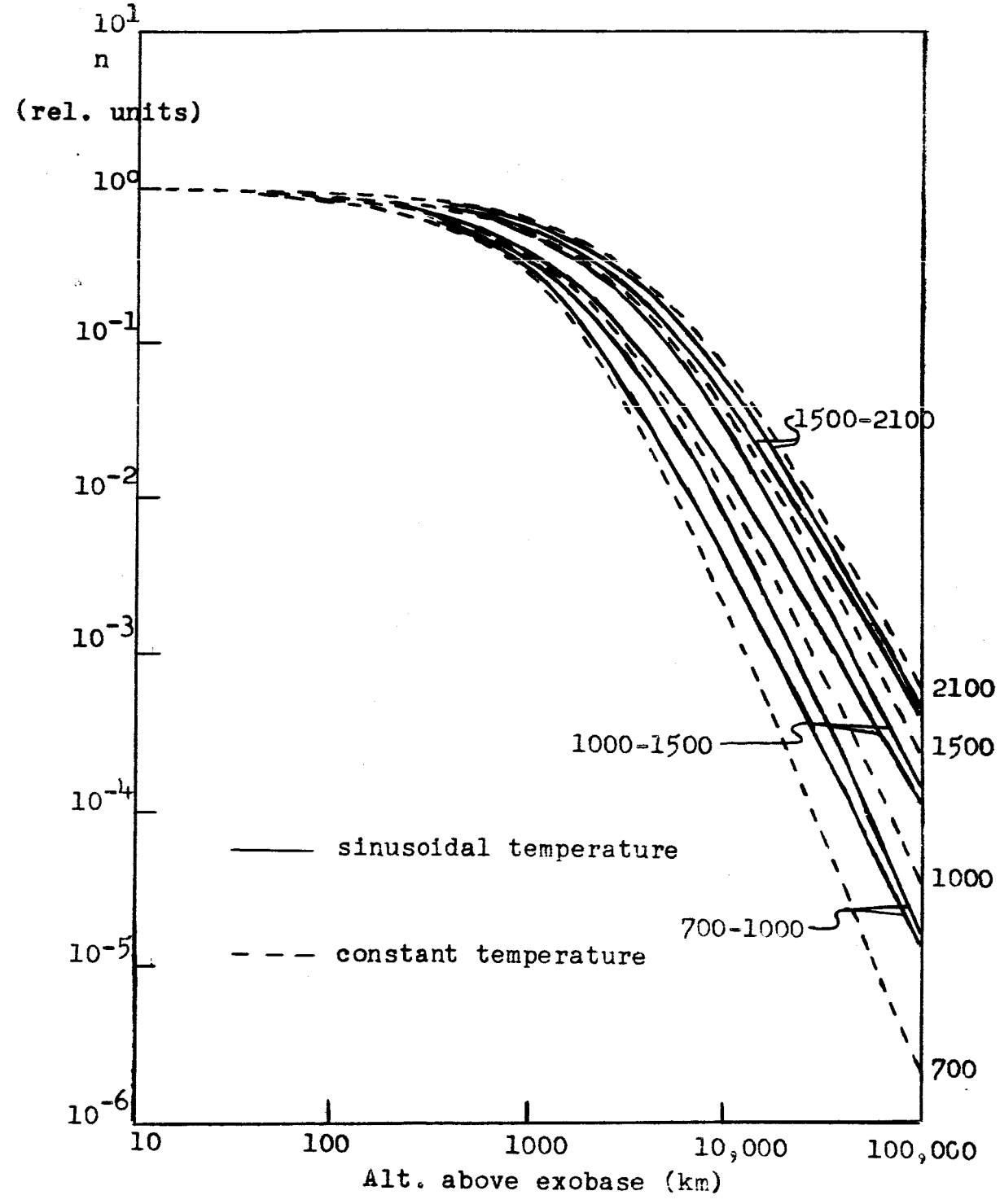

Figure 47. Exospheric hydrogen densities for a constant exobase density and sinusoidal temperature variations.

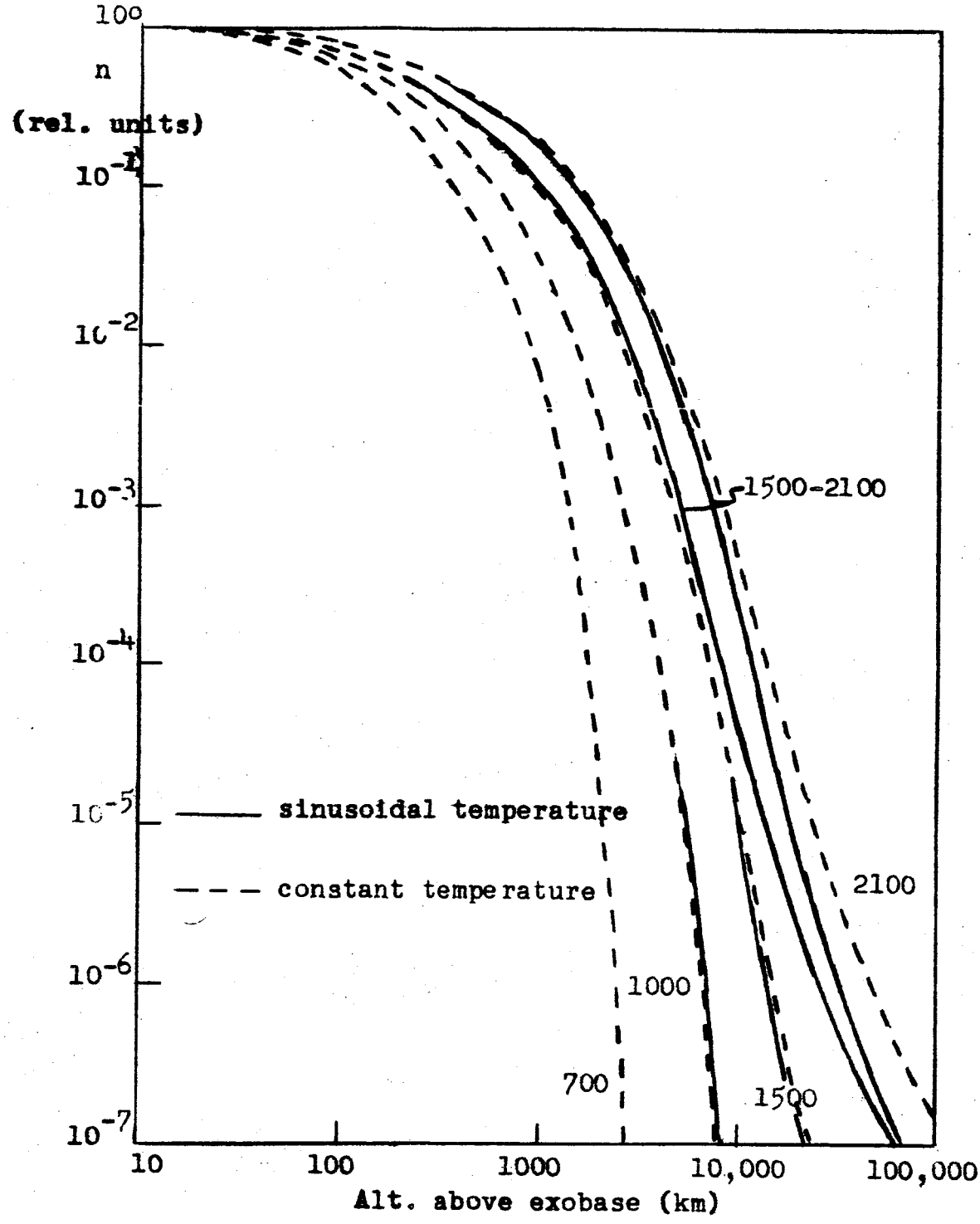

Figure 48. Exospheric helium densities for a constant exobase density and sinusoidal temperature variations.

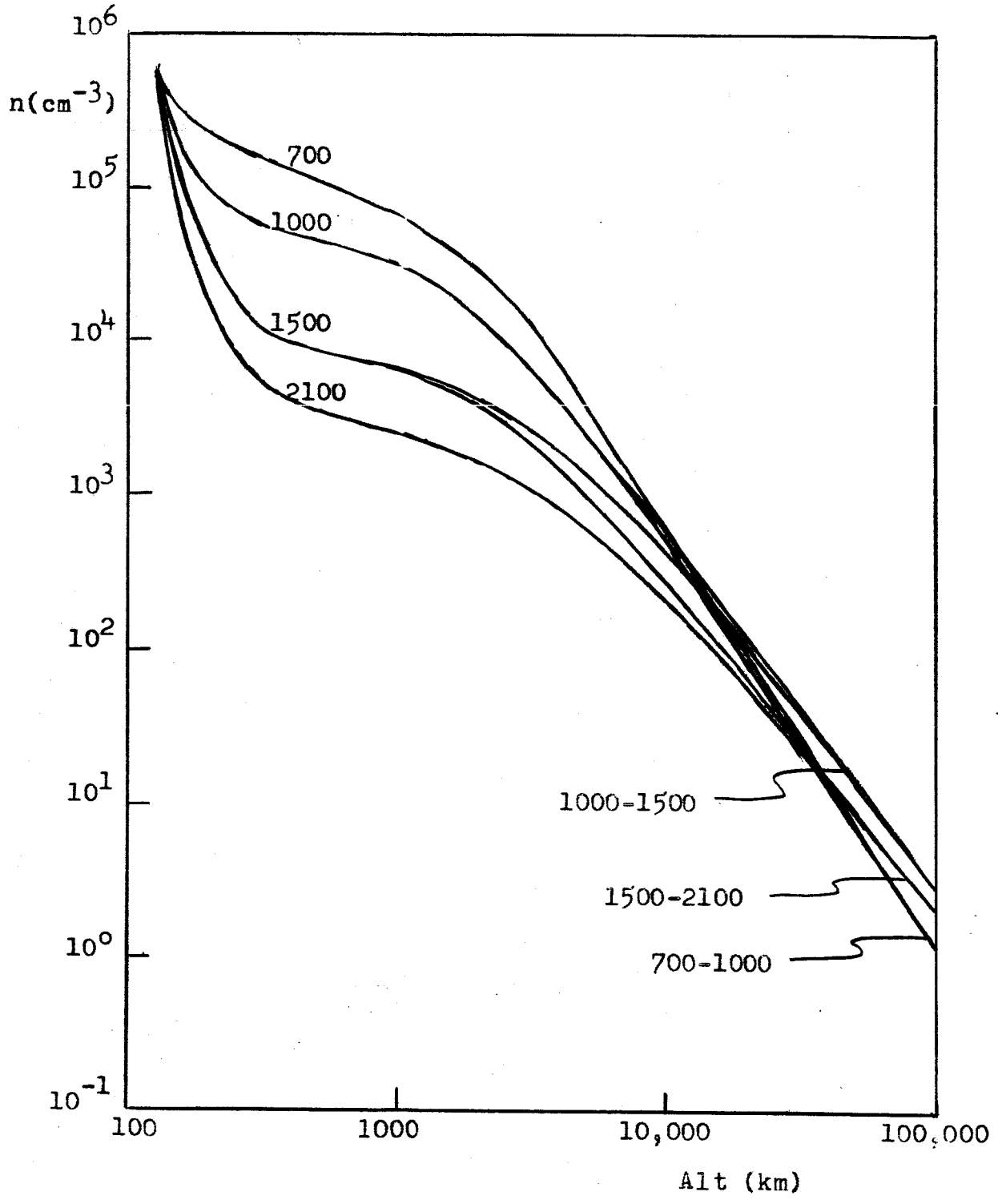

Figure 49. Hydrogen densities for various sinusoidal exobase temperature variations, diffusion below the exobase, no-collision theory above.

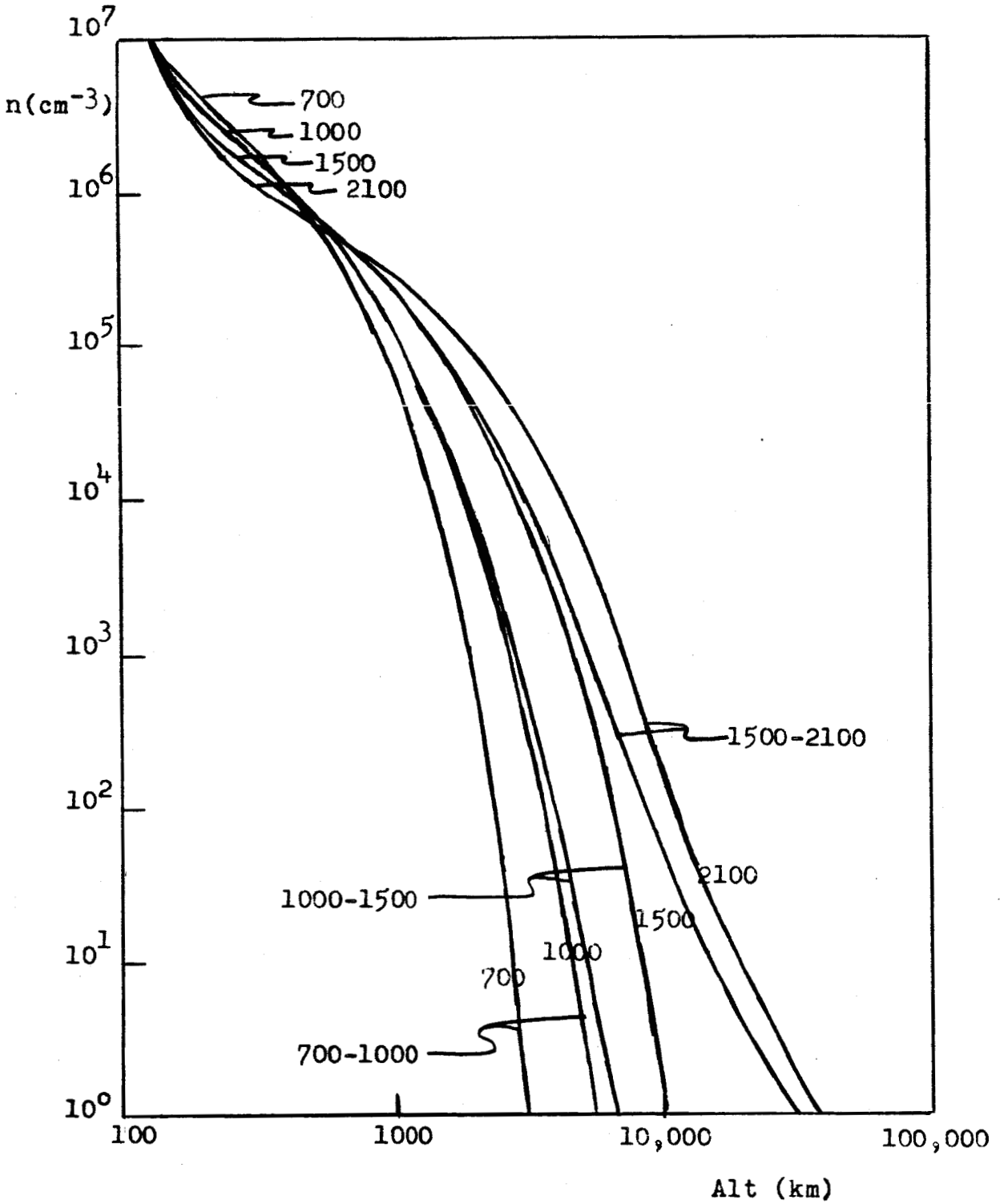

Figure 50. Helium densities for various sinusoidal exobase temperature variations, diffusion below the exobase, no-collision theory above.

5.22. Measurements in the Exosphere

Another feature of a lateral flow concerns its possible effect on various exospheric measurements by virtue of the net flow velocity. For instance, it is possible that this might produce perturbations in the orbits of high altitude satellites. Also photometric measurements concerning radiation emitted in the exosphere would contain Doppler shifts due to the net relative velocity.

An estimate may be made of the average flow velocity by considering the total lateral flow above the exosphere base through a semi-infinite strip of unit width, exactly the reverse of converting lateral flow to vertical flux. This flow $\mathcal{F}$ may be written in terms of the vertical flux, F, as

$$\mathcal{F}_i(\theta_o) = \frac{-R_b}{\sin\theta_o}\int_0^{\theta_o} F_i(\theta)\sin\theta d\theta. \tag{40}$$

and the average flow velocity would be this flux divided by the total column density, N, or

$$v_{ave} \equiv \frac{\mathcal{F}_i(\theta_o)}{N_i(R_b,\theta_o)} = \frac{-R_b\int_0^{\theta_o} F_i(\theta)\sin\theta d\theta}{\sin\theta_o n_i(R_b,\theta_o)H_i(R_b,\theta_o)} \tag{41}$$

where the approximation

$$N_i(R_b,\theta_o) \sim n_i(R_b,\theta_o)H_i(R_b,\theta_o)$$

has been made. Two values for v_{ave} which were lateral

maximums ($\theta_o \sim 90^o$) are $5x10^3$cm sec^{-1} and $5.4x10^4$cm sec^{-1} for the 1000-1500° helium and hydrogen cases respectively. These were the largest values that occurred for each. In terms of the rms velocities, the helium is about 5% and the hydrogen about 10% while they are about 1% and 8% of satellite velocities respectively. However the local lateral flow velocity will increase with altitude so that in the relatively dense region near the exobase it will be smaller than the average flow velocity and conversely, at high altitudes it will be larger. Hence if these effects are at all observable, it would be at high altitudes.

6.0. CONCLUSIONS

The conclusions that may be drawn from calculations of lateral flow are rather definite with respect to the gross effects. First, the flow for the heavier constituents, atomic oxygen, and molecular nitrogen and oxygen, is small enough to occur without altering the picture of a density distribution from a diffusive equilibrium one. Second, the flow for hydrogen and helium is sufficiently large to prohibit ignoring the effect in calculations of their density distributions. The energy flow may be neglected in any case.

These statements must be tempered by two conditions, namely the approximation of the diffusion coefficient in calculating maximum diffusive fluxes and more important the adoption of the criterion for establishing the exobase. The second is important because the lateral flow is directly proportional to the density and will vary in the same manner. Fortunately, the helium and hydrogen densities vary slowly in the exobase region so that it would take a large change in exobase altitude to seriously alter the lateral flow.

Several conclusions may be drawn from the form of the flow, but they are rather unspecific in nature. The lateral flow will demand an asymmetry as pointed out by Donahue and McAfee[10] from earlier work. This is most easily seen from the density distributions yielding zero net flow. They contain an approximate 2.5-1 maximum to minimum density ratio. A distribution lying between this and the escape flux distribution for hydrogen would have a larger ratio and

between this and the diffusive equilibrium distribution for helium would have a smaller ratio. Added effectiveness of the zero flow distributions is in the fact that they are general, and independent of exobase choice.

The problem of calculating the exact effect of the flow on density distributions has not yet been attempted. It could be approached in two ways. If a steady state solution is desirable, diffusion equations in the exosphere could be coupled to lateral flow in the exosphere, much as escape is included in the diffusion equations for hydrogen. Unfortunately an exact solution is not readily available. Perhaps the best way to proceed would be by successive approximations with alternate calculation of lateral flow and vertical densities using the information from one in the other. In this case the fluxes would have to be scaled down, however, to avoid divergences.

The second approach would be to consider a time dependent atmosphere with both vertical and lateral diffusion, the lateral diffusion replacing lateral flow as calculated here. This is probably permissible in the lower exosphere since the atmosphere seems to act like a diffusive one in this region anyway.

Each of these processes must contain assumptions about the boundary conditions, not only with respect to the densities, themselves, but also with respect to the flows. A definite knowledge of such conditions must be known before a real description of the effects of lateral flow can be made.

It does not seem likely that evidence could be gathered experimentally directly involving the lateral flow as in section 5.22. Experimental support would then have to arise from measurements on an atmosphere that has been altered due to the presence of the flow. Obviously, density measurements on helium and hydrogen would be the most likely.

In summation, then, the particular features of the lateral flow are:

1) The flow is negligible for O, N_2, and O_2.
2) The flow is large for He and H.
3) Diffusive equilibrium is unlikely for He.
4) Hydrogen should have a very complicated lateral and vertical variation, at least with respect to its theoretical determination.
5) Real distributions of H and He will be determined by diffusion and lateral flow and also by the boundary conditions on both density and flow.

APPENDIX A. DIFFUSION EQUATIONS

According to Chapman and Cowling[35] the general equation of diffusion for a binary gas of constituents 1 and 2 may be written:

$$\underset{\sim}{\bar{c}_1}-\underset{\sim}{\bar{c}_2}=\frac{-n^2}{n_1 n_2}D_{12}\left\{\underset{\sim}{\nabla}\left(\frac{n_1}{n}\right)+\frac{n_1 n_2}{n\rho}(m_2-m_1)\underset{\sim}{\nabla}\ln P\right.$$

$$\left.-\frac{\rho_1\rho_2}{\rho P}(\underset{\sim}{F_1}-\underset{\sim}{F_2})+\frac{n_1 n_2}{n^2}\alpha_T\frac{1}{T}\underset{\sim}{\nabla}T\right\}, \qquad (42)$$

where:

$\underset{\sim}{\bar{c}_1},\underset{\sim}{\bar{c}_2}$ = diffusion velocities,

n_1, n_2 = number densities,

m_1, m_2 = masses,

$\underset{\sim}{F_1},\underset{\sim}{F_2}$ = accelerations due to external forces,

ρ_1, ρ_2 = mass densities,

D_{12} = diffusion coefficient,

n = total number density,

P = total pressure,

ρ = total mass density,

α_T = coefficient of thermal diffusion,

T = temperature.

The four terms represent diffusion due to the non-uniformity of composition, pressure, and temperature and due to external forces.

If the region of atmosphere of interest is considered to be plane parallel, the vertical diffusion will be:

$$w_1 - w_2 = \frac{-n^2}{n_1 n_2} D_{12} \left\{ \frac{\partial}{\partial z}\left(\frac{n}{n_1}\right) + \frac{n_1 n_2}{n\rho}(m_2 - m_1)\frac{1}{P}\frac{\partial P}{\partial z} + \frac{n_1 n_2}{n^2} \alpha_T \frac{1}{T}\frac{\partial T}{\partial z} \right. \tag{43}$$

where w_1 and w_2 are the vertical components of diffusion velocity. Using the relationships

$$n_1 + n_2 = n$$

$$\rho = \bar{m}\, n$$

where $\bar{m}$, the mean molecular mass, is defined by:

$$\bar{m} = \frac{m_1 n_1 + m_2 n_2}{n},$$

and applying the ideal gas law,

$$P = nkT,$$

and the hydrostatic equation

$$\frac{\partial P}{\partial z} = -\rho g,$$

equation (43) reduces to:

$$w_1 - w_2 = -D_{12}\left[\frac{n}{n-n_1}\right]\left\{\frac{1}{n_1}\frac{\partial n_1}{\partial z} + \frac{m_1 g}{kT} + \left[1 + \frac{n-n_1}{n}\alpha_T\right]\frac{1}{T}\frac{\partial T}{\partial z}\right\} \qquad (44)$$

In the case of diffusive equilibrium, $w_1 - w_2 = 0$, and

$$\frac{1}{n_1}\frac{\partial n_1}{\partial z} + \frac{m_1 g}{kT} + \left[1 + \frac{n-n_1}{n}\alpha_T\right]\frac{1}{T}\frac{\partial T}{\partial z} = 0. \qquad (45)$$

If thermal diffusion is neglected, i.e. $\alpha_T = 0$, equation (45) has the solution:

$$\overline{n_i(z)} = n_i(a)\left[\frac{T(a)}{T(z)}\right]\exp\left[-\frac{m_i}{k}\int_a^z \frac{g(z')}{T(z')}dz'\right] \qquad (46)$$

where the index i refers to the ith component. This is the familiar barometric formula for diffusive separation.

If component 1 is not in diffusive equilibrium but it is a minor component such that

$$n_1 << n_2$$

$$w_2 << w_1$$

then equation (44) may be written for this ith component:

$$w_i = -D_i\left\{\frac{1}{n_i}\frac{\partial n_i}{\partial z} + \frac{m_i g}{kT} + (1+\alpha_T)\frac{1}{T}\frac{\partial T}{\partial z}\right\}. \qquad (47)$$

One case of importance that involves a non-zero diffusion is the steady state flow. If there is a source and sink

at different altitudes with no loss or gain between, continuity (now written as in a spherical geometry) imposes a restriction on the diffusive flux, $S_i(z)$, namely

$$S_i(z) \equiv n_i(z) w_i(z) = S_i(a) \left(\frac{R_a}{R_z}\right)^2 \tag{48}$$

where R_h is the geocentric radius of level h. Equation (44) then becomes upon substitution of (48)

$$S_i(a) \left(\frac{R_a}{R_z}\right)^2 + D_i \left\{ \frac{\partial n_i}{\partial z} + \frac{n_i m_i g}{kT} + n_i (1+\alpha_T) \frac{1}{T} \frac{\partial T}{\partial z} \right\} = 0, \tag{49}$$

and has the solution:

$$n_i(z) = \overline{n_i(z)} \left\{ 1 - \int_a^z \frac{S_i(a)}{D_i(z') \overline{n_i}(z')} \left(\frac{R_a}{R_z}\right)^2 dz' \right\}, \tag{50}$$

again ignoring thermal diffusion.

For small values of $S_i(a)$, the steady state solution, $n_i(z)$, is that for diffusive equilibrium, $\overline{n_i(z)}$. For larger positive values (flow out at the top), this solution will be reduced from that for diffusive equilibrium, while for large negative values (flow in at the top) the solution is enhanced.

For a sufficiently large positive value of $S_i(a)$, the steady state solution becomes negative at some altitude. Hence a maximum flux, $S_i^{max}(a)$, in the steady state case between levels a and z may be defined by that flux which will reduce the density to zero at level z, or in terms of

equation (47),

$$S_i^{max}(a) = \frac{1}{\int_a^z \frac{1}{D_i(z')\overline{n_i(z')}}\left(\frac{R_a}{R_{z'}}\right)^2 dz'} \quad . \tag{51}$$

Any flow greater than $S_i^{max}(a)$ will give the non-physical situation of negative densities somewhere between levels a and z.

The diffusion coefficient, $D_i(z)$, for the case of hard sphere elastic collisions, again as derived in Chapman and Cowling[35], may be written:

$$D_i(z) = \frac{3\sqrt{\pi/2}}{8\sigma_i}\left[1+\frac{\bar{m}}{m_i}\right]^{1/2}\left[\frac{kT}{\bar{m}}\right]^{1/2}\frac{1}{n} \tag{52}$$

where σ_i is the collisional cross-section.

In the particular case where planetary escape acts as a sink at the top of the atmosphere and an equivalent source is available from below, $S_i(a)$ may be determined by relating it to the escape flux:

$$S_i(b) = S_i(a)\left(\frac{R_a}{R_b}\right)^2 = n_i(b)w_i^{esc} \tag{53}$$

where b is the exobase altitude and w_i^{esc} the effusion velocity as defined in section 2.3. Substitution for $n_i(b)$

from equation (47) in equation (53) yields

$$S_i(a)=\overline{n_i(b)}w_i^{esc}\left(\frac{R_b}{R_a}\right)^2\left\{1-\int_a^b\frac{S_i(a)}{D_i(z')\overline{n_i(z')}}\left(\frac{R_a}{R_b}\right)^2dz'\right. \tag{54}$$

and solving for $S_i(a)$ gives

$$S_i(a)=\frac{\overline{n_i(b)}w_i^{esc}(R_b/R_a)^2}{1+\overline{n_i(b)}w_i^{esc}(R_b/R_a)^2\int_a^b\frac{1}{D_i(z')\overline{n_i(z')}}\left(\frac{R_a}{R_z}\right)^2dz'}. \tag{55}$$

Diffusion in a lateral direction, say the y direction, for a minor constituent without thermal diffusion, from equation (43) is

$$w_i^{lat}=\frac{-n}{n_i}D_i\left\{\frac{\partial}{\partial y}\left(\frac{n_i}{n}\right)+\frac{n_i}{\rho}(\bar{m}-m_i)\frac{1}{P}\frac{\partial P}{\partial y}\right\}. \tag{56}$$

If there is no lateral flow of the bulk atmosphere,

$$\frac{\partial P}{\partial y}=0$$

and using this and the perfect gas law

$$P=nkT$$

reduces equation (56) to

$$w_i^{lat}=-D_i\left\{\frac{1}{n_i}\frac{\partial n_i}{\partial y}+\frac{1}{T}\frac{\partial T}{\partial y}\right\}. \tag{57}$$

APPENDIX B. ORBITAL RELATIONSHIPS

Given a particle of velocity v at an angle α to the radial direction when at the radial distance R_b, its trajectory in the earth's gravitational field is given by:

$$\frac{1}{r}=\frac{1}{R_b}\left\{-\cot\alpha\sin\psi+\left[1-\frac{1}{2x^2\sin^2\alpha}\right]\cos\psi+\frac{1}{2x^2\sin^2\alpha}\right\} \qquad (58)$$

where

$$x \equiv \frac{v}{v_{esc}}$$

$v_{esc} = 2g(b)R_b$ = escape velocity at R_b

ψ = angle traversed by particle in orbital plane.

If equation (58) is solved for ψ, the trajectory may be expressed as:

$$\cos\psi = \frac{[A+\cos\gamma][A+y\cos\gamma+1-y] \pm \sin\gamma\sqrt{[A+\cos\gamma]^2+1-[A+y\cos\gamma+1-y]^2}}{[A+\cos\gamma]^2+\sin^2\gamma} \qquad (59)$$

$$\sin\psi = \frac{\sin\gamma[A+y\cos\gamma+1-y] \mp [A+\cos\gamma]\sqrt{[A+\cos\gamma]^2+1-[A+y\cos\gamma+1-y]^2}}{[A+\cos\gamma]^2+\sin^2\gamma} \qquad (60)$$

where

$$\gamma \equiv 2\alpha$$

$$y \equiv R_b/r$$

$$A \equiv \frac{1}{x^2} - 1.$$

For the particular case of $y=1$, i.e. the angle traversed by the particle between leaving the sphere $r=R_b$ and returning, equations (59) and (60) become

$$\cos\psi = \frac{[A+\cos\gamma]^2 \pm \sin^2\gamma}{[A+\cos\gamma]^2+\sin^2\gamma} \tag{61}$$

$$\sin\psi = \frac{\sin\gamma[A+\cos\gamma][1\mp 1]}{[A+\cos\gamma]^2+\sin^2\gamma} \quad . \tag{62}$$

In a similar manner, if equation (58) is solved for $\gamma=2\alpha$,

$$\cos\gamma = \frac{\left\{-(y-\cos\psi)[A(1-\cos\psi)+1-y] \pm \sin\psi\sqrt{(y-\cos\psi)^2+\sin^2\psi-[A(1-\cos\psi)+1-y]^2}\right\}}{(y-\cos\psi)^2+\sin^2\psi} \tag{63}$$

$$\sin\gamma = \frac{\left\{[A(1-\cos\psi)+1-y]\sin\psi \pm (y-\cos\psi)\sqrt{(y-\cos\psi)^2+\sin^2\psi-[A(1-\cos\psi)+1-y]^2}\right\}}{(y-\cos\psi)^2+\sin^2\psi} \quad . \tag{64}$$

These in turn when $y=1$ reduce to:

$$\cos\gamma = \frac{-A(1-\cos\psi) \pm \sqrt{1+\cos\psi}\sqrt{2-(1-\cos\psi)A^2}}{2} \tag{65}$$

$$\sin\gamma = \frac{A\sin\psi \pm \sqrt{1-\cos\psi}\sqrt{2-(1-\cos\psi)A^2}}{2} \quad . \tag{66}$$

Finally, solving equation (58) for x yields

$$x^2 = \frac{1-\cos\psi}{\sin\gamma\sin\psi+(1-\cos\gamma)(y-\cos\psi)} \quad . \tag{67}$$

APPENDIX C. LATERAL FLOW UNDER SYMMETRY CONDITIONS

The validity of the lateral flux equation may be checked by consideration of the case of a spherical symmetry in both density and temperature. Under these conditions equation (32) may be written:

$$F^{in} = \frac{n}{4}\left(\frac{E}{\pi}\right)^{3/2} v_{esc} \int dx x^3 \exp\left[-Ex^2\right] \int \frac{d\theta' \sin\theta' (1+A^2\cos\theta')}{\sqrt{1+\cos\theta'}\sqrt{2-A^2(1-\cos\theta')}} \int d\phi' \tag{68}$$

where now

$$E \equiv \frac{m v_{esc}^2}{2kT}$$

With the proper limits of integration this becomes

$$F^{in} = \frac{n}{4}\left(\frac{E}{\pi}\right)^{3/2} v_{esc} \left\{ \int_0^{1/\sqrt{2}} dx x^3 \exp\left[-Ex^2\right] \int_1^{1-2/A^2} \frac{(-d\cos\theta')(1+A^2\cos\theta')}{\sqrt{1+\cos\theta'}\sqrt{2-A^2(1-\cos\theta')}} \int_0^{2\pi} d\phi' \right.$$

$$\left. + \int_{1/\sqrt{2}}^{1} dx x^3 \exp\left[-Ex^2\right] \int_1^{-1} \frac{(-d\cos\theta')(1+A^2\cos\theta')}{\sqrt{1+\cos\theta'}\sqrt{2-A^2(1-\cos\theta')}} \int_0^{2\pi} d\phi' \right\}. \tag{69}$$

For each of the two terms the ϕ' integration is 2π. The Θ' integrations are of the form:

$$I = \int \frac{d\xi (1+A^2\xi)}{\sqrt{1+\xi}\sqrt{2-A^2(1-\xi)}} = \sqrt{1+\xi}\sqrt{2-A^2(1-\xi)}.$$

Substitution of these into equation (69) yields:

$$F^{in} = \frac{\pi n}{2}\left(\frac{E}{\pi}\right)^{3/2} v_{esc}\left\{\int_0^{1/\sqrt{2}} dx x^3 \exp\left[-Ex^2\right]\left[\sqrt{1+\xi}\sqrt{2-A^2(1-\xi)}\right]_{1-2/A^2}^{1} + \int_{1/2}^{1} dx x^3 \exp\left[-Ex^2\right]\left[\sqrt{1+\xi}\sqrt{2-A^2(1-\xi)}\right]_{-1}^{1}\right\}$$

$$F^{in} = \frac{\pi n}{2}\left(\frac{E}{\pi}\right)^{3/2} v_{esc}\left\{\int_0^{1/\sqrt{2}} dx x^3 \exp\left[-Ex^2\right](2-0) + \int_{1/\sqrt{2}}^{1} dx x^3 \exp\left[-Ex^2\right](2-0)\right\}$$

$$F^{in} = \pi n\left(\frac{E}{\pi}\right)^{3/2} v_{esc}\int_0^1 dx x^3 \exp\left[-Ex^2\right]. \qquad (70)$$

The equation for the outgoing flux is:

$$F^{out} = n\left(\frac{E}{\pi}\right)^{3/2} v_{esc}\int_0^1 dx x^3 \exp\left[-Ex^2\right]\int_0^{\pi/2} \sin\alpha\cos\alpha\, d\alpha \int_0^{2\pi} d\beta$$

$$F^{out} = n\left(\frac{E}{\pi}\right)^{3/2} v_{esc}\int_0^1 dx x^3 \exp\left[-Ex^2\right]\left(\tfrac{1}{2}\right)(2\pi)$$

$$F^{out} = \pi n\left(\frac{E}{\pi}\right)^{3/2} v_{esc}\int_0^1 dx x^3 \exp\left[-Ex^2\right]. \qquad (71)$$

Equations (70) and (71) are identical and hence the net flux is zero as it must be in a symmetrical situation.

APPENDIX D. INFLUENCE OF LATERAL FLOW ON THE DIURNAL VARIATION IN EXOSPHERIC HYDROGEN

REFERENCES

1. G. Kockarts and M. Nicolet, Ann. Geophys. 18, 269 (1962).
2. G. Kockarts and M. Nicolet, Ann. Geophys. 19, 370 (1962).
3. M. Godart and M. Nicolet, Space Research IV, North Holland, Amsterdam (1964).
4. T. Van Zandt and R. W. Knecht, Space Physics, Wiley, New York (1964).
5. J. H. Jeans, Kinetic Theory of Gases, Cambridge University Press, Cambridge (1962).
6. T. M. Donahue, J. Geophys. Res. 69, 1301 (1964).
7. G. E. Thomas, J. Geophys. Res. 68, 2639 (1963).
8. T. M. Donahue and G. E. Thomas, J. Geophys. Res. 68, 2661 (1963).
9. W. B. Hanson and T. N. L. Patterson, Planet. Space Sci. 11, 1035 (1963).
10. T. M. Donahue and J. R. McAfee, Planet. Space Sci. 12, 1045 (1964).
11. E. A. Reber and M. Nicolet, Investigation of the Major Constituents of the April-May 1963 Heterosphere by the Explorer XVII Satellite, NASA Report X-650-65-64 (1965).
12. J. E. Blamont, T. M. Donahue and M. L. Lory, Planet. Space Sci. 5, 185 (1961).
13. J. E. Blamont, T. M. Donahue and M. L. Lory, Phys. Rev. Letters 6, 403 (1961).
14. J. E. Blamont, M. L. Lory, J. P. Schneider, and G. Courtes, Space Research II, North Holland, Amsterdam (1962).
15. J. E. Blamont, M. L. Lory and G. Courtes, Ann. Geophys. 16, 435 (1960).
16. J. E. Blamont and M. L. Lory, Space Research III, North Holland, Amsterdam (1963).
17. J. E. Blamont and M. L. Lory, C. R. Acad. Sc. Paris 257, 1135 (1963).
18. J. E. Blamont and M. L. Lory, Nature 201, 593 (1964).

19. A. E. Hedin, C. P. Avery and C. D. Tschetter, J. Geophys. Res. 69, 4637 (1964).

20. A. E. Hedin and A. O. Nier, J. Geophys. Res. 70, 1273 (1965).

21. E. Zipf, private communication.

22. E. B. Meadows and J. W. Townsend, Space Research I, North Holland, Amsterdam (1960).

23. A. A. Pokhunkov, Planet. Space Sci. 9, 269 (1962).

24. E. Meadows-Reed and C. R. Smith, J. Geophys. Res. 69, 3199 (1964).

25. E. J. Schaefer and M. H. Nichols, J. Geophys. Res. 69, 4649 (1964).

26. A. O. Nier, J. H. Hoffman, C. Y. Johnson, and J. C. Holmes, J. Geophys. Res. 69, 4629 (1964).

27. T. M. Donahue, private communication.

28. P. J. Nawrocki and R. Papa, Atmospheric Processes, Prentice-Hall, Englewood Cliffs (1963).

29. E. J. Öpik and S. F. Singer, Phys. Fluids 3, 653 (1961).

30. J. Herring and L. Kyle, J. Geophys. Res. 66, 1980 (1961).

31. C. S. Shen, J. Atmos. Sci. 20, 69 (1963).

32. J. W. Chamberlain, Planet. Space Sci. 11, 901 (1963).

33. F. S. Johnson, Astrophys. J. 133, 701 (1961).

34. S. Chapman and T. G. Cowling, The Mathematical Theory of Non-uniform Gases, Cambridge University Press, Cambridge (1961).